Electrochimica Acta 444 (2023) 141970

Contents lists available at ScienceDirect

Electrochimica Acta

journal homepage: www.journals.elsevier.com/electrochimica-acta

Lanthanide nickelates for their application on Solid Oxide Cells

M.A. Morales-Zapata, A. Larrea, M.A. Laguna-Bercero *

Instituto de Nanociencia y Materiales de Aragón, CSIC-Universidad de Zaragoza, c/ María de Luna 3, 50018 Zaragoza, Spain

ARTICLE INFO

Keywords:
SOFC
SOEC
Lanthanide nickelate
Ruddlesden-Popper phase
Oxygen electrode

ABSTRACT

High-temperature technologies like solid oxide cells (SOC) have been employed to provide power-to-fuel and vice versa for energy conversion and storage. These technologies are a work in progress due to durability and compatibility issues between components at high temperatures. For this reason, the pursuit of optimal physical, mechanical, and chemical properties of SOC materials at lower temperatures has become more diligent. Finding suitable air electrodes has become one of the more notable obstacles to complete implementation in the industry. One of the most recent alternatives is the use of lanthanide nickelates with the Ruddlesden-Popper (RP), $Ln_{n+1}Ni_nO_{3n\pm1}$ (Ln = La, Nd or Pr), and perovskite, $LnNiO_{3-\delta}$, structures. These materials present fast ionic and electronic transport, as well as flexible oxygen stoichiometry that makes them compelling for this purpose. As part of an ongoing study on alternative air electrode advanced materials, this review is focused on documenting the relevant findings of RP nickelates over the years, especially focusing on the current status in research and development while comparing the electrochemical performance of nickelate air electrodes.

1. Introduction

Current global energy demands entail huge capacities of energy conversion and storage because most of the renewable energy is available as electricity from sources like solar photovoltaics, wind, and water streams, which are sporadic in comparison to nuclear and carbon-fueled sources. Economic output has been soaring at almost the same rate of energy use since the 20th century [1]. To be prepared for this, some perspectives on how sustainable energy-powered reversible solid oxide cells (SOC), i.e. the combination of solid oxide fuel cells (SOFC) and solid oxide electrolysis cells (SOEC), [2,3] may be applied on a large scale for the transportation sector via power-to-fuel technology and for integration with power systems together with seasonal storage. In reversible-SOCs, the manipulation of H_2O and/or CO_2 gasses is pivotal, as the recycling of product gasses can become a viable solution in energy systems storage. Furthermore, the benefits of reversible SOC over current battery designs are evident based on the criteria of equivalent power density that favors the conversion of energy density by electrolysis into a chemical energy storage system [4].

To be commercially viable, long-term stability in SOC performance is the final goal, where compatibility between components becomes essential. Stable performances for more than 100,000 h in SOFC [5] (in a short stack operating at 700 ºC) and 80,000 in SOEC [6] (at 850 ºC) have been achieved recently. In addition, the reversible-SOC operation has demonstrated an improvement on the overall long-term stability of SOCs [2,7,8]. Examples of this include long reversible-SOC tests performed for 4000 h in single cells [8] (with 50 vol.% steam at 800 ºC for 80 cycles of 1 h SOEC and 5 h SOFC) and 9200 h in stacks (70% H_2 utilization for 326 cycles at 750 ºC in SOFC and 820 ºC in SOEC) [9]. Another indispensable property of oxygen electrodes is to have the ability to induce mixed electronic and ionic conductivity. For a SOC oxygen electrode, the phase structures of candidate materials and the corresponding structural stability under working conditions are critical parameters since they are closely related to the catalytic activity and operational stability. This is particularly important in the intermediate-to-low temperature range, as the activity of the polarized electrodes could be insufficient depending on the synthesis and/or operating conditions.

The continuous research to improve SOC electrochemistry has converged in studies focused on lanthanide nickelates over the past 20 years [7,10], emphasizing their remarkable performances as air electrodes (also called oxygen electrodes), the approach to reducing long-term degradation, and their structural advantages for enhanced oxygen kinetics [11–15].

The lanthanide nickelates can be found in different phases: the parent phase is the $Ln_2NiO_{4+\delta}$ nickelate with one corner-sharing layer of NiO_6 octahedra along the ***c*** direction. The next tier is the higher-order nickelate $Ln_{n+1}Ni_nO_{3n\pm1}$ (n = 2), like in $Ln_3Ni_2O_{7-\delta}$, constructed in two $LnNiO_3$ layers connected in the ***c*** direction between the rock-salt

* Corresponding author.
E-mail address: malaguna@unizar.es (M.A. Laguna-Bercero).

https://doi.org/10.1016/j.electacta.2023.141970
Received 14 October 2022; Accepted 28 January 2023
Available online 30 January 2023

layers. Since the Ni oxidation state and electronic correlations along the ***c*** direction increase relative to Ln_2NiO_4, the electrical conductivity is enhanced significantly in comparison to the parent phase. The multi-layered nickelate $Ln_4Ni_3O_{10-\delta}$ ($n = 3$), first documented in 1959 [16], presents a phase with a La/Ni ratio between that of $LaNiO_3$, and LNO. The main advantage of lanthanide nickelate-based electrodes is the oxygen exchange mechanism that is driven cooperatively by both interstitial oxygen from the rock salt layers and regular oxygen from the perovskite layers. With the increased interest in electrolysis, co-electrolysis and reversible operation in SOC, $Nd_2NiO_{4+\delta}$ (NNO) [17, 18], $La_2NiO_{4+\delta}$ (LNO) [12], and $Pr_2NiO_{4+\delta}$ (PNO) [7] have been studied extensively because of their promising performance under these particular operating conditions. Recent reviews of these materials include studies about nickelate air electrode performance in proton conducting fuel cells (PCFC) for perovskite [19,20] and RP nickelates [21], nickelate air electrodes SOFC performance [19,22], and structure and oxygen kinetics of the RP phases [23]. In this literature, relevant aspects such as crystalline structure, main physical properties, and transport mechanisms are often mentioned, while offering some oxygen ion and proton conduction strategies. In particular, nickelate perovskites show fast oxygen surface exchange kinetics and intermediate-to-low temperature stability, making them attractive for oxide- and proton-conducting applications [19,21,24,25]. In addition, perovskite-type nickelates have been studied as current-collector components in oxygen electrodes as in the case of $LaNi_{0.6}Fe_{0.4}O_{3-\delta}$ (LNF64) [26–28], and composites like LNF64-SDC (Scandia-doped Ceria) [26] and $La_{0.79}Sr_{0.20}CoO_3$ (LSC) [29].

Previously, La-based oxygen electrodes like lanthanum and strontium manganites (LSM) were preferred because of thermal stability at the typical SOC temperatures. However, intermediate temperature range operation in any SOC mode hinders its ionic conductivity. For other perovskite and double-perovskite electrodes, severe degradation due to surface segregation causing thermal expansion coefficients (TEC) incompatibility with conventional electrolytes [30] and the formation of carbonates [31] are issues that need to be solved before implementation. In this regard, nickelates present several advantages depending on the compositional order, type of conductivity, phase stability, and compatibility between materials. While RP nickelates do not present a high electronic conductivity like several perovskite materials, their ionic conductivity is high (over 0.01 $S{\cdot}cm^{-1}$) at intermediate-to-low temperatures [23]. To demonstrate the viability of these materials as oxygen electrodes, Bassat et al. [13] measured their ionic conductivity (from the oxygen diffusion data, using the Nernst–Einstein relation), finding that LNO presented a higher value than that of $La_{1-x}Sr_xFe_{0.7}Ni_{0.3}O_{3-\delta}$ (LSFN) or $La_{0.6}Sr_{0.4}Fe_{0.8}Co_{0.2}O_{3-\delta}$ (LSFC). The oxygen reduction reaction (ORR) activity of these materials is comparable to Lanthanum Strontium Manganite (LSM) electrodes, particularly for LNO and $Nd_2NiO_{4+\delta}$ (NNO) [32], while $Pr_2NiO_{4+\delta}$ (PNO) exhibits the lowest cathodic polarization resistance (R_{pol}) [33] and the highest oxygen permeation rate [34,35]. PNO was reported to have the best ORR performance and highest oxygen bulk diffusion and surface exchange coefficients at the intermediate temperature range (600 - 800 °C) among the Ln_2NiO_4 materials [36]. However, practical applications up to date are still limited, as the stability of some RP nickelate phases in oxidation conditions at usual SOC temperatures is still a matter of discussion. Currently, many of the approaches for phase stabilization of nickelate electrodes circle the ability to order the oxygen excess [37,38]. High-ordered ($2<n<3$) RP phases ($Ln_3Ni_2O_7$ and $Ln_4Ni_3O_{10}$), which can appear as the high-temperature decomposition of the $Ln_2NiO_{4+\delta}$ parent phase, have also been studied in SOC air electrode configurations [15, 39–43]. These phases exhibit better structural stability at high temperatures, low TEC, and better electrical conductivity (over 100 $S{\cdot}cm^{-1}$) than the parent phases (LNO, NNO, PNO) [39]. An improved ORR activity is typically observed for high-ordered RP phases [40,44].

Given the spread of information about SOC nickelates air electrodes, this review aims to identify the main methods that have been used to improve their electrochemical properties, while also focusing on the reported performances of single cells by the different research groups, mainly for ionic-conducting electrolytes. We review and compare the different strategies that could be useful for future developments and applications.

2. General properties of lanthanide nickelate materials

A useful approach toward the study of the properties of lanthanide nickelates is centered on the influence of the methodology employed for the enhancement of the physicochemical properties of SOC air electrodes and the resulting phase stability under different testing conditions. For better comprehension, we made a systematic comparison between the different syntheses found in the literature for parent phases and high-order lanthanide nickelates and their influence on particle size and agglomeration, final sintering temperature, formation of secondary phases, reactivity between air electrode and electrolyte, and SOC performance.

2.1. Structural and functional properties

Balz and Plieth [45] described, for the first time, the characteristic K_2NiF_4 structure of lanthanide nickelates. A few years later, their formal structure was determined by Ruddlesden and Popper in 1958 [46]. They identified these phases as "the stacking of finite perovskite layers ($LnNiO_3$), between rock salt layers (LnO) along the crystallographic ***c*** direction (LnO $LnNiO_3)_n$". Further descriptions of Ruddlesden-Popper (RP) nickelates and phase transformations at high temperatures were described in several contributions over the years [47–51]. In this section, we mention the most relevant of these contributions centering on the microstructure and functional properties of the nickelates such as mechanical stability, phase evolution, chemical compatibility with other SOC components, oxygen transport, and electrical conductivity. Along the oxide composition descriptions, terms related to oxygen content like "over stoichiometry" or "substoichiometric" are employed. The term "over-" indicate any oxygen composition that exceeds the nominal stoichiometric value (δ) of oxygen content on the oxides. Likewise, the "sub-" denomination is used to describe low δ values.

2.1.1. Microstructural stability of RP phases in SOC operation

The compatibility between SOC components plays an important role to prevent reactivity and/or TEC mismatches. The reactivity between nickelate electrodes and electrolytes depends heavily on the temperature, where secondary phases may also be formed. The use of interlayers often provides a solution for these issues. Phase compatibility of RP nickelates with other SOC components has been studied for CGO (cerium gadolinium oxide) and YSZ (yttria-stabilized zirconia) [52] and LSGM (lanthanum strontium gallium manganite) [53], revealing that YSZ and CGO are highly reactive with PNO and LNO at 900 ºC for over 24 h, while reactivity is not as evident in LSGM for up to 72 h at 1000 ºC. Doped-ceria interacts with these nickelates decomposing them and also producing a Pr-doped ceria phase [7]. Even with the presence of interdiffusion, the degradation rate of the SOCs is expected to be low in the long term [54]. In addition, Lalanne et al. [55] studied the optimal sintering temperatures on a series of Nd-deficient NNO oxygen electrodes with an anode-supported cell configuration of Ni-YSZ/YSZ/NNO, revealing, that at 1200 °C a large crack in all over the electrode surface is present, while the best performance was obtained at a sintering temperature of 1100 °C.

When sintered at 1100 °C, most RP nickelates experience a strong anisotropic lattice expansion, with a chemical expansion caused by the release or incorporation of oxygen in the lattice [56]. This, and the type of synthesis can influence the resulting microstructure and performance of the electrodes. This is best exemplified by the experiments performed by Montenegro-Hernández et al. [57], where a series of NNO powders prepared by the solid-state reaction, hexamethylenetetramine, and

citrates methods, were used and compared in terms of microstructural features. For the NNO starting material prepared by the solid-state reaction, a low porosity was present. This influenced the oxygen kinetic and electrochemical impedance performances, as the bulk diffusion and the combination of adsorption and gas diffusion processes were believed as the rate-determining steps. On the other hand, in the electrodes with the starting powders prepared from the other two methods, the surface oxygen exchange and dissociative adsorption processes were critical for the ORR.

One of the most important concerns on SOCs is the mechanical strength of the components, where similar thermal expansions between layers and the prevention of detrimental reactivity between air electrode and electrolyte play an important role. Mechanical stability is usually analyzed by dilatometry studies. Using this technique, we can determine the optimal thermomechanical compatibility between different SOC components. The TEC of parent RP nickelate phases has been studied in detail over the years, concluding that nickelates are, in general, compatible with the commonly employed electrolytes. A compendium of the RP nickelate TEC values obtained by several research groups is detailed in Table 1. Typical values between RT and 1000 °C are in the range of 12.1–14.5 $\times 10^{-6}$ K^{-1} for LNO, 11.1–15.5 $\times 10^{-6}$ K^{-1} for PNO, and 11.5–15.0 $\times 10^{-6}$ K^{-1} for NNO. These variations correspond to the specific test conditions employed during the experiments. For instance, Flura et al. [58] studied the thermal expansion of RP nickelates in air and at low O_2 content (10^{-4} atm), finding a diminution of TEC values when using low pO_2. This difference in TEC values was more noticeable over 450 °C for LNO (varies from 13.0 to 12.1 $\times 10^{-6}$ K^{-1}), 600 °C for PNO (13.4 to 11.1 $\times 10^{-6}$ K^{-1}), and 300 °C in NNO (12.4 to 11.5 $\times 10^{-6}$ K^{-1}). The authors noticed that the decrease in TEC values coincided with the unchanged lattice volume under low pO_2, concluding that the samples did not exhibit a chemical expansion. In the NNO case, the oxygen over stoichiometry increases with pO_2 accompanied by a phase transition at 500 °C. PNO follows the same trend but evolves at 400 °C, while LNO over stoichiometry behaves almost proportionally to temperature. In the latter, they also found that the space group determined in air is F*mmm*, differing from the one identified under N_2 atmosphere (B*mab*). The TEC values of RP nickelate phases are compatible with YSZ and CGO10 (10 atom% of Gd) at high temperatures in air.

In high-order nickelates, a phase transition from tetragonal (I4/*mmm*) to orthorhombic (F*mmm*) product of oxygen deficiency is normally shown [40]. For this reason, an increase in TEC values is expected in the 275–800 °C range, as detailed in Table 1. The nickelate order in the RP phases does not seem to have a great influence on TEC values at high temperatures. Except in high-order La-based nickelates, where its TEC values are lower than in parent phases at less than 275 °C. Other high-order RP nickelate TEC values are only found in the literature for $Pr_4Ni_3O_{10-\delta}$ compositions [59]. Doping strategies on A- and B- sites of the nickelate parent phases also influence the thermomechanical expansion, as will be discussed in subsequent sections.

2.1.2. Strategies to decrease TEC values

As outlined in the previous section, the thermomechanical compatibility of the nickelates with standard ionic and proton conducting electrolytes should be evaluated for their viability as an oxygen electrode. Lenka et al. [93] developed several strategies involving A-site cation substitutions and ensuing TEC variations. In NNO A-site substitutions, the results showed an increase in the values with Ba and Sr doping, while decreasing with Ca doping. Also, $Nd_{1.7}Ca_{0.3}NiO_{4+\delta}$ showed the lowest area-specific polarization resistance (ASR) and lowest activation energy for ORR. Remarkable comparisons are made in Ca-doped NNO ($Nd_{1.4}Ca_{0.6}NiO_{4+\delta}$) with values as low as 11.8 $\times 10^{-6}$ K^{-1} [90]. Increasing copper amounts in LNO also decreases TEC values from 14.2 $\times 10^{-6}$ K^{-1} ($La_2Ni_{0.8}Cu_{0.2}O_{4+\delta}$ [56]) to 12.8 $\times 10^{-6}$ K^{-1} ($La_2Ni_{0.5}Cu_{0.5}O_{4+\delta}$ [24]).

Tarutin et al. [94] observed a tendency for NNO TECs to increase with Ba doping, from 13.5 $\times 10^{-6}$ K^{-1} in undoped NNO to 14.7 $\times 10^{-6}$

Table 1
TEC values of RP nickelates reported from dilatometry data in the RT to 1000 °C range (values are obtained in air unless noted). TEC values of the most common electrolytes are included for comparison.

Composition	TEC (x 10^{-6} K^{-1})	Reference
La-based		
LNO	12.1 (10^{-4} atm of pO_2)	[58]
	12.6	[60]
	13.0	[36,58]
	13.1 (RT-275 °C)	[40]
	13.5	[61]
	13.8 (275–800 °C)	[40]
	14.5 (air at 0.001 and 0.03 atm)	[62]
$La_3Ni_2O_{7+\delta}$	10.5 (RT-275 °C)	[40]
	13.7 (275–800 °C)	[40]
$La_4Ni_3O_{10+\delta}$	11.2 (RT-275 °C)	[40]
	13.5 (275–800 °C)	[40]
$La_{1.95}Ba_{0.05}NiO_{4+\delta}$	13.2	[63]
$La_{1.8}Sr_{0.2}NiO_{4+\delta}$	12.6	[64,65]
$La_{1.75}Sr_{0.25}NiO_{4+\delta}$	11.2	[66]
$La_{1.7}Sr_{0.3}NiO_{4+\delta}$	13.9	[67]
$La_{1.6}Sr_{0.4}NiO_{4+\delta}$	13.1	[68]
$La_{1.2}Sr_{0.8}NiO_{4+\delta}$	12.4	[68]
$La_{1.7}Sr_{0.3}Ni_{0.9}Mn_{0.1}O_{4+\delta}$	15.3	[69]
$La_{0.2}Sr_{1.8}NiO_{4+\delta}$	13.8	[65]
$La_{1.8}Ca_{0.2}NiO_{4+\delta}$	14.5	[70]
$La_{1.7}Ca_{0.3}NiO_{4+\delta}$	13.9	[67]
	14.2	[71]
$La_{1.6}Ca_{0.4}Ni_{0.9}Fe_{0.1}O_{4+\delta}$	14.6	[70]
$La_{1.6}Ca_{0.4}Ni_{0.9}Cu_{0.1}O_{4+\delta}$	14.9	[70]
$La_{1.9}Gd_{0.1}NiO_{4+\delta}$	12.2 (air at 0.001 atm) to 12.3 (air at 0.03 atm)	[62]
$La_{1.8}Gd_{0.2}NiO_{4+\delta}$	13.6 (air at 0.001 and 0.03 atm)	[62]
$La_{1.7}Gd_{0.3}NiO_{4+\delta}$	12.8 (air at 0.001 atm) to 13.1 (air at 0.03 atm)	[62]
$La_{1.6}Gd_{0.4}NiO_{4+\delta}$	12.5 (air at 0.001 atm) to 12.4 (air at 0.03 atm)	[62]
$La_{1.5}Gd_{0.5}NiO_{4+\delta}$	13.6 (air at 0.001 atm) to 13.5 (air at 0.03 atm)	[62]
$La_{1.5}Pr_{0.5}NiO_{4+\delta}$	15.0	[72]
$La_{1.7}Ba_{0.3}NiO_{4+\delta}$	15.2	[67]
$La_2Ni_{0.6}Cu_{0.4}O_{4+\delta}$	13.0	[73]
$La_2Ni_{0.9}Co_{0.1}O_{4+\delta}$	13.8	[56]
$La_2Ni_{0.9}Fe_{0.1}O_{4+\delta}$	13.8	[56]
	12.7	[74]
$La_2Ni_{0.8}Cu_{0.2}O_{4+\delta}$	14.2	[56]
$La_2Ni_{0.5}Cu_{0.5}O_{4+\delta}$	12.8	[24]
Pr-based		
PNO	11.1 (10^{-4} atm of pO_2)	[58]
	13.2	[29]
	13.3	[61]
	13.4	[58]
	13.6	[36]
	13.9	[75]
	14.2	[76]
	15.5	[77]
$Pr_4Ni_3O_{10+\delta}$	12.0	[59]
$Pr_{1.95}Ba_{0.05}NiO_{4+\delta}$	13.9	[63]
$PrLaNiO_{4+\delta}$	14.1	[78]
$Pr_{1.7}Sr_{0.3}NiO_{4+\delta}$	12.0	[79]
	15.0	[80]
$Pr_{1.2}Sr_{0.8}NiO_{4+\delta}$	12.9	[79]
$Pr_{1.5}Sr_{0.5}Ni_{0.75}Co_{0.25}O_{4+\delta}$	13.0	[81]
$Pr_{1.7}Sr_{0.3}Ni_{0.6}Cu_{0.4}O_{4+\delta}$	13.8	[82]
$Pr_{1.7}Ca_{0.3}NiO_{4+\delta}$	14.5	[71]
$Pr_{1.6}Ca_{0.4}NiO_{4+\delta}$	13.7	[77]
$PrNdNiO_{4+\delta}$	13.7	[76]
$Pr_2Ni_{0.75}Cu_{0.25}Ga_{0.05}O_{4+\delta}$	12.7	[83]
$Pr_2Ni_{0.9}Co_{0.1}O_{4+\delta}$	16.2	[84]
$Pr_2Ni_{0.9}Mo_{0.1}O_{4+\delta}$	13.5	[75]
Nd-based		
NNO	11.5 (10^{-4} atm of pO_2)	[58]
	12.7	[36]
	13.0	[76]
	13.4	[85]
	14.5	[86]
	15.0	[71]

(*continued on next page*)

Table 1 (*continued*)

Composition	TEC (x 10^{-6} K^{-1})	Reference
$Nd_{1.95}Ba_{0.05}NiO_{4+\delta}$	13.4	[63]
$Nd_{1.8}Sr_{0.2}NiO_{4+\delta}$	12.9	[87]
$Nd_{1.6}Sr_{0.4}NiO_{4+\delta}$	13.0	[88]
$Nd_{1.2}Sr_{0.8}NiO_{4+\delta}$	14.4	[88]
$NdSrNiO_{4+\delta}$	12.3	[89]
$Nd_{1.9}Ca_{0.1}NiO_{4+\delta}$	15.1	[71]
$Nd_{1.8}Ca_{0.2}NiO_{4+\delta}$	14.3	[71]
$Nd_{1.7}Ca_{0.3}NiO_{4+\delta}$	13.5	[71]
$Nd_{1.7}Ca_{0.3}NiO_{4+\delta}$	13.5	[71]
$Nd_{1.6}Ca_{0.4}NiO_{4+\delta}$	14.1	[90]
$Nd_{1.4}Ca_{0.6}NiO_{4+\delta}$	11.8	[90]
Electrolyte Materials		
CGO20	12.0 (air 0.001 atm) to 12.2 (air 0.03 atm)	[62]
	12.3	[91]
LSGM9182	12.0	[92]
8YSZ	10.4	[58]

K^{-1} with the Ba-doped ones. When heating the $Nd_{2-x}Ba_xNiO_{4+\delta}$ phases, a $Ni^{3+}\rightarrow Ni^{2+}$ transition occurs, increasing the average ionic radii of nickel-ions coupled with a stronger expansion of the lattice, as well as other dimension-related parameters.

Compatibility of TEC values between the nickelates and electrolyte is also found in $La_2Ni_{0.9}Co_{0.1}O_{4+\delta}$ (13.8×10^{-6} K^{-1} [56]) and $La_2Ni_{0.9}Fe_{0.1}O_{4+\delta}$ (12.7×10^{-6} K^{-1} [74]), $Pr_{1.2}Sr_{0.8}NiO_{4+\delta}$ (12.9×10^{-6} K^{-1} [79]). Molybdenum can also decrease TEC values as exemplified in the comparison with cobalt substitutions in B-site in PNO (16.2×10^{-6} K^{-1} in $Pr_2Ni_{0.9}Co_{0.1}O_{4+\delta}$ [84] vs 13.5×10^{-6} K^{-1} in $Pr_2Ni_{0.9}Mo_{0.1}O_{4+\delta}$ [75]). Zhang et al. [95] reported a TEC of 13.9×10^{-6} K^{-1} for a composition of $Nd_{1.5}Pr_{0.5}NiO_{4+\delta}$, but optimal compatibility with SOC components was achieved with Mo- and Cu-doped B-cation.

2.1.3. Crystal symmetry of RP nickelates

RP nickelates present different crystal symmetries depending on the amount of oxygen over stoichiometry and the structural ordering of the material. LNO usually crystallizes in the orthorhombic space group F*mmm,* but his phase diagram is separated into two regions by the interleaving of an I4/*mmm* tetragonal phase in the oxygen compositional range of $0.11 < \delta < 0.15$ [96]. PNO (B*mab* at low δ, F*mmm* at high δ) and NNO (F*mmm*) also crystallize in the orthorhombic space group [97] and their oxygen excess often reaches over stoichiometry ($\delta < 0.15$) at high temperatures, where their favorable oxygen transport makes them more suitable for electrolysis operation [98,99]. Pr-content increase in the A-site of $La_{0.5}Pr_{1.5}NiO_{4+\delta}$ also crystallized in the B*mab* space group [100]. In addition, the increase in A-site La content of high-order RP nickelates $La_3Ni_2O_{7\pm\delta}$ [40], $La_4Ni_3O_{10\pm\delta}$ [101], $La_3PrNi_3O_{10\pm\delta}$ [102], and $La_2Pr_2Ni_3O_{10\pm\delta}$ [103] yields a crystallization in the F*mmm* space group. These high-order nickelate phases crystallize in the tetragonal I4/*mmm* space group at high temperatures, as determined by neutron diffraction [104]. Song et al. [23] identified this transition in the 300–450 °C range. Other authors have identified that in $n = 3$ RP nickelates, as in $LaPr_3Ni_3O_{10\pm\delta}$, there is a considerable number of vacancies in the rock-salt layers, although most vacancies are present in the perovskite layers [105]. They also observed a transition to the I4/*mmm* space group at 800 °C. Tsai et al. [106] confirmed by neutron diffraction that $Pr_4Ni_3O_{10\pm\delta}$ presents a monoclinic $P2_1/a$ space group. This has also been studied in $La_4Ni_3O_{10\pm\delta}$ and $Nd_4Ni_3O_{10\pm\delta}$ [23], where for La-rich high-order nickelates a transition from $P2_1/a$ to I4/*mmm* is more energetically favorable at ~700–750 °C [23,107]. However, tested cells containing lanthanide nickelates showed structural integrity after stability tests, evidencing the absence of detrimental phase transitions.

The structural transition of parent RP nickelates (at 450 °C for LNO) [58] is analogous to $Ln_2CuO_{4+\delta}$, where three types of tetragonal phases (I4/*mmm* space group) are identified [108]. The most stable at RT is the T* tetragonal phase with mixed $3^+/4^+$ valence due to a combination of oxygen coordination numbers 8 and 9. Over 450 °C, the phase transition to T' structure is present, then converging into a T tetragonal structure at higher temperatures, favoring trivalent Ln cations. In PNO and NNO, this phase transition is normally observed at 400 °C and 500 °C, respectively [58]. Ideally, the presence of Ln^{3+} cations enhances the overall activation of the nickelate electrodes, and could help the suppression of phase decomposition with the aid of barrier layers [109].

The oxygen over stoichiometry in these materials is usually attributed to intergrowths of RP-type phases [110,111], deviations in the metal-ion ratio [112], the variable valence of the transition metal ion [113], and incorporation of interstitial oxygen defects [114]. The large spread of transition temperatures was also reported [115], where multiple nickelate phase formations were detected at high temperatures [116]. Tailoring of oxygen over stoichiometry (δ) can enhance the ionic conductivity due to the higher oxygen content, which produces more charge carriers available for transport, as demonstrated by Aguadero et al. [117], who reported $\delta = 0.30$ for LNO.

2.2. Oxygen kinetics

RP lanthanide nickelate oxides (parent and high-order phases) show rapid ionic and electronic transport properties [39,118], with a versatile oxygen stoichiometry capable of accommodating the oxygen excess under high pO_2 atmospheres in the crystallographic interstices and supporting the low pO_2 atmospheres through the loss of interstitial oxygen [119]. In all processes, three parameters are essential for describing its electrochemical transport properties: (i) electronic conductivity, (ii) ionic conductivity, and (iii) oxygen diffusivity (D_{chem}) and surface exchange rates (k_{ex}), or the rate at which ambient oxygen is transferred to a surface lattice site and vice versa.

The enhanced oxygen kinetics of these materials is an important parameter for their application as SOC air electrodes [120,121]. The consensus in the literature is that lanthanide nickelates can accommodate excess oxygen by incorporating it into the interstices of the ***a-b*** plane (rock-salt layers) and as Frenkel defects in the ***c*** direction (perovskite layers) [122]. This mechanism provides an appealing alternative to vacancy-based conduction in perovskite or fluorite oxides. In particular, PNO has the highest recorded values of D_{chem} (10^{-8} $cm^2 \cdot s^{-1}$) and k_{ex} (10^{-6} $cm \cdot s^{-1}$) among the traditionally used nickelate air electrodes [36,123], with smaller activation energies. D_{chem} values are not significantly influenced by the morphology of particles, while k_{ex} is more likely to be influenced by the surface state. The ionic conductivity of these materials is directly related to the D_{chem} value; therefore, the ionic conductivity is the highest in the case of PNO. Corresponding values of k_{ex} are also associated with good electrocatalytic activity and, therefore, with the ORR. Reported ionic conductivities at 700 °C for LNO ($\sigma_i = 0.013$ $S \cdot cm^{-1}$ [124] to $\sigma_i = 0.015$ $S \cdot cm^{-1}$ [13,36,125]), PNO ($\sigma_i = 0.026$ $S \cdot cm^{-1}$ [13,126]) and NNO ($\sigma_i = 0.017$ $S \cdot cm^{-1}$ [13,126]) compare favorably to commonly used perovskites like LSFC, with values over ten times higher [105]. On the other hand, the calculated values for high-order RP nickelate phases reported by Song et al. [23] using the Nernst-Einstein equation, are considerably lower than the values reported for the other RP nickelate phases, with distinctive ionic conductivities in the range of 10^{-5} $S \cdot cm^{-1}$. This result is probably influenced by the oxygen sub-stoichiometric nature presented in these samples.

The oxygen surface exchange kinetics of $Ln_2NiO_{4+\delta}$ oxides has been investigated many times [12,13,36,38,125,127–130] by methods like the isotope exchange depth-profiling with secondary ion mass-spectrometry (IEDP-SIMS) [36], gas phase equilibration isotope exchange (IE-GPE) [131], and electronic conductivity relaxation (ECR) [132]. The oxygen diffusion in LNO has been studied on monocrystalline samples [13], polycrystalline ceramics [127], and thin films [38]. The oxygen migration in these materials has been determined as highly anisotropic, exemplified by the difference in activation energies of oxygen migration paths calculated by atomistic simulations in the ***a–b***

plane (0.29 eV) and the ***c*** direction (2.90 eV) of LNO [122]. The activation energies for oxygen diffusion and surface exchange coefficient of most polycrystalline samples fall in this range, as it includes the overall contribution in the different planes. To influence oxygen kinetics, this anisotropic behavior has been studied in epitaxial LNO [133]. In LNO films grown on perovskites in ***a*** and ***a*** + ***b*** directions, the tracer diffusion and surface exchange coefficients are approximately two orders of magnitude higher along the ***a-b*** plane than in the ***c*** axis [38]. The anisotropic effect was also explored by Tsvetkov et al. [134] for an electrochemical optimization of the nickelates. They studied the surface exchange coefficients of NNO films under tensile and compressive strain and compared their values with non-strained samples in the low-temperature SOC range. An improvement of the oxygen exchange kinetics was also found on epitaxial NNO films, accompanied by a tensile strain of about ten times faster than in compressive strain along the ***c*** axis. Yatoo et al. [105] also observed a large ***a-b*** plane anisotropy of the apical O(4) sites, more evidently at high temperatures, which is an indicator of faster oxygen diffusion. More interestingly, the vacancy diffusion of the RP structure differs from that of nickelate perovskites [135], almost exclusively through the ***a-b*** plane, while vacancy transport is limited along the ***c*** axis. Vacancies do not seem to contribute, at all, to the total diffusion over a wide range of oxygen stoichiometries [136–138].

The k_{ex} of different perovskites varies within two orders of magnitude ($\sim 10^{-8}$ to 10^{-6} cm·s^{-1} at 700 °C) [139–141], while the variation range of nickelates is still higher, as it is shown in Table 2 for some of the most utilized methods in the literature. Possible causes of the differences in the values can be explained by the diversity of microstructures, surface morphologies, and the density of the samples. The tracer diffusion coefficients (D^*) correspond to isotopic tracer techniques like IEDP-SIMS and IE-GPE, while the D_{chem} are related to net mass transport measurements like ECR or EIS.

More recently, Stangl et al. [147] studied the oxygen incorporation and transport in LNO thin film growth by Pulsed Injection Metal Organic Chemical Vapor Deposition. They identified by ECR an enhanced surface activity in thick nano-tailored films. They noted that this enhancement was possible by changes in the grain orientation and additional features on the lateral side of the nano-columns such as kinks and edges, as these defects are expected to modify surface electronic states involved in the reaction mechanism. Another study about oxygen incorporation and dissociative adsorption rates by PIE [129] concluded that k_{ex} and D_{chem} values for LNO are limited by dissociative adsorption of oxygen influenced by Ln-ion. An oxygen exchange kinetics analysis of k_{ex} in an LNO polycrystalline sample using GPE data [128], showed that oxygen dissociative adsorption is the rate-determining stage for LNO at the intermediate temperature range (600–800 °C), and the pO_2 range of 0.003–0.027 atm. Oxygen from the gas phase immediately incorporates into the LNO lattice, while grains that did not incorporate became part of the rate-determining stage. In the upper-temperature threshold, the value of the LNO effective D_{chem} was closer to the value of D_{chem} along the ***a-b*** plane, while at the lower temperature threshold, the value of the LNO diffusion coefficient was closer to the value of D_{chem} along the ***c***-axis. In the case of PNO, there is still no determination of what the rate-determining stage of oxygen exchange kinetics is.

Table 2
Oxygen diffusion and surface exchange coefficients for RP nickelates in literature at 700 °C.

RP nickelate	Method used	D^* or D_{chem} (cm^2·s^{-1})	k^* or k_{chem} (cm^2·s^{-1})	Reference
LNO	IEDP-SIMS	4.8×10^{-8}	2.1×10^{-7}	[36]
LNO	IE-GPE	1.1×10^{-8}	1.4×10^{-7}	[131]
LNO	ECR	8.3×10^{-5}	2.6×10^{-5}	[142]
LNO	EIS	–	8.6×10^{-7}	[143]
NNO	IE-GPE	4.5×10^{-8}	–	[144]
NNO	IEDP-SIMS	4.5×10^{-8}	3.4×10^{-7}	[36]
NNO	ECR	–	1.3×10^{-7}	[132]
NNO	ECR	–	1.2×10^{-4}	[145]
NNO	EIS	5.6×10^{-8}	1.8×10^{-7}	[146]
$Nd_{1.95}NiO_{4+\delta}$	IEDP-SIMS	3.5×10^{-8}	9.0×10^{-7}	[36]
PNO	IE-GPE	7.0×10^{-8}	9.5×10^{-5}	[144]
PNO	IEDP-SIMS	7.2×10^{-8}	1.4×10^{-6}	[36]
PNO	ECR	–	4.7×10^{-5}	[84]

2.3. Electrical conductivity

RP nickelates are semiconductive in nature and for this reason, can only induce limited electronic conductivity [148], however, their conductivity still compares favorably to perovskite nickelates at intermediate temperatures [97]. Reference values for electrical conductivities at 650 °C of LNO, NNO and PNO are 90 S·cm^{-1} [149], 105 S·cm^{-1} [150] and 110 S·cm^{-1} [97], respectively. These values increase with a higher pO_2 product of superior oxygen over stoichiometry [23].

High-order nickelates present a metallic behavior on dense samples (>96%) with reported high electronic conductivities in $La_3Ni_2O_{7\pm\delta}$ (260 S·cm^{-1}), $Pr_4Ni_3O_{10\pm\delta}$ (340 S·cm^{-1}), $Nd_4Ni_3O_{10\pm\delta}$ (400 S·cm^{-1}) and $La_4Ni_3O_{10\pm\delta}$ (450 S·cm^{-1}) at 650 °C [23]. On the electrical conductivity of the $Pr_4Ni_3O_{10\pm\delta}$ phase, Tsai et al. [106] noticed that the higher-order oxide showed a high content of Ni^{3+} in an alternated distribution sandwiched in the perovskite layers. A metallic behavior was observed in dense (92%) $Pr_4Ni_3O_{10\pm\delta}$ at high temperatures in air and electrical conductivity of 235 S·cm^{-1} at 700 °C and 250 S·cm^{-1} at 600 °C.

Moham Ram et al. [47] introduced the discussion about the effect of Ni^{3+} concentration, and the proportional increase with ***n*** in $Ln_{n+1}Ni_nO_{3n+1}$, to explain the difference of magnetic and electrical properties as a function of the nickelate order. Yatoo et al. [105] recently commented on this, implying that due to a lower Fermi level, a higher neighboring density of states is produced. This phenomenon is better explained by Zhang and Greenblatt [118], who showed how the interactions between Ni 3d and O 2p orbitals along the c-direction can substantially increase with Ni valence. The electrons in a small energy range near this level contribute to electrical transport. The electrical conductivity thus increases as a result, and the inherent p-type conductivity of RP nickelates changes to n-type conductivity when the Ni valence is 3^+.

2.4. Cr poisoning and CO_2 effects on RP nickelates

In terms of vulnerability to Cr contamination and CO_2 poisoning, NNO shows the best phase stability under SOFC operating conditions [151,152] among the different nickelates. Egger et al. [153] investigated the long-term oxygen exchange kinetics of NNO under H_2O- and CO_2-containing atmospheres at 700 °C. In dry Ar with 1% O_2 content, NNO exhibited excellent stability over 1000 h with minimal changes on introducing an additional 5% CO_2, as the k_{ex} remained in the same range of values in similar a long-term span. Yang et al. [154] later discussed that the Cr-species effect on the k_{ex} of NNO was negligible, attributed to the Sr-free nature. However, Schuler et al. [152] identified that in A-site deficient NNO, Cr-poisoning is not prevented and the electrochemical reduction of Cr^{4+} (g) to Cr^{3+} (s) is more responsible for contributing to faster performance degradation of the oxygen electrode. Schrodl et al. [155] investigated the chromium deposition influence on the operation modes of a PNO air electrode. After Cr-species under humidified conditions are introduced, the cell performance deteriorates, and the polarization resistance contribution of the SOC air electrode increases. PNO air electrodes also displayed a superior resilience against Cr-poisoning than LNO without apparent degradation in SOEC mode.

2.5. Cation substitutions

In the literature, it is also commonly found that A- and B-site cation substitutions influence the electrochemical and thermal stability of RP nickelate air electrodes. Cation solubility in RP nickelates has been

demonstrated with elements like La [156], Pr [157], Nd [158], Sm [39], Ca [159], Sr [160], Eu [161] and Ba [94] (A-site cations), and Cu [157], Co [40], Fe [162], Mo [163] and Mn [164] (B-site cation). This often represents a compromise linking structural and performance optimization, as cation substitutions are known to affect the oxygen stoichiometry while leading to a change in the oxygen transport properties [165]. B-site modifications seem to have more influence on the oxygen ion transport in RP oxides than in the A-site [138]. Alternatively, substitutions with different ionic sizes and valence states than lanthanide elements could alter the electronic structure of the B-site cations in the lattice, in turn modifying SOC performance. Low valence ions in the A-site can cause oxidation of the B-site ion to a smaller radius due to charge compensation [24,70,166].

In a recent review, Tarutin et al. [21] outlined a general trend when increasing the content of alkaline-earth metal cations in the A sublattice of $Ln_{2-x}A_xNiO_{4+\delta}$ (Ln = La, Pr, Nd; A = Ca, Sr, Ba) that is accompanied by a decrease in the oxygen content (δ) and an increase in the electron-hole concentration. Based on this premise, we found several strategies to enhance the performance of the RP nickelate oxygen electrodes in terms of electronic (σ_{el}) and ionic (σ_{ion}) conductivity, phase stability, and thermomechanical expansion within SOC components.

2.5.1. Strategies to improve the electronic conductivity

A decrease in oxygen content with a reduction in pO_2 is accompanied by a decrease in σ_{el} for compositions with a moderate ($x = 0.3$) and large ($x = 1.0$) substitutional level, while solid solutions with low dopant contents demonstrate nearly pO_2-independent oxygen nonstoichiometry ($\delta = 0$) and electronic conductivity at 600–900 °C and pO_2 in the range of 10^{-5} to 1.0 atm [87,150,167]. For example, the σ_{el} of LNO (x = 0–0.15) gradually decreases with an increase in the concentration of A-site cation vacancies [168]. A-site deficiency is charge-compensated by a decrease in δ and hole concentration, resulting in less electronic transport.

A summary of the compiled electronic conductivities of RP nickelates and the aforementioned doping strategies to improve this property is presented in Fig. 1. In mixed lanthanide A-site cations, the σ_{el} is influenced by the properties of the dominant element; i.e., when increasing Pr content in $La_{2-x}Pr_xNiO_{4+\delta}$, the σ_{el} raise until $x = 1.0$ [169], and then weakly in the $1.0<x<2.0$ range. Electronic transport in the $(Pr_{1-x}Nd_x)_2NiO_{4+\delta}$ system declines gradually with an increase in Nd fraction [170]. Samaria-doped LNO ($La_{2-x}Sm_xNiO_{4+\delta}$) increases the conductivities of the parent phase and maintains the over stoichiometry

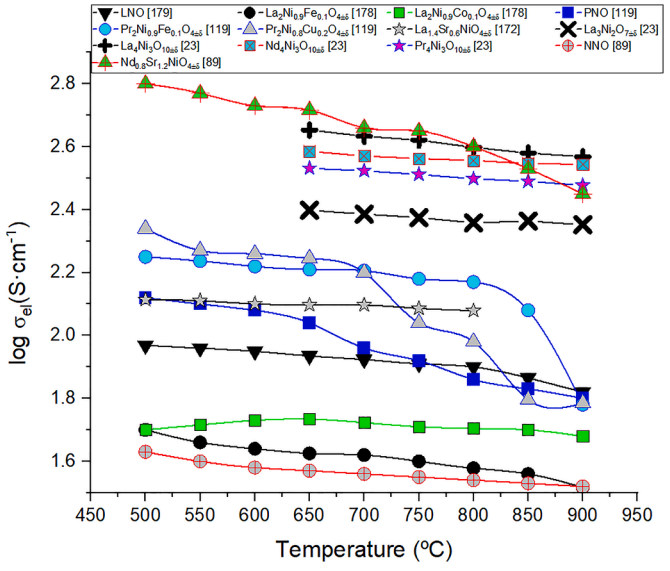

Fig. 1. Electronic conductivity (σ_{el}) of different doped RP nickelates in comparison with parent and high-order nickelate phases.

in the composition, but is not varying systematically as the best performance is obtained in $x = 0.5$ with a $\sigma_{el} = 125$ S·cm^{-1} at 600 °C [39].

Comparing other strategies, Shen et al. [171] reported that the σ_{el} of A-site doped LNO and its electronic transport in $La_{1.7}A_{0.3}NiO_{4+\delta}$ was found to increase in the sequence $A = Sr < Ba < Ca$. Another instance is in the strontium-rich composition $Nd_{0.8}Sr_{1.2}NiO_{4+\delta}$, which presented a maximum electron-hole concentration and σ_{el} in the 500–1000 °C range [89]. The σ_{el} is 510 S·cm^{-1} at 600 °C in air but diminishes over time due to an increase in oxygen vacancy concentration. In reduction conditions ($pO_2 = 10^{-5}$ atm), $LaSrNiO_{4+\delta}$ showed structural changes resulting in localization of electronic charge carriers and a transition to semiconducting behavior at 1000 °C under mildly reducing conditions [172].

Low Ba-doping in $Nd_{2-x}Ba_xNiO_{4+\delta}$ using the nitrate-citrate route showed an increase in the ***c*** lattice parameter and a decrease in the ***a*** and ***b*** parameters [94,173], accompanied by a transition from the orthorhombic to a tetragonal structure at 550 °C. The highest σ_{el} was obtained in $x = 0.2$, with a value of 125 S·cm^{-1} at 500 °C [94].

Zhu et al. [66] studied the effect of strontium- and bismuth-doped LNO ($La_{1.65}Bi_{0.1}Sr_{0.25}NiO_{4+\delta}$), finding that the σ_{el} increases slightly from 99.3 S·cm^{-1} to 100.3 S·cm^{-1} at 550 °C.

The incorporation of metal cations with a stable valency (common examples are Mg^{2+} and Al^{3+}) into the Ni sublattice of the RP nickelates reduces the hole concentration, where less interaction is happening in Ni-O-Ni bonds, lowering the σ_{el} values [174,175]. The only exception found in the literature so far is in the case of $La_2Ni_{0.95}Al_{0.05}O_{4+\delta}$, where the hole mobility was reported to be slightly higher compared to undoped LNO [174].

B-site doped LNO ($La_2Ni_{1-x}Cu_xO_{4+\delta}$) has a metal-insulator behavior as temperature increases in air, with metallic-like properties at high temperatures [176]. Using this reasoning, the decline in electronic transport with Cu doping should be attributed to a decrease in oxygen non-stoichiometry and hole concentration. Also, in Cu-substituted LNO, σ_{el} was improved over LNO at 500 °C (90 S·cm^{-1} vs 75 S·cm^{-1}).

Using different transition metal dopants in the NNO B-site, the σ_{el} at 700 °C in air was reported to be the highest with Ni (44 S·cm^{-1}), and the lowest for Fe and Mn (~33 S·cm^{-1}) [177]. Taking the same approach, in LNO doped B-site, the highest σ_{el} at 700 °C was Ni (87 S·cm^{-1}), while the lowest declined even sharply in the Fe doping (44 S·cm^{-1}) [178]. The σ_{el} data of the doped PNO resulted in a notable increase in the values for $Pr_2Ni_{0.9}Fe_{0.1}O_{4+\delta}$ and $Pr_2Ni_{0.9}Cu_{0.1}O_{4+\delta}$ on cooling in air [119].

2.5.2. Strategies to improve ionic conductivity

A strategy to improve the oxygen ion conductivity is the substitution of A-site cations (typically composed of Ln^{3+}) with cations of lower valence (typically alkaline-earth metal ions, such as Sr^{2+} [160] and Ca^{2+} [159]), which can facilitate the formation of oxygen vacancies to maintain charge neutrality. A-site deficiency provided a lower σ_{ion} of 8.7×10^{-3} S·cm^{-1} at 700 °C [125], but it proved to be enhanced by Sr substitutions as in the case of $La_{1.9}Sr_{0.1}NiO_{4+\delta}$ ($\sigma_{ion} = 0.012$ S·cm^{-1} at 700 °C [179]). A further increase of Sr content diminishes σ_{ion}, i.e., in $La_{1.5}Sr_{0.5}NiO_{4+\delta}$ $\sigma_{ion} = 5.8 \times 10^{-5}$ S·cm^{-1} at 800 °C [180]. Ca-substituted nickelates have performed better, with values as high as 2.7×10^{-3} S·cm^{-1} at 700 °C in $La_{1.7}Ca_{0.3}NiO_{4+\delta}$ [181]. Slight B-site doping with transition metals can significantly increase σ_{ion}, particularly with iron. This is exemplified in $La_2Ni_{0.9}Fe_{0.1}O_{4+\delta}$ (0.228 S·cm^{-1} at 900 °C [178]). Aluminum also provides an improved σ_{ion} in $La_2Ni_{0.95}Al_{0.05}O_{4+\delta}$ (0.085 S·cm^{-1} at 800 °C [174]). A small copper content in the B-site of RP nickelates can also enhance significantly the σ_{ion}, as reported for LNO ($La_2Ni_{0.5}Cu_{0.5}O_{4+\delta}$, $\sigma_{ion} = 7 \times 10^{-3}$ S·cm^{-1} at 700 °C [182]) and PNO ($Pr_{1.9}Ni_{0.75}Cu_{0.25}O_{4+\delta}$, $\sigma_{ion} = 0.040$ S·cm^{-1} at 700 °C [183]). Barium doping is another option, but it induces $BaCO_3$ impurities that decrease ion conductivity [184]. However, in combination with small amounts of F anion substitution, it provides better ionic conductivity. For the composition $Nd_{1.9}Ba_{0.1}NiO_{4+\delta}F_{0.05}$, the calculated σ_{ion} is 0.023 S·cm^{-1} at 700 °C [185]. Another common strategy to increase the σ_{ion} is the B-cation substitution with elements like copper (50

vol.% [186] and 40 vol.% [187]), cobalt ($La_2Ni_{0.8}Co_{0.2}O_{4+\delta}$ (LNCO20) and $Pr_2Ni_{0.8}Co_{0.2}O_{4+\delta}$ (PNCO20) [188]), and mixtures of Cu and Ga with A-cation lanthanide substitutions, $(Pr_{0.9}La_{0.1})_2(Ni_{0.74}Cu_{0.21}Ga_{0.05})O_{4+\delta}$ (PLNCG) [156,189]. The composition PLNCG yields a σ_{ion} of 0.061 $S{\cdot}cm^{-1}$ at 700 ºC [183]. The latter approach was applied in NNO electrodes, including cerium substitution in the A-site cation with a final composition of $Nd_{1.8}Ce_{0.2}Cu_{0.5}Ni_{0.5}O_4$ [190]. In addition, it was previously demonstrated that Ga and Cu substitutions increased the ionic conductivity to the LSGM level (~0.015–0.016 $S{\cdot}cm^{-1}$ at 600 ºC) [35].

2.6.3. Strategies to improve phase stability

A smaller size mismatch between the dopant and host cations can be useful to suppress dopant segregation as the diffusivity of Sr, Ce, and Ca cations, at intermediate-to-low temperatures is normally slower and can also slow down segregation [191]. In the referred work, Lee et al. demonstrated that the La/Ce pair was less likely to show dopant segregation due to a low mismatch between the cations. Also, dopant segregation tends to be less probable in expansion under low pO_2 conditions. Fig. 2 shows the possible energy minimization and size mismatch strategies on A- and B-site cations and the effects of pO_2 that drive dopant segregation to the lanthanide nickelate surface.

When comparing the surface composition of $Pr_{1-x}La_xNiO_{4+\delta}$ (PLNO) and LCSF electrodes using the low-energy ion scattering (LEIS) technique, no segregation of lanthanide cations is observed in PLNO, contrary to Sr segregation at the surface of LSFC [192]. This may be related to the possible weakening of the electrostatic driver that depends on oxygen distribution and cation vacancies and could be related to a dominant chemical expansion. As shown in Section 2.1.1., the TEC of RP nickelates is not very high, so the former hypothesis is more plausible for these particular materials. For example, the A-site substitution with a low Sr valence does not create oxygen vacancies, decreasing the interstitial oxygen concentration and the lattice oxygen activity, but this is usually compensated by increasing the heat treatment temperatures to produce more oxygen vacancies [89]. With adequate B-site cation contributions, their performance can also be more efficient. For instance, the high-order Sr-rich phase $Sr_{2.8}Pr_{0.2}Ni_{0.75}Fe_{1.25}O_{7-\delta}$ showed good electrochemical stability and 100% Faradaic efficiency in the ORR potential range [193]. In two compounds, $Sr_{2.8}Pr_{0.2}Ni_{0.75}Fe_{1.25}O_{5.73}$ (with Fe^{3+}/Ni^{2+}) and $Sr_{2.8}Pr_{0.2}Ni_{0.75}Fe_{1.25}O_{6.73}$ (with Fe^{4+}/Ni^{3+}), the overall efficiency was improved in the latter as it produced more gas per power input. In this case, the higher oxygen stoichiometry contributed to the valence change in the dopants and the better overall performance. Anomalous Sr segregation from perovskite to the interface and the RP phase seems to form during synthesis as observed by direct X-ray methods [194], where no significant changes were found during annealing of $(La_{1-x}Sr_x)_2CoO_{4\pm\delta}$ / LSC layers in O_2.

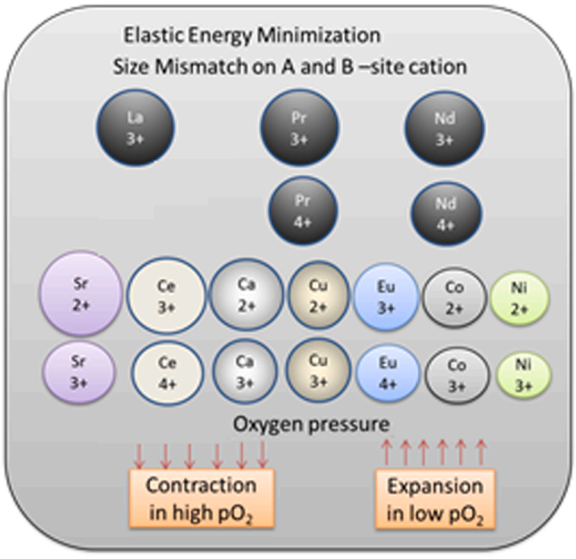

Fig. 2. Illustration of the possible energy minimization and size mismatch strategies on A- and B-site cations and the effects of pO_2 that drive dopant segregation to lanthanide nickelate surface. Adapted from reference [191].

Boehm et al. [37] studied the oxygen transport properties of $La_2Ni_{1-x}Cu_xO_{4+\delta}$, finding good thermal stability of the oxygen over stoichiometry and TEC, with a high σ_{el} = 70 $S{\cdot}cm^{-1}$ at 600 ºC in $La_2Ni_{0.75}Cu_{0.25}O_{4+\delta}$. The substitution of Ni for Cu produces a structural transition of $Ln_2Ni_{1-x}Cu_xO_4$ [60], as well as a decrease in oxygen over-stoichiometry due to the fixed low valence state of Cu and the improved sintering capability of the material [34,37]. However, the k_{ex} and D_{chem} parameters, which are strongly related to the ORR, decreased by Cu substitutions [37]. In this sense, Aguadero et al. [60,73] investigated the ORR activities of the $La_2Ni_{1-x}Cu_xO_{4+\delta}$ ($0 \leq x \leq 1$) series. Two consecutive phase transitions were observed along the series, from orthorhombic (F*mmm*) to tetragonal (F4/*mmm*) at x = 0.2 and single-face centered orthorhombic (B*mab*) for x = 1. The formation of the tetragonal phase is equivalent to $Ln_2CuO_{4-\delta}$ [108]. These phase transformations have been interpreted in terms of strain between the perovskite and the rock-salt layers due to the Cu^{2+} Jahn–Teller effect and variations of the ionic radii of Ni^{2+} vs Cu^{2+}. They also found the best electrochemical performance for the $La_2Ni_{0.6}Cu_{0.4}O_4$ electrode on an LSGM electrolyte. The authors attributed this to the high σ_{el} of $La_2Ni_{0.6}Cu_{0.4}O_4$ and better TEC compatibility between electrode and electrolyte [73]. Yashima et al. [195] further explored the role of Cu^{2+} adding Ga^{3+} in a PNO-based oxide, concluding that the Jahn–Teller effect helped to stabilize the tetragonal structure at high temperature and to improve the mobility of apical oxygens, which is important for bulk oxygen diffusion. The higher symmetry of the tetragonal I4/*mmm* phase is determinant in obtaining lower activation energy for oxygen permeation rate, compared to the lower symmetry of the orthorhombic (B*mab*) PNO.

Other trends are focused on long-term stability studies in multiple cation substitutions, i.e. in $(Nd_{0.9}La_{0.1})_2(Ni_{0.74}Cu_{0.21}Al_{0.05})O_{4+\delta}$ (NLNCA) electrodes with excellent oxygen permeation under CO_2-containing atmospheres for 250 h at 975 ºC [196]. A similar performance is obtained in cells with PLNCG nickelates [156,197]. In addition, Vibhu et al. [188] studied nickelate air electrodes with mixtures of Pr and La, reporting better long-term stability than in non-mixed lanthanide nickelates. Nicollete et al. [198] later identified good chemical stability, up to one month, with more La content in PLNO, independently of the operating temperature. This result improves in terms of stability over pure PNO, which decomposed in air at 600 °C (into Pr_6O_{11} and $PrNiO_{3-\delta}$) and over 700 °C (with additional $Pr_4Ni_3O_{10-\delta}$) [199]. The same approach applies to combining NNO and PNO assets (good stability and electrochemical activity, respectively) as demonstrated by Dogdibegovic et al. [158]. Long-term operation of $(Pr_{1-x}Nd_x)_2NiO_{4+\delta}$ (PNNO) electrodes shows suppressed phase transitions and its decompositions (PrO_x and NiO) with an increase in Nd content. Reaction with the CGO buffer layer was also suppressed with an increase in Nd content. The elimination of phase decompositions helps to obtain thermal expansion compatibility between electrode and electrolyte materials. Tarutin et al. [94] have observed that barium-doped NNO employed in PCFCs, show little interdiffusion of Ba-ions from the electrolyte to electrode during long-term operation. A moderate Ba content is also beneficial in reducing impurities formed at the interface.

Furthermore, the substitution of nickel for cobalt in the B-site cation seems to activate the electrochemical performance of the PNO oxygen electrode/electrolyte interface. Also, the inclusion of Co into LNO contributes to optimizing the oxygen surface exchange process, as proved by the improved k_{ex} and reduced activation energy [200–203]. The activation enthalpy for oxygen migration in $La_2Ni_{1-x}Co_xO_{4+\delta}$ increased with an increasing Co content according to Kilner et al. [201]. In LNO, the activation energy of surface exchange coefficients was around 120 $kJ{\cdot}mol^{-1}$, while, when 50% Ni was replaced by Co, the activation energy

decreased to a value of 20 kJ·mol^{-1} [203]. The impact of Co on bulk diffusion is weak at low doping content (<50%), but a greatly reduced activation energy was observed when the amount of Co was higher. Despite this, the electrochemical performance of Co-doped LNO is seldom reported. This may be related to its poor phase stability at high-temperature, where the $La_3Ni_2O_7$ phase appeared after short-term calcination at elevated temperatures [204].

2.7. Infiltration techniques

The electrochemical performances of the nickelate SOC air electrodes improve substantially when using infiltration techniques (also called impregnation) and co-impregnation [205]. This involves the fabrication of electrodes by the infiltration of a porous ceramic backbone with a solution of cation salts [206,207]. The infiltration objective is to ensure that the porous skeleton is mechanically strong enough to withstand the stresses caused by the volumetric expansion of the phase upon oxidation. Optimization of catalyst loading is greatly influenced by the solution concentration and the microstructure also varies with the amount of solid loading [208]. Normally, an increase in precursor molarity increases the infiltrated particle size. R_{pol} variations can also be influenced the level of solid loading [209].

For lanthanide nickelates, the influence of the infiltration solution concentration on the electrochemical performance is of great importance, as it might change the way the lanthanide particles are formed and crystallize. One general issue is that a highly-concentrated solution does not fully penetrate inside the whole backbone, as the viscosity of the solution typically increases with concentration.

The importance of the temperature at which the nickelate phase is formed in the infiltration was underlined by Railsback et al. [210], who studied on symmetrical cells the effect of a PNO-infiltrated into an LSGM scaffold (14 vol.% solid loading). They discovered that the minimum calcination temperature required to form the nickelate phase is in the range of 950–1000 °C. Nicollet et al. [211] prepared PNO infiltrations on a CGO scaffold noting that PNO crystallization is highly dependent on the annealing atmosphere. The authors emphasized that the formation of a single-phase nickelate using infiltration solutions is more difficult than employing the synthesis of the powder. However, the annealing of PNO at 900 °C under an N_2 atmosphere hastened the formation of this phase and the secondary PrO_x species at 800 ºC. Specifically, the Pr_6O_{11} phase could contribute to improving the cell performance and evidence of this is the low R_{pol} value obtained at 600 °C in air (0.075 Ω·cm^2) in a symmetrical PNO-infiltrated CGO cell [211]. For other nickelates, the optimum temperature of formation in NNO-infiltrated SOC was reported at 900 ºC [18,212], and in lanthanum nickelates infiltrations, the temperatures reported are 900 ºC for LNO (in CGO scaffolds) [198] and 850 ºC for high-order nickelates (in YSZ scaffolds) [213].

Phase reactivity and phase decomposition issues have been successfully avoided by Zhou et al. [214], who infiltrated LNO into a porous (Ba,Sr)(Co,Fe)O_3 (BSCF, barium strontium cobalt ferrite) scaffold followed by microwave plasma treatment. The latter treatment produced a protecting layer of a cone-shaped 3D geometry. The best performance was registered with a 26 wt% LNO solid loading, where they observed the formation of larger cone shapes particles after the microwave plasma treatment (Fig. 3).

To improve ORR activity, Yang et al. [215] prepared a symmetrical LNO electrode infiltrated into LSGM. The nanosized LNO electrode displayed high ORR activity, partially decomposing into La_2O_3 and metallic Ni particles of smaller size, which distributed homogeneously and showed good catalytic activity for fuel oxidation. Furthermore, an LNO-SDC/SDC/LNO-SDC cell was successfully operated for a period of 210 h without apparent degradation at 650 °C. High-order $La_4Ni_3O_{10}$ was also infiltrated into YSZ scaffolds as oxygen electrodes, achieving a better performance than in LNO-infiltrated YSZ [213].

3. Performance of lanthanide nickelates as oxygen electrodes

3.1. RP oxygen electrodes performance

One of the main issues in the performance of SOC with nickelates as oxygen electrodes is obtaining good phase stability during cell sintering and operation. Neodymium addition can stabilize (and even suppress) phase decompositions due to their higher nuclear charge in comparison with La and Pr atoms, decreasing the overlapping of the f-electrons with the surrounding atoms, as explained by Petit et al. [216]. Contrary to Nd atoms, Pr is more prone to tetravalence. The existence of trivalent A-site cation in the lanthanide is pivotal to tailoring the nickelate conductivity and obtaining a suitable electrochemical performance for any kind of

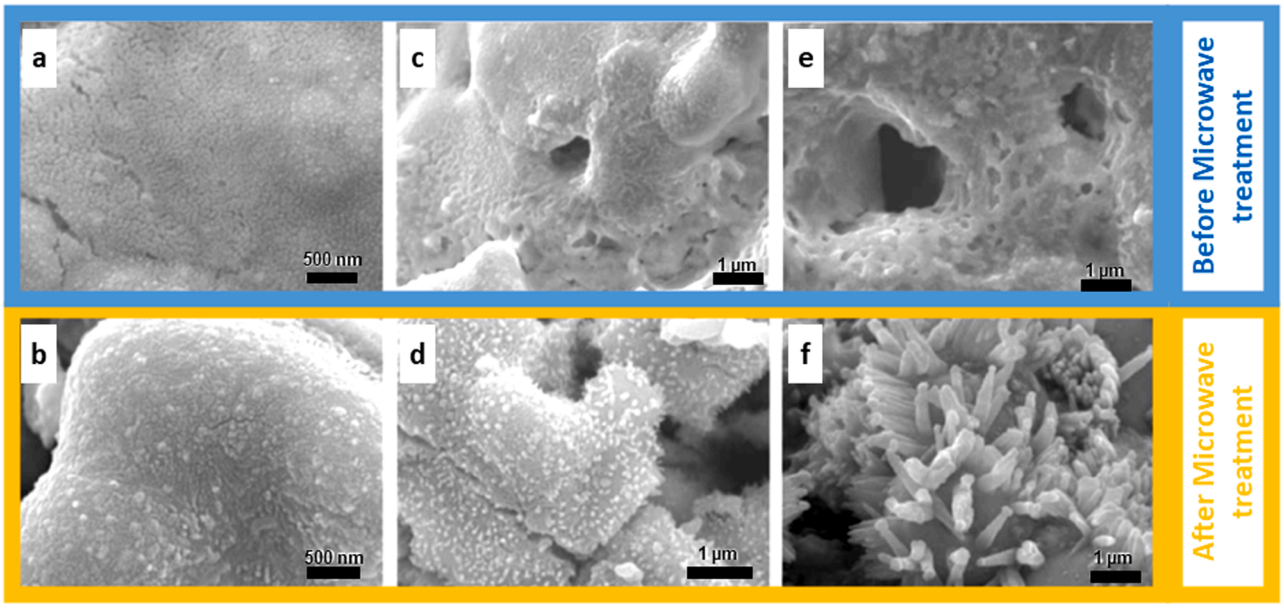

Fig. 3. Scanning Electron Microscopy (SEM) micrograph showing the LNO-infiltrated BSCF electrode with dense cone-like structure using different solid loadings: 6 wt% (a and b), 12 wt% (c and d), and 26 wt% (e and f). The images a), c) and e) are obtained before the microwave plasma treatment, while b), d) and f) after the treatment [214].

SOC operation. To compare the electrochemical performance of the different LNO, NNO, and PNO pure electrodes, Tables 3-5 present detailed electrochemical performance results for symmetrical, single, and reversible SOC, respectively, including RP-oxygen electrodes with different electrolyte materials for both solid oxide and proton conducting cells.

3.1.1. LNO electrochemical performance

The electrochemical performance of LNO as an oxygen electrode for SOCs was studied in detail by many authors. For example, Montenegro-Hernandez et al. [217] studied the performance of LNO symmetrical cells using CGO and YSZ electrolytes, which were deposited by aerography and treated at 900 °C for 1 hour to promote electrode adhesion. They found the lowest polarization resistance for the LNO/YSZ cell at 800 ºC (R_{pol} = 5.6 Ω·cm^2). Their Transmission electron microscopy (TEM) study suggested that $La_2Zr_2O_7$ could be present at the LNO/YSZ interface, concluding that the formation of this compound due to the chemical reaction between LNO and YSZ is the cause of a continuous increment with the time of ASR values. In addition, they observed that ASR values for LNO / CGO cells are much higher than those determined for the LNO / YSZ cell, suggesting that the reactivity between LNO- CGO is higher than that of LNO–YSZ.

In terms of single cells, Zhao et al. [218] studied LNO electrodes by screen-printing using SDC as electrolyte and Ni-SDC as anode supports. Their single cells presented a maximum power density (MPD) of about 0.30 W cm^{-2} at 800 °C, which was further increased to 0.46 W cm^{-2}

Table 3
Electrochemical performance of symmetrical cells of RP-oxygen electrodes with different electrolyte materials. * Indicates PCFC.

Configuration	R_{pol} (Ω·cm^2)	Temperature (°C)	Comments	Reference
8YSZ/CGO/PNO	0.03	700	Delamination occurred at the interface between PNO and CGO layers	[97,224]
SDC/$Nd_{1.5}Pr_{0.5}Ni_{0.9}Cu_{0.1}O_{4+\delta}$	0.03	800	Electrolyte-supported cell, 330 μm thick. Identical performance to PNNO electrode, but better than with Mo and Co-doped electrodes at the same temperature	[95]
CGO/$Nd_{0.8}Sr_{1.2}Ni_{0.8}M_{0.2}O_{4+\delta}$ (M = Ni, Co, Fe)	0.04	800	Pechini method modification with PrO_x. M=Ni+23 wt% PrO_x. Oxygen-deficient in air above 700 °C. Incorporation of Co or Fe into Ni sublattice reduces δ and electrical conductivity	[262]
8YSZ/CGO/PNO	0.04	800	Commercial 8YSZ pellets. CGO and PNO layers are coated by scree-printing (SP). CGO interlayer sintered at 1350 °C	[274]
8YSZ/CGO/$Pr_4Ni_3O_{10-\delta}$	0.05	700	Co-sintering of CGO/electrode layers. $Pr_4Ni_3O_{10+\delta}$ phase synthesized by glycine nitrate. R_{pol} starts at 0.03 Ω·cm^2 and the value reported is after 678 h in SOFC mode.	[97]
CGO/$La_{0.99}Co_{0.4}Ni_{0.6}O_{3-\delta}$(LCO)-CGO/LCO	0.05	750	LCO-infiltrated LCO—CGO	[269]
SSZ/NNO-SSZ	0.06	750	Prepared by tape casting. co-firing and impregnation	[85]
CGO/$La_4Ni_3O_{10\pm\delta}$	0.05	800	3D-type microstructure with $La_4Ni_3O_{10\pm\delta}$ deposited on a CGO substrate by ESD and nickelate current collector by screen-printing (SP) on a CGO electrolyte	[101]
SSZ/$LaNi_{0.6}Fe_{0.4}O_3$–CGO20	0.05	800	Impregnated functional layer. CGO20-impregnated into LNF backbone enhanced TPBs	[232]
LSGM/$La_4Ni_{2.6}Co_{0.4}O_{10\pm\delta}$	0.06	800	Synthesized by Pechini (ethylene glycol and citric acid). Annealing at 1050 °C, over 6 days	[40]
SSZ/NNO-SSZ	0.07	750	NNO-impregnated SSZ. Under SOEC (1.3 V), current densities are −1081 and −677 mA·cm^{-2} for 800 and 750 ºC, respectively	[275]
8YSZ/CGO/$PrNiO_{3-\delta}$	0.07	750	Co-sintering of CGO/electrode. Powders prepared by a modified Pechini method	[97]
3YSZ/PNO	0.08	600	N_2 annealing of PNO-infiltrated into CGO at 900 ºC. Pr_6O_{11} subproduct contributed to the low R_{pol} value. Electrode deposition by SP on 3YSZ	[211]
PNO/CGO/YSZ	0.08	600	Stacking of two layers: a 3D tree-like microstructure (20 μm thick) over a thin dense layer (100 nm) fabricated by ESD topped by a screen-printed (SP) current collecting of the same composition	[221]
YSZ/LP5NO	0.09	700	Chemically stable long-term in SOEC, large degradation in SOFC	[224]
PNO/LSGM	0.11	650	PNO wet-infiltrated into porous LSGM to form oxygen electrodes	[210]
CGO/PNO	0.11	700	Electrolyte pellet support. Synthesis by nitrate-citrate	[33]
YSZ/PNO	0.14	800	Commercial 8YSZ pellets. CGO and PNO layers are coated by scree-printing (SP). At 600 ºC, PNO, NNO, and LNO R_{pol} are 1.77, 4.47, and 15.30 Ω·cm^2, respectively	[274]
YSZ/LNO - CGO/LNF64	0.15	600	SP cathode + commercial electrolyte support + Current collector. Porous CGO + Nitrate infiltration + calcination	[198]
CGO/PNO	0.15	600	Synthesized by glycine nitrate, co-sintered half cells	[100]
LSGM/$La_4Ni_3O_{9.78}$	0.16	800	Synthesized by Pechini (ethylene glycol and citric acid). Annealing at 1050 °C. over 6 days	[40]
CGO/$Pr_4Ni_3O_{10\pm\delta}$	0.16	600	Synthesized by glycine nitrate. Sintering at 950 °C for 2 h is stable under oxygen at 1000 °C. Further increase decomposes into PNO and NiO under both air and oxygen. Lower R_{pol} than samples sintered at 1050, 1150, and 1200 ºC	[59]
LNF64-SDC+Ag	0.18	700	Ag-infiltrated LNF64-SDC	[276]
0.89ZrO_2–0.10Sc_2O_3–0.01Al_2O_3/LNF-CPGO/LNF	0.24	800	CPGO contribution diminished R_{pol}	[239]
$PrFe_{1-x}Ni_xO_{3-\delta}$	0.32	800	Comparable to LSCF, higher than LNF64 electrodes (0.14 Ω·cm^2)	[277]
CGO/$Pr_{2-x}Sr_xNiO_{4+\delta}$ (x = 0.7)	0.39	700	Synthesized by microwave combustion. Electrodes by spin coating	[160]
SDC/$Pr_{1.7}Ca_{0.3}NiO_{4+\delta}$/LNF64	0.40	700	Co-precipitated electrode layers	[159]
SDC/LNO(+ PNO additive)	0.44	650	Synthesized by the citrate-nitrate method. The stoichiometric ratio of Pr: Ni as 2:1. Non-ohmic polarization is almost doubled using LNO additive at this temperature	[278]
CGO/$Nd_{1.8}Ce_{0.2}Cu_{1-x}Ni_xO_{4+\delta}$	0.44	700	Symmetrical cathodes deposited by spin coating	[190]
CGO/NNO	0.50	700	Cathode deposited by spray pyrolysis	[223]
50 w t% LNO + 50 wt% $La_4Ni_3O_{10}$	0.53	700	Functionally-graded porous LNO+$La_4Ni_3O_{10}$ and porous $La_4Ni_3O_{10}$ as a current collector	[279]
PNO/$BaCe_{0.9}Y_{0.1}O_{3-\delta}$(BCY)	0.58	600	Prepared using proton-conducting BCY from two perovskite compounds. BSCF and LSFC, and PNO. R_{pol} was comparable to double perovskite $PrBaCo_2O_{5+\delta}$	[280]*
LNO/CPO/TZ3Y	0.64	600	Use of CPO layer enhances performance in place of CGO buffer layer	[231]
CGO/70 wt% LNF – 30 wt% CGO	0.73	800	LNF's high Ni fraction on B-site with an average B–O bonding energy ~170 kJ mol^{-1}. The low energy could not tolerate the A-site deficiency and Ni is expelled to form NiO	[281]
LNO/YSZ	0.75	800	LNO is synthesized by HMTA (hexamethylenetetramine). Lower R_{pol} than with CGO	[217]
SASZ/LNF64	0.77	800	SP LNF64 on SASZ. After 114 h of current loading (255 mA·cm^{-2}), R_{pol} decreased	[282]
$Nd_{1.6}Sr_{0.4}NiO_4$	0.93	700	Impregnated nano-sized NNO accelerates oxygen dissociation and diffusion processes	[88]
SDC20/$La_{1.8}Eu_{0.2}NiO_{4+\delta}$	1.30	700	Eu- doping enhances the structural and electrical properties. Deposited by spin coating	[161]

Table 4
Power output electrochemical performance of RP-oxygen electrodes in different single-cell configurations. * Indicates PCFC.

Configuration	R_{pol} ($\Omega \cdot cm^2$)	MPD (mW. cm^{-2})	Voltage at MPD (V)	Temperature (°C)	Comment	Reference
Ni-YSZ/YSZ/CGO/$Pr_4Ni_3O_{10\pm\delta}$	0.01	1600	0.50	800	Anode-supported (Ni-YSZ//YSZ) cell. $Pr_4Ni_3O_{10\pm\delta}$ synthesized by glycine nitrate method. Co-sintered CGO/ $Pr_4Ni_3O_{10\pm\delta}$ layers	[59]
Ni-SASZ/SASZ/LNF64	0.10	1560	0.60	800	Loading of 3000 mA·cm^{-2} for several days to activate LNF64. Power output was 5–10 times higher after activation. The best performance is in the sample sintered at 1000 ºC. Initially, R_{pol}=0.10 $\Omega \cdot cm^2$ and after loading the low-frequency resistance is 0.7 $\Omega \cdot cm^2$	[266]
Ni-YSZ (support)/Ni-SSZ/SSZCGO/ LCNO—CGO/LCO	0.05	1300	0.60	750	LCO-infiltrated LCO—CGO. Substantially lower R_{pol} than LSM-YSZ. Slightly lower MPD than LCO—CGO at 750 ºC	[269]
NiO-YSZ/SSZ/NNO-SSZ	0.04	1260	0.50	800	Anode support. Impregnation improves performance. R_{pol} of 0.06, 0.09 and 0.17 $\Omega \cdot cm^2$ at 750, 700 and 650 ºC, respectively	[85]
Ni–YSZ/YSZ/CGO/LNO	0.40	1250	0.50	800	Anode-supported cells, with aerosol-deposited CGO thin layer as interlayer between the electrolyte and cathode	[219]
Ni-YSZ/YSZ/$La_4Ni_3O_{10}$	0.15	1162	0.55	800	Powders are synthesized via a sol-gel route. R_{pol} is lower than on LSGM electrolyte at 800 °C	[149]
Ni-YSZ/YSZ/$La_3Ni_2O_7$	0.20	1138	0.50	800	Powders are synthesized via a sol-gel route. Stable under a constant current of 600 mA·cm^{-2} for over 30 h at 750 °C	[43]
NiYSZ/YSZ/NNO/$La_{0.6}Sr_{0.4}CoO_3$ (LSC)	0.18	1100	0.65	800	Tape-casted planar Ni–YSZ anode support. The best performance was obtained at a sintering temperature of 1100 ºC	[55]
NiO-SDC/SDC/ $PrNi_{0.6}Co_{0.4}O_3$ (PNC)–SDC50	0.03	1090	0.45	700	Anode-supported single cell. Cathode powders are prepared by glycine–nitrate process. wt ratio of PNC: SDC (50:50) yields the lowest ASR and double MPD than the sole PNC electrode	[270]
NiO-$Ba(Zr_{0.1}Ce_{0.7}Y_{0.1}Yb_{0.1})O_{3-\delta}$ (BZCYYb)/AFL/BZCYYb/ $Pr_2BaNiMnO_{7-\delta}$	0.08	1070	0.50	700	Proton conducting electrolyte in the anode-supported cell. No degradation at 0.70 V for 100 h at 600 ºC. At 500 and 400 °C, MPD reaches 259 and 135 mW·cm^{-2}, respectively. High amount of Ni^{3+} (78 wt%) and Mn^{3+} (81 wt%) determined was by XPS	[164]*
Ni-YSZ/SDC/LNO/BSCF	0.13	1000	0.50	700	Shell-covered porous oxygen electrode infiltration followed by microwave plasma treatment	[214]
Ni-BCZY/BCZY/31 wt% LNO - 69 wt % LNF	0.03	969	0.50	700	LNF-infiltrated LNO. The powders were synthesized by citric acid-nitrate combustion. Fabricated by co-pressing and SP. MPD = 369 mW·cm^{-2} and R_{pol} = 0.31 $\Omega \cdot cm^2$ at 600 ºC	[283]*
NiO-YSZ/YSZ/$La_4Ni_3O_{10}$-YSZ	0.25	889	0.70	750	Anode-supported cell. Nickelate infiltration into YSZ is improved using $La_4Ni_3O_{10}$ over $La_3Ni_2O_7$ (754 mW·cm^{-2}) and LNO (717 mW·cm^{-2}) at an external loading of 0.70 V	[213]
Ni-YSZ/YSZ/ $Pr_{1.8}La_{0.2}Ni_{0.74}Cu_{0.21}Ga_{0.05}O_{4+\delta}$ (PLNCG)	0.41	876	0.55	750	Sol-gel route based on citric acid and EDTA as complexing and gelation agents. Anode precursor hollow fibers fabricated using wet spinning/phase inversion. Stable under CO_2 concentrations variations from 0 to 10 vol.% at 700 and 750 ºC	[156]
Ni-YSZ/AFL/YSZ/LNO-EBO	0.35	850	0.40	750	$Er_{0.4}Bi_{1.6}O_{3-\delta}$ (EBO) promotes the operational stability of LNO at 750 °C within a testing period of 200 h. Cathodic polarization has a critical effect on accelerating the La surface segregation and migration to the YSZ surfaces	[263]
NiO-BZCY/AFL/BZCY/LSNF ($La_{1.2}Sr_{0.8}Ni_{0.6}Fe_{0.4}O_{4+\delta}$)	0.08	781	0.55	700	Proton conducting electrolyte in anode-support. MPD of 138.5 mW·cm^{-2} at 500 ºC. Excellent stability for 100 h at 600 ºC	[284]*
NiO-BZCY/BZCY/PLNCN-BZCY	0.13	770	0.42	700	43.6 wt% $(Pr_{0.9}La_{0.1})_2(Ni_{0.74}Cu_{0.21}Nb_{0.05})O_{4+\delta}$ (PLNCN)-infiltrated $BaZr_{0.1}Ce_{0.7}Y_{0.2}O_{3-\delta}$ (BZCY). Fabricated by co-pressing and SP. MPD = 420 mW·cm^{-2} at 600 ºC. Stable for 200 h at 600 ºC	[157]*
NiYSZ/SDC20+NiO/PNO/ $La_{0.79}Sr_{0.20}CoO_3$	0.05	700	0.80	750	Anode-supported button cells/electrolyte bilayers. Ni-mesh anode current collector. Degradation rate at 0.80 V = 3% per 1000 h up to 2000 h. Best performance with PNO thickness of 24 μm	[29]
NiYSZ/YSZ/CGO/$Pr_4Ni_3O_{10\pm\delta}$/LNF	0.03	680	0.40	700	Anode-supported cell, LNF current collector. $Pr_4Ni_3O_{10\pm\delta}$ is synthesized by glycine nitrate. Delamination between CGO/PNO after loading of 300 mA·cm^{-2} for 500 h at 0.76 V	[97]
NiYSZ/YSZ/CGO/PNO/LNF	~0.33	680	0.70	790	Similar performance after 500 h operation. The use of the LNF current collector provided better performance than LSC and Au	[226]
NiO-Fe_2O_3/LSGM/ $PrSr_3Fe_{2.9}Ni_{0.1}O_{10-\delta}$	0.26	679	0.50	800	Pelletizing electrolytes under isostatic pressure. Ni =10 mol% doping, decreases TEC. η= 0.13 V @ 1250 mA.cm^{-2}	[162]
Ni-BZCY/$BaZr_{0.1}Ce_{0.7}Y_{0.2}O_3$/LNF64	0.05	668	0.50	700	Synthesized via citrate–nitrate combustion. The dry-pressing method is employed for anode support. MPS of 431 mW·cm^{-2} at 650 °C, 232 mW·cm^{-2} at 600 °C and 109 mW·cm^{-2} at 550 °C	[28]*
Sr_2MgMoO_6 (SMMO)/LDC (buffer layer)/LSGM/$LaNi_{0.75}Mo_{0.25}O_3$ (LNMO)		660	0.55	850	Electrolyte-supported SOC. LNMO was obtained by the citrate technique. LNMO deposited by SP. Segregation of La_2MoO_6 from LNMO introduces La vacancies giving mixed Ni^{2+}/Ni^{3+} content. No impedance data is given	[163]
Ni-CGO/YSZ/NNO—CGO/LSC	0.30	620	0.70	800	NNO—CGO composites sintered on CGO and YSZ at 1000 ºC. LSC is used as a current collector. 70NNO-30CGO composite cathode exhibited the best results. NNO-YSZ composites formed insulating zirconate phases	[285]
Ni-BCZY/BCZY/70 wt% LNO- 30 wt % LNF	0.09	590	0.50	700	Fabricated by co-pressing and painting. MPD = 288 mW·cm^{-2} at 600 ºC. R_{pol} = 0.49 $\Omega \cdot cm^2$ at 600 ºC. Stable for more than 70 h at 700 ºC in SOFC mode.	[286]*
NiO—CGO/CGO/PNO–CPO	0.09	570	0.40	800		[235]

(*continued on next page*)

Table 4 (*continued*)

Configuration	R_{pol} ($\Omega \cdot cm^2$)	MPD (mW. cm^{-2})	Voltage at MPD (V)	Temperature (°C)	Comment	Reference
					PNO—CPO composite synthesized by solid-state mixing and modified sol-gel. Calcined at 900 ºC	
Ni-BCZY15/BCZY15/PNO	0.28	560	0.50	600	A microwave heat-treatment method was used to increase the interfacial adhesion between the $BaZr_{0.3}Ce_{0.55}Y_{0.15}O_{3-\delta}$ electrolyte and the PNO cathode. Fabricated by co-pressing and SP. $R_{pol} = 0.24$ Ω·cm2 at 500 ºC.	[287]*
LNO-SDC/SDC/LNO-SDC	0.04	550	~0.50	800	Electrolyte-supported symmetrical SOC. LNO-infiltrated SDC. Synthesized via EDTA−citrate sol−gel. LNO synthesis via GNP. Operated for 210 h no sign of degradation at 650 °C. Better performance than LNO-LSGM/LSGM/LNO-LSGM (520 $mW \cdot cm^{-2}$).	[215]
Ni-3YSZ/Ni-8YSZ/8YSZ/CGO/ LPNO double layer	~0.20	500	0.49	750	Stacking of two layers (3D tree microstructure of 20 mm thick) over a thin dense layer (100 nm) fabricated by ESD and topped by SP current collector. Degradation of 20% for 408 h at 700 ºC.	[221]
Ni-SDC/SDC/SDC (functional layer)/PNO		487	0.45	800	Anode-supported cell. PNO is prepared by GNP and chemical solution deposition. 5 SDC layers are fabricated by co-pressing and spin coating. Infiltration solution filled the pores in electrolyte avoiding delamination. No EIS data is given.	[227]
Ni-SDC/YSZ+SDC20/LNO/Au	0.23	464	0.42	800	Anode-supported cell. Synthesized using a polyaminocarboxylate complex. Electrodes deposited by SP. Au layer current collector.	[218]
Ni-BCZY/BCZY/LNO	0.17	461	0.50	700	The powders were synthesized by citric acid-nitrate combustion. Fabricated by co-pressing and SP. MPD = 210 $mW \cdot cm^{-2}$ and R_{pol} = 0.88 $\Omega \cdot cm^2$ at 600 ºC.	[283]*
NiO-SDC/SDC/PNNO ($Nd_{1.5}Pr_{0.5}NiO_{4+\delta}$)	0.03	456	0.45	800	Electrolyte-supported cell; NiO-SDC (65:35 wt ratio). Similar performance with Cu-substitution (443 $mW \cdot cm^{-2}$) and slightly higher than with Mo (386 $mW \cdot cm^{-2}$) and Co (353 $mW \cdot cm^{-2}$).	[95]
NiO−Fe_2O_3 /LSGM/PNCG/Au	~0.26	450	0.45	800	Single-cell with 3 mol% Au dispersed on air electrode. PNCG and NiO−Fe_2O_3 slurries were deposited by SP.	[288]
Ni-CGO/CGO/PLNCG	0.04	407	0.40	800	Electrolyte supported cell. SP PLNCG on CGO electrolyte. TEC is compatible with CGO. Electrode R_{pol} at 600 ºC is 0.25 $\Omega \cdot cm^2$.	[189]
Ni-8YSZ/YSZ/CGO20-Co/PNO	0.40	400	0.50	600	Anode-supported cell. Under O_2, PNO decomposes into $Pr_4Ni_3O_9$ and $PrO_{1.71}$. The addition of Co improves performance over CGO and yttria-doped ceria (YDC) buffer layers and LSCF composites.	[254]
Ce-Pd-YSZ/YSZ/$La_4Ni_3O_{10-\delta}$ -YSZ	0.13	385	0.57	700	The electrolyte-supported cell is made by tape casting. $La_4Ni_3O_{10-\delta}$-infiltrated YSZ. Better performance without Sr in A-site as R_{pol} increases due to Sr segregation (0.195, 0.274 $\Omega \cdot cm^2$ for 0.4 and 0.8 Sr content, respectively).	[228]
PNO-0.40SDC/SDC/PNO-0.40SDC	0.07	375	0.40	800	In-situ exsolution of Ni nanoparticles is embedded on the surface of the PNO scaffold. Operated at a current density of 356 $mA \cdot cm^{-2}$ at 750 ºC for 168 h. Stability under H_2/air cycling.	[246]
Ni-SDC/SDC/LSGM/LNO	0.31	322	0.50	850	Similar performance with and without SDC functional layer.	[220]
Ni-SDC/SDC/$Pr_2Ni_{0.6}Cu_{0.4}O_4$	0.07	308	0.45	800	PNC is prepared by glycine nitrate using Pr_6O_{11}, NiO, CuO powders, HNO_3, and $C_2H_5NO_2$ as raw materials. Commercial NiO and SDC are prepared by gel-casting for anode substrates.	[187]

when the current collection was improved using a gold layer on the surface. In addition, Lee and Kim [219] also studied the performance of LNO single cells, where in this case the electrode material was synthesized with a modified EDTA process using citric acid. LNO oxygen electrodes were sintered at 1100 °C, and they obtained fuel cell performances of 1.25 W cm^{-2} at 800 ºC.

LNO electrodes show a better compatibility with LSGM, as demonstrated in Ni-SDC / LSGM / LNO single cells [220], where no apparent degradation was observed at 800 °C for 144 h under a polarization current density of 0.45 $A \cdot cm^{-2}$ (MPD measured at 0.16 $W \cdot cm^{-2}$ and 0.32 $W \cdot cm^{-2}$ at 750 ºC and 850 ºC, respectively) [53,220]. Improved interfaces between LNO or PNO and CGO were also achieved using sequentially electrostatic spray deposition (ESD) and screen-printing (SP) techniques [221]. For example, a reduction in R_{pol} from 3.33 to 0.42 $\Omega \cdot cm^2$ and from 0.83 to 0.08 $\Omega \cdot cm^2$ was obtained at 600 °C for LNO and PNO, respectively. Another interesting result is the one reported by Zhou et al. [214], obtaining an ASR of 0.13 $\Omega \cdot cm^2$ at 575 °C in an LNO-infiltrated BSCF oxygen electrode.

3.1.2. NNO electrochemical performance

Montenegro-Hernandez et al. [217] also studied the performance of NNO symmetrical cells using CGO and YSZ electrolytes. In this case, the ASR values obtained for the two cells present a slight increase with time (about 10%). They concluded that the reactivity of NNO samples should be much lower than in LNO samples. This was an expected effect because the chemical reactivity of NNO/YSZ and NNO/CGO is much lower than that of LNO/YSZ and LNO/CGO. In addition, A-site deficient NNO cathode-supported microtubular cells were proposed for SOC applications [212]. They obtained modest power densities at 750 ºC, about 0.04 Wcm^{-2} at 0.5 V, showing the first electrochemical measurements reported using NNO cathode-supported microtubular cells. In any case, further developments in the fabrication process are needed for this type of cell to compete with the standard microtubular SOC cells.

In addition, high performances were also obtained on microtubular cells using air electrodes of porous YSZ supports infiltrated with NNO salt precursors [18]. In SOFC mode, an MPD = 0.40 $W \cdot cm^{-2}$ at temperatures as low as 600 °C was achieved, while no degradation was observed for up to 24 h under the current load. The performance was even more promising in SOEC mode, where a configuration of Ni-YSZ/8YSZ/NNO-infiltrated YSZ (65 wt% NiO in fuel electrode) yielded a current density of −1.38 $A \cdot cm^{-2}$ at 1.5 V and 800 °C (H_2O: H_2 ratio of 1:1) using calcined YSZ, twice the value without calcined YSZ [222]. The R_{pol} at OCV was ~0.20 $\Omega \cdot cm^2$.

Finally, Mesguich et al. [223] studied the influence of crystallinity and particle size on the electrochemical properties of spray pyrolyzed NNO powders, obtaining by EIS R_{pol} values below 0.5 Ω cm^2 at 700 °C. Furthermore, they concluded that electrochemical performances could be still enhanced after the optimization of the processing parameters,

Table 5
SOEC and Reversible-SOC electrochemical performance of RP-oxygen electrodes in different SOC configurations. * Indicates PCFC.

Configuration	SOFC performance in MPD ($mW \cdot cm^{-2}$)	Voltage at MPD (V)	SOFC Temperature (°C)	SOEC performance in j ($mA \cdot cm^{-2}$)	Voltage at j (V)	SOEC Temperature (°C)	Comment	Ref.
Ni-BCZYYC/BCZYYC/ $La_{1.2}Sr_{0.8}NiO_{4+\delta}$ -BCZYYC	1220	0.60	700	3020	1.30	700	Infiltration solution solid loading of 42.2 wt% of $La_{1.2}Sr_{0.8}NiO_{4+\delta}$ into BCZYYC. Reversible SOC operational mode using moist hydrogen (3% H_2O) as fuel and moist air (20% H_2O) as oxidant. SOEC OCV = 0.99 V. MPD = 548 $mW \cdot cm^{-2}$ at 600 °C. R_{pol} = 0.36 $\Omega \cdot cm^2$ at 600 °C.	[252] *
SDC-infiltrated Ni-YSZ/ Nd_2O_3—NNO-SSZ				2050	1.30	800	Nd_2O_3—NNO-SSZ electrode in a metal-supported (430 L) cell with an SDC-infiltrated Ni-YSZ fuel electrode and a scandia-stabilized zirconia (SSZ) electrolyte. 50% H_2 and 50% H_2O feed gas mixture. Showed stability for over 350 h (-0.17 $A \cdot cm^{-2}$) at 600 °C with 30% steam content.	[251]
Ni-BCZYYC/BCZYYC/ $La_{1.2}Sr_{0.8}NiO_{4+\delta}$	850	0.50	700	1960	1.30	700	BCZYY and BCZYYC2 electrolyte, as well as $La_{1.2}Sr_{0.8}NiO_{4+\delta}$ (LSN) oxygen electrode powders, were synthesized by a modified Pechini method. Incorporation of Cu^{2+} into $BaCe_{0.7}Zr_{0.1}Y_{0.1}Yb_{0.1}O_{3-\delta}$ boosted its sintering. Reversible-SOC was carried out in moist air (20% H_2O) and moist hydrogen (3% H_2O) at 700 °C for 100 h, respectively. SOEC OCV = 1.01 V. Performance is portrayed at 60 h.	[289] *
Ni-8YSZ/8YSZ/PNCO20/ LNF	1200	0.60	800	1900	1.50	800	SP cathode + commercial electrolyte support. PNCO shows a lower degradation rate than LNCO20 (98 and 238 $mV \cdot kh^{-1}$). 250 h under SOEC (-1000 $mA \cdot cm^{-2}$). 50% H_2 and 50% H_2O feed gas mixture.	[188, 290]
Ni-BCZYYb/BCZYYb/ $Nd_{1.9}Ba_{0.1}NiO_{4+\delta}$ /LNF (current collector)				1800	1.30	750	Nickelates were synthesized via the solid-state synthesis method. The electrode slurries were sprayed on opposite sides of the electrolyte discs. 50 vol% H_2O used in SOEC. SOEC OCV = 0.9 V.	[185] *
Ni-BCZYYb/BCZYYb/ PNO				1643	1.30	700	$La_2Ce_2O_7$ and $BaZr_{0.1}Ce_{0.7}Y_{0.1}Yb_{0.1}O_{3-\delta}$ electrolyte powders were synthesized by the EDTA-citric sol−gel method. SOEC performance with BCZYYb is better than with the LCO electrolyte. SOEC OCV = 0.95 V. PNO coated by SP.	[291] *
Ni-YSZ/YSZ/ $La_{0.8}Sr_{0.2}Co_{0.8}Ni_{0.2}O_{3-\delta}$ -CGO	1336	0.40	800	1600	1.30	800	Fuel electrode substrate fabricated by tape casting. SP deposition of YSZ and AFL (functional layer) on support. R_{pol} doubles after 20 h in SOEC (750 °C). Initial low R_{pol} = 0.10 $\Omega \cdot cm^2$ value at OCV. In SOEC, j reaches -1.00 $A \cdot cm^{-2}$ (750 °C) at 1.3 V, with 90 vol.% absolute humidity (AH).	[250]
Ni-YSZ/8YSZ/NNO-YSZ	760	0.80	800	1380	1.50	800	The configuration Ni-YSZ/8YSZ/NNO-infiltrated YSZ (65 wt% NiO in fuel electrode) was tested in an H_2O: H_2 ratio of 1:1. It was fabricated using calcined YSZ, and its performance is twice the value than without calcined YSZ.	[18, 222]
Ni-BCZY/BCZY/ $La_{1.2}Sr_{0.8}NiO_{4+\delta}$/BCZY	460	0.50	700	1410	1.30	700	Powders for the supports prepared by solid-state reaction. A 30 wt% of carbon microspheres were used to control porosity in the H_2 electrode. 20 vol.% H_2O on SOEC. SOEC OCV = 0.98 V.	[292] *
Ni-BZCY7/AFL/BZCY/ $La_{1.2}Sr_{0.8}NiO_{4+\delta}$/BZCY	460	0.50	700	1370	1.30	700	Synthesized by the modified Pechini method. Dry-pressed and SP air electrodes. 20 vol.% H_2O on SOEC.	[293] *
Ni-BZCY7/AFL/BZCY/ $Pr_{1.2}Sr_{0.8}NiO_{4+\delta}$/BZCY	350	0.50	700	1120	1.30	700	Synthesized by the modified Pechini method. Dry-pressed and SP air	[293] *

(*continued on next page*)

Table 5 (*continued*)

Configuration	SOFC performance in MPD ($mW{\cdot}cm^{-2}$)	Voltage at MPD (V)	SOFC Temperature (°C)	SOEC performance in j ($mA{\cdot}cm^{-2}$)	Voltage at j (V)	SOEC Temperature (°C)	Comment	Ref.
							electrodes. 20 vol.% H_2O on SOEC. Over 40 h stability. SOEC OCV = 0.97 V.	
Ni-YSZ/SSZ/NNO-SSZ				1080	1.30	800	NNO-impregnated SSZ. Under SOEC (1.3 V), current densities are −1081, −677 and −441 $mA{\cdot}cm^{-2}$ for 800, 750 ºC, and 700 ºC respectively. 50% H_2 and 50% H_2O feed gas mixture. Slight degradation after 23 h under −0.37 $A{\cdot}cm^{-2}$ loading.	[275]
Ni-YSZ/YSZ/ PNO—CGO/PNO	550	0.50	800	980	1.20	800	Microtubular cell (anode-supported). Extruded tubular NiO-YSZ. No air electrode degradation for 150 h in reversible SOC. 50 vol.% H_2O.	[3]
Ni-BZCY/BZCY/PNO-BZCY				977	1.30	700	The powders were synthesized by the EDTA-citric sol-gel method. Co-pressed and SP air electrodes. SOEC OCV = 0.98 V (pH_2O = 0.40 atm in air).	[294] *
Ni-BCZD/BCZD/ $Pr_{1.95}Ba_{0.05}NiO_{4+\delta}$/ LNF				850	1.30	700	Tubular fuel electrode support. The powders were prepared via a citrate-nitrate synthesis. The half-cell of the PCFC was fabricated using tape-calendering. 3%H_2O–H_2/30% H_2O–air was used in SOEC. SOEC OCV = 0.94 V.	[295] *
Ni-BCZD/BCZD/ $Nd_{1.95}Ba_{0.05}NiO_{4+\delta}$				830	1.30	750	NBN powder is synthesized via a citrate-nitrate synthesis. PCFC is fabricated by the tape-calendering method. pH_2O=0.5 atm in air used in SOEC measurements. SOEC OCV = 0.85 V.	[296] *
Ni-CGO/T3YSZ/NNO				640	1.30	800	Electrolyte-supported cell. Reduced at 750 °C in an Ar/H_2 with increasing H_2, up to 100%. NNO is powder prepared by the nitrate–citrate route and deposited by SP. The ratio H_2O/H_2 is 0.9 at the H_2 electrode. SOEC OCV = 0.86 V.	[17]
Ni-BCZD/BCZD/LNO-BCZD (70:30 wt%)	221	0.50	750	450	1.50	750	BCZD is prepared by the citrate–nitrate synthesis. The cells were fabricated by tape calendering. 90% H_2O was used in the SOEC test.	[297] *

demonstrating the importance of spray pyrolysis synthesis for SOCs materials. One of the most relevant works for single-cell applications is that of Chauveau et al. [17]. They proposed NNO as the oxygen electrode for both fuel cell and electrolysis applications. They performed the study using 3YSZ electrolyte-supported cells with a Ni-CGO hydrogen electrode. They found that ASR values are slightly lower in electrolysis mode in comparison with fuel cell mode. Their performances in SOEC mode were compared with a commercial LSM-based cell, obtaining a significant increase in terms of performance for the NNO cell. At the thermoneutral voltage (1.3 V), they obtained current densities of 0.64 and 0.87 $A{\cdot}cm^{-2}$ at 800 and 850 °C, respectively, confirming that NNO is an excellent candidate for high-temperature steam electrolysis applications.

3.1.3. PNO electrochemical performance

Vibhu et al. [224] studied the electrochemical aging of PNO as oxygen electrodes for solid oxide fuel or electrolysis cells. PNO was screen printed on dense 8YSZ ceramics coated with a thin CGO barrier layer. These experiments also confirmed that PNO decomposed into a mixture of Pr_6O_{11}, $PrNiO_{3\pm\delta}$, $Pr_4Ni_3O_{10+\delta}$, and NiO [225]. Despite this, the electrochemical stability was confirmed over one month under operation. However, under polarization (i_{dc} = 300 $mA{\cdot}cm^{-2}$), PNO suffered delamination at the interface between PNO and CGO, which was believed to come from a poor supply of oxygen inside the porosity of the electrode. In addition, the behavior of PNO in SOEC mode was remarkable, as polarization resistances of about 0.03 $\Omega{\cdot}cm^2$ at 700 °C for 1800 h were obtained. These results confirmed that PNO is an excellent candidate as a SOEC electrode, and is also in line with those reported for the same material in SOEC using microtubular configuration [7].

The performance of PNO in single cells was also studied by Dogdibegovic et al. [226] in a long-term stability test on PNO cells for up to 500 h. They did not observe degradation, as power densities remained almost constant at 0.66 W cm^{-2} at 750 ºC and 0.8 V. EIS analysis also showed that the slow degradation of the cell performance is consistent with an increase in electrode polarization, both of which resulted from the electrode evolution. In addition, Lin et al. [227] also studied the performance of PNO cells prepared by the glycine-nitrate method. They obtained maximum power densities of about 0.49 W cm^2 at 800 °C and 0.77 V. In their cells, they reported that an SDC solution infiltrating and filling the pores in the electrolyte membrane was required to avoid delamination between the electrolyte and the oxygen electrode.

Finally, Laguna-Bercero et al. [3,7] studied a series of microtubular cells (mT-SOCs) using PNO as the oxygen electrode along with different electrolyte–electrode interlayers, observing that the stability and performance of the cells strongly depend on the barrier layer used. In the SOFC mode, they showed power densities of about 0.63 W cm^{-2} at 800 °C and 0.7 V, when using PNO—CGO composite barrier layers. In addition, these cells presented excellent stability as no degradation was observed after 100 h under the operating conditions. Their current density in electrolysis mode was −0.78 A cm^{-2} at 800 °C and 1.3 V. In

concordance with previous findings by other authors, oscillatory current behavior was observed and ascribed to the partial decomposition reaction of the $Pr_2NiO_{4+\delta}$ phase into $PrNiO_3$ and PrO_{2-y} which, on the other hand, seems not to deteriorate the electrochemical properties of the cell. They concluded that the PNO–CGO in situ reaction, forming mixed praseodymium, cerium, and gadolinium oxides (CPGO) at the electrolyte–oxygen electrode interface, is a key parameter for the good stability and performance of the cells.

3.1.4. Mixed RP phase compositions

Partial substitution with La is often used to compensate for the lack of stability in PNO electrodes, as LNO electrodes are generally more chemically stable. In this sense, Sharma et al. [221] evaluated oxygen electrodes on CGO electrolytes, consisting of the stacking of two PLNO layers fabricated by different methods: an electrostatic-sprayed functional layer and a screen-printed current collector. The resulting anode-supported single cell (Ni-3YSZ/Ni-8YSZ/8YSZ/CGO), including a PNO (maximum Pr content in PLNO) double layer air electrode (Fig. 4), showed an MPD of 0.44 $W{\cdot}cm^{-2}$ at 700 °C. Different SEM micrographs of the PLNO oxygen electrode on a CGO substrate are shown in Fig. 4. However, the best stability, up to 500 h in air under no polarization, was obtained with lower Pr contents in PLNO (50 at% in A-site). Outstanding long-term stability was reported by Vibhu et al. [224] for PLNO ($La_{1.5}Pr_{0.5}NiO_{4+\delta}$). Their cells lasted up to 1800 h at 700 ºC in SOEC and SOFC modes (± 0.30 $A{\bullet}cm^{-2}$).

3.2. High-order nickelate-based oxygen electrodes

Although the synthesis of pure-phase nickelates, particularly high-order RP materials, is difficult, some contributions to SOC applications have developed significantly in recent years. The performance of high-order RP materials is in general higher than that of the parent RP phases and perovskite nickelates. The better electrochemical performance is attributed to higher electrical conductivity and a larger area where reactive sites occur. In infiltrated La nickelate solutions, the Brunauer–Emmett–Teller (BET) surface areas of LNO, $La_3Ni_2O_7$, and $La_4Ni_3O_{10}$ are 0.54, 0.79, and 2.06 $m^2{\cdot}g^{-1}$, respectively [213]. This is owed to the increase of the electrochemical reactive sites due to the usual smaller grain size of the high-order nickelate phases.

Vibhu et al. reported [59] full stability of $Pr_4Ni_3O_{10\pm\delta}$ electrodes under oxygen at 1000 °C in co-sintered symmetrical cells, whereas a further increase of temperature under air and oxygen leads to decomposition into PNO and NiO. This decomposition seemed to appear after 106 h of aging [97]. The R_{pol} using co-sintered CGO and two-step sintered symmetrical cells registered a value of 0.16 $\Omega{\cdot}cm^2$ at 600 °C under air, which is comparable with the highest performing PNO at the same temperature [169]. The anode-supported SOC (Ni-YSZ / YSZ / CGO / $Pr_4Ni_3O_{10\pm\delta}$) displayed $R_{pol} = 0.03$ $\Omega{\cdot}cm^2$ at 700 °C and MPDs of 1.60 $W{\cdot}cm^{-2}$ at 800 °C and 0.68 $W{\cdot}cm^{-2}$ at 700 °C. These results are among the best recorded for RP nickelates. Interestingly, using the same fabrication methods for PNO and $Pr_4Ni_3O_{10\pm\delta}$ results in similar R_{pol} values (~0.03 $\Omega{\cdot}cm^2$ at 700 °C) [97].

One interesting innovation is the application of electrostatic spray deposition (ESD) for $La_4Ni_3O_{10\pm\delta}$ films explored by Sharma et al. [101], who also noticed the difficulties in the synthesis of pure phases that require prolonged homogenization and reheating procedures. Low R_{pol} values were obtained for the double layer (a 3D coral layer adjacent to the electrolyte fabricated by ESD topped by a screen-printed layer). In particular, R_{pol} values of 2.01, 0.30, and 0.05 $\Omega{\cdot}cm^2$ were measured at 600, 700, and 800 °C, respectively. These results give light on the strong influence of the microstructure on the electrochemical properties of $La_4Ni_3O_{10\pm\delta}$ oxygen electrodes.

Regarding infiltration, Choi et al. [213] integrated these nickelates into YSZ scaffolds using anode-supported SOCs. The ensuing MPDs were 0.72, 0.75, and 0.89 $W{\cdot}cm^{-2}$ at 750 °C using LNO, $La_3Ni_2O_7$, and $La_4Ni_3O_{10}$ electrodes, respectively. Kim et al. [228] studied the effects of Sr-doping in the nanocomposites $La_4Ni_3O_{10\pm\delta}$- YSZ and LNO- YSZ. The LNO-YSZ composite barely showed a better performance than the Sr-doped sample ($La_{3.6}Sr_{0.4}Ni_3O_{10-\delta}$– YSZ), both in R_{pol} (0.128 $\Omega{\cdot}cm^2$ vs 0.190 $\Omega{\cdot}cm^2$) and MPD (0.38 $W{\cdot}cm^{-2}$ vs 0.37 $W{\cdot}cm^{-2}$) at 700 °C. In addition, Chaianansutcharit et al. [162] used Sr- and Fe-doped $Pr_4Ni_3O_{10\pm\delta}$ in A- and B-cation, respectively, finding that unit cell parameters and crystal size decreased when Ni was substituted at the Fe-site. However, the electrical conductivity of $PrSr_3Fe_{2.9}Ni_{0.1}O_{10-\delta}$ (PSFNO10) barely changed by the addition of Ni and the presence of dominant hole conduction is present in any case. They also found remarkable power density of a planar SOC using PSFNO10, achieving an MPD = 0.68 $W{\cdot}cm^{-2}$ at 800 ºC. This performance was higher than the

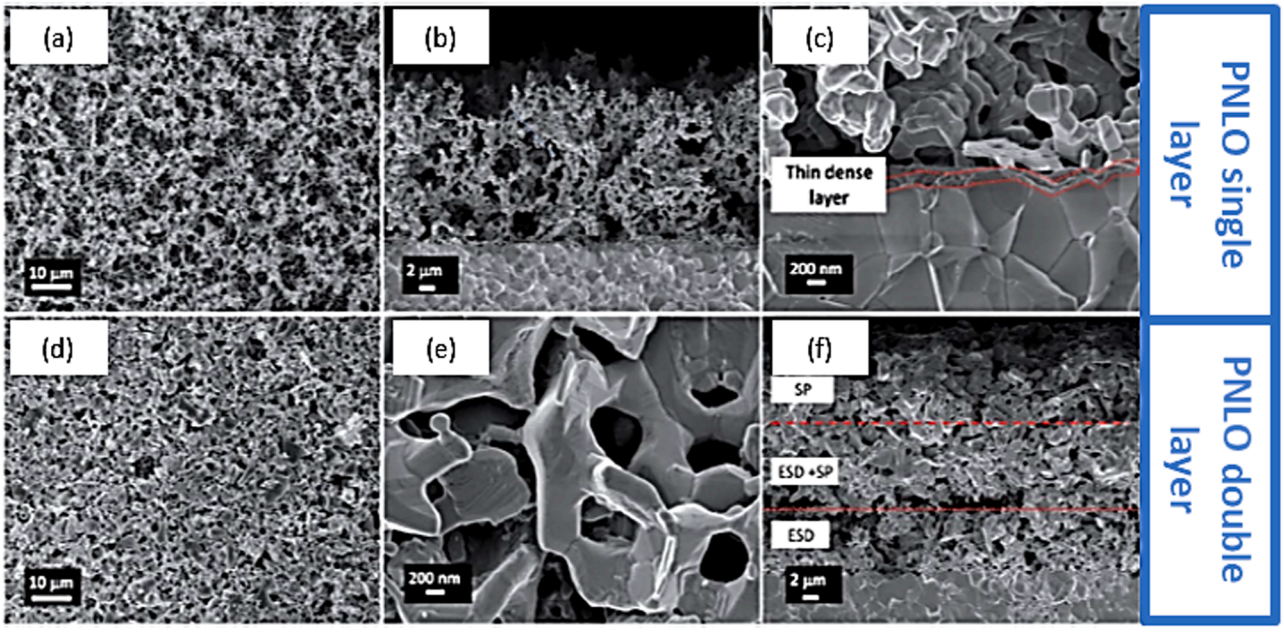

Fig. 4. SEM micrograph of PLNO oxygen electrode on a CGO substrate. PLNO single layer: a) surface, b) and c) cross sections at different magnifications. PLNO double layer: d) surface, e) and f) cross sections [221].

MPD's of $PrSr_3Fe_3O_{10-\delta}$ (0.51 W·cm^{-2} at 800 °C) and LSFC (0.44 W·cm^{-2} at 800 °C) under a similar configuration [229].

3.3. Interlayers and RP nickelate-CGO composite electrodes

As mentioned before, electrolyte materials can accelerate the decomposition of nickelates as cation interdiffusion occurs between CGO or YSZ and the different nickelates during sintering at high temperatures [230]. Exceptionally, in the case of Pr- or Sm-doped-ceria layers, doped-ceria layers can help to mitigate or correct these obstacles.

Electrochemical impedance spectroscopy (EIS) was measured by Flura et al. [231] on LNO / doped-ceria / 3YSZ symmetrical cells. In this work, the R_{pol} values were compared as a function of the doped ceria interlayer used (Pr or Gd doped). They also determined that the R_{pol} parameter characterizes the overall incorporation of O_2 as O^{2-} into LNO at the gas//electrode interface, then the diffusion of O^{2-} from the LNO electrode toward the electrolyte. In conclusion, they found slightly better performances for the LNO electrode when using CPO (R_{pol} = 0.64 Ω·cm^2) as interlayer instead of CGO (R_{pol} = 0.88 Ω·cm^2), for LNO and doped-ceria interlayers sintered in the same conditions. In addition, it was shown that no cation interdiffusion occurs at the LNO / CPO interface, contrarily to the LNO / CGO interface, which is responsible for this difference in R_{pol}.

Further strategies to avoid cation interdiffusion were issued by Zhou et al. [29], who compared the performance of Ni-YSZ / YSZ / $Ce_{0.8}Sm_{0.2}O_{1.9}$ / PNO with a Ni-YSZ / YSZ / $Ce_{0.8}Sm_{0.2}O_{1.9}$ / BSCF cell. While the power density achieved in the BSCF single cell is higher, the performance degraded during the stability test. In the same study, it was outlined that similar deterioration is present in a single cell with LSFC as an oxygen electrode. It is also worth noting that the performance of NNO impregnated into SSZ [85] showed comparable results (R_{pol} of 0.04 Ω·cm^2 in symmetrical cells and MPD = 1.26 W·cm^{-2} at 800 ºC in single cells) to functionally-graded LNF-CGO (0.054 Ω·cm^2 at 800 ºC [232]), LSFC-YSZ (~0.16 Ω·cm^2 at 800 ºC [233]), and LSF (~0.10 Ω·cm^2 at 700 ºC [234]), using the same type of synthesis. The key result was obtained at 650 ºC with a R_{pol} = 0.17 Ω·cm^2 and MPD = 0.520 W·cm^{-2}.

In addition, Dogdibegovic et al. [109] employed a CPGO interlayer to diminish the decomposition in nickelates induced by CGO, finding an increase of 48% in power density [158]. The microstructural analysis confirmed the presence of multiple phases in the PNO electrode, including PrO_x and NiO phases [7,158]. It was found that at 1100 ºC, Pr from PNO diffuses into CGO forming the CPGO phase [7], showing also good ionic and adequate electronic conductivity.

The performance under reversible cycling showed a MPD = 0.55 W·cm^{-2} (0.5 V) in single-cell configuration of Ni-YSZ / YSZ / CPGO / PNO, and a R_{pol} = 0.32 Ω·cm^2 in CGO / CPGO / PNO cells at 800 °C [3]. No apparent degradation was observed in the CPGO electrode during 150 h of SOFC / SOEC operation. For reference, Chen et al. [235] manufactured PNO—CPO composites synthesized by solid-state techniques and modified sol-gel methods, obtaining in a single Ni-CGO / CGO / PNO—CPO cell a R_{pol} = 0.09 Ω·cm^2 and MPD = 0.57 W·cm^{-2} at 800 ºC.

Mixed Ce-Pr oxides with combined 3+/4+ valence at high temperatures produce an improved electronic conductivity [236,237] and could simultaneously increase the oxygen vacancies [238]. Chiba et al. [239] have previously studied this effect in symmetrical cells of LNF - CPGO / $(ZrO_2)_{0.89}(Sc_2O_3)_{0.10}(Al_2O_3)_{0.10}$, and compared the performance of SDC, CPGO, and CPO layers. They found that $Ce_{0.8}Pr_{0.1}Gd_{0.1}O_{1.95-\delta}$ performed better as a buffer layer with R_{pol} = 0.24 Ω·cm^2.

In Pr-doped ceria, one important shortcoming is the relatively large TEC compared to YSZ or CGO electrolytes (~10×10^{-6} and ~12×10^{-6} K^{-1}, respectively [240]), especially at temperatures higher than 500 °C [241]. The TEC can reach as high as ~20–30$\times10^{-6}$ K^{-1}, mainly influenced by the thermal reduction of Pr and the formation of oxygen vacancies [242,243]. To counter this, it was reported that thermal expansion could be diminished by introducing additional Zr or Gd atoms into the lattice, despite the decrease of combined ionic/electronic conductivity performance [244,245]. Samarium has proven to be effective as well, like in SDC-infiltrated PNO [246], where after reduction in H_2 at high temperature the in-situ exsolution of Ni nanoparticles are adhered to the surface of the PNO scaffold, improving catalytic activity for H_2 oxidation. The SDC electrolyte-supported symmetrical cells achieved an MPD = 0.37 W·cm^{-2} at 800 °C. No apparent degradation is observed for the PNO-40SDC / SDC / PNO-40SDC symmetrical cell after operation at j = 0.36 A·cm^{-2} at 750 °C for 168 h.

LNO-infiltrated CGO electrodes, with a R_{pol} = 0.15 Ω·cm^2 at 600 °C, display one of the best performances reported for SOC oxygen electrodes [97,198]. As the CGO conductivity is not controlling the electrode ionic conductivity, the main benefit of such infiltrated electrode comes from a higher specific area, compared to screen-printed electrodes, and better interfaces between LNO, the CGO backbone, and the electrolyte. The infiltration of LNO using different electrolyte supports of LSGM and SDC also achieved a respectable MPD (0.52 W·cm^{-2} with an LNO-LSGM composite and 0.55 W·cm^{-2} with an LNO-SDC composite, both at 800 °C) in SOFC mode [215]. A symmetrical LNO-SDC/SDC/LNO-SDC cell using 3% H_2O-humidified H_2 was stable under a constant polarization of j = 0.15 A·cm^{-2} at 650 °C for a period over 200 h. The performance of this composite yields more than double the MPD of the LNO oxygen electrode (0.37 W·cm^{-2} for LNO-SDC vs 0.17 W·cm^{-2} for LNO at 800 ºC) [247]. The reported MPD of the PNO-SDC layer / SDC /NiO-SDC single cell is similar (0.49 W·cm^{-2} at 800 ºC) [227]. In any case, the good ionic conductivity of SDC improves the charge transfer process in LNO [248]. This behavior was also studied by Pérez-Coll et al. [247] in a single cell with an LNO-SDC electrode (80–20 wt%), drawing an MPD of 0.37 W·cm^{-2} at 800 °C. This performance doubled the result obtained without the layer under the same operating conditions.

A good performance can be found in, PNO—CGO composites, like the ones reported by Philippeau et al. [33] showing a low R_{pol} = 0.28 Ω·cm^2 at 600 °C. Furthermore, an improved nickelate performance was observed using LSGM porous scaffolds. Railsback et al. [210] obtained a better performance at 650 ºC, with a R_{pol} = 0.11 Ω•cm^2, using PNO-infiltrations in LSGM. They infiltrated the LSGM scaffold 12 times to obtain this performance, observing that the main R_{pol} increased rapidly with decreasing temperature, shifting to a lower frequency. To verify this effect, they conducted a detailed experiment to identify contributions to the overall R_{pol} response (500 h test in air at 650 ºC), identifying significant changes in the first 100 h and a new response at ~1 Hz. However, they could not conclude if R_{pol} eventually stabilizes or continues to increase. They related this performance to the PNO surface area due to coarsening and a possible phase transformation of the parent nickelate phase, although the XRD results suggested that this was mostly suppressed. Druce et al., [249] based on a LEIS analysis, suggested that A-site surface enrichment may occur in RP nickelates, which may also account for the resistance increase.

Partial substitutions in the nickelate composition have also been used in composites as in Tan et al. [250], who employed impregnated $La_{0.8}Sr_{0.2}Co_{0.8}Ni_{0.2}O_{3-\delta}$–$Ce_{0.9}Gd_{0.1}O_{2-\delta}$ (LSCN - CGO) as oxygen electrode in reversible SOCs. In SOFC mode, a MPD = 1.34 W·cm^{-2} at 800 °C is obtained, mainly due to the low R_{pol} = 0.10 Ω·cm^2 value at OCV. In SOEC, the current density reaches −1.00 A·cm^{-2} (750 ºC) and −1.60 A·cm^{-2} (800 ºC) at thermoneutral voltage (1.3 V) with 90 vol.% absolute humidity. Additionally, the $Pr_{1.2}Sr_{0.8}NiO_{4+\delta}$-$Sm_{0.2}Ce_{0.8}O_{1.9}$ (PSNO-SDC, weight ratio of 1:1) composite was successfully characterized in single NiO-SDC/SDC/PSNO-SDC cells [79]. Good chemical stability was shown with a $Sm_{0.2}Ce_{0.8}O_{1.9}$ (SDC) electrolyte with a low ASR = 0.112 Ω·cm^2 at 800 ºC. For a low OCV of 0.75 V, the cells showed an MPD = 0.30 W·cm^{-2} at 700 ºC.

Chen et al. [251] developed a Nd_2O_3- and NNO- impregnated scandia-stabilized zirconia (SSZ) electrode in a metal-supported cell with an SDC-infiltrated Ni-YSZ fuel electrode and an SSZ electrolyte. The resulting test in SOEC mode (30% steam content) at 600 ºC showed

stability for over 350 h (-0.17 A·cm^{-2}). With the same SOC configuration, the peak performance under SOEC was -2.05 A·cm^{-2} at 800 ºC (1.3 V), which is among the best SOEC current density recorded for nickelate-based air electrodes. Currently, the highest recorded SOEC current density in nickelate electrodes was presented by Sun et al. [252], with $j = -3.02$ A·cm^{-2} (1.3 V) at 700 °C using 42.2 wt% solid loading of infiltrated $La_{1.2}Sr_{0.8}NiO_{4+\delta}$ into the skeleton of a $BaCe_{0.68}Zr_{0.1}Y_{0.1}Yb_{0.1}Cu_{0.02}O_{3-\delta}$ electrolyte.

3.4. Cobalt-doped nickelate oxygen electrodes

The non-ohmic polarization measured for pure RP nickelates is significantly larger than those of cobalt-doped electrodes [188,253]. As proof, the R_{pol} in Cobalt-doped $La_3Ni_2O_{7-\delta}$ was diminished when increasing the dopant amount (from 1.12 Ω·cm^2 in $La_3Ni_{1.9}Co_{0.1}O_{7-\delta}$ to 0.35 Ω·cm^2 in $La_3Ni_{1.6}Co_{0.4}O_{7-\delta}$ at 650 ºC) [253]. To compare electrochemical properties, Vibhu et al. [188] prepared oxygen electrodes by screen printing with a Ni: Co ratio of 4:1 in $Pr_2Ni_{1-x}Co_xO_4$, achieving an MPD = 1.20 W·cm^{-2} (0.6 V) at 800 °C. Other reports imply single PNO cells with a Co-doped CGO20 layer [254], resulting in a R_{pol} = 0.08 Ω·cm^2 at 800 °C. Also, long-term stability may improve in cobalt-doped nickelate air electrodes, especially in SOEC mode [188]. To illustrate this idea, the long-term stability experiments performed in single cells containing LNCO20 and PNCO20 electrodes under SOFC conditions at 800 °C ($j = 1.00$ A·cm^{-2}), yielded good stability for up to 250 h. The PNCO20 cell showed a lower degradation rate of 98 mV·kh^{-1} than the 238 mV·kh^{-1} of the LNCO cell, however, under SOEC the rates are even lower (22 mV·kh^{-1} and 113 mV·kh^{-1} for PNCO20 and LNCO, respectively) [188]. Previous work in LSCN electrodes includes the use of the LSCN composition ($La_{1.7}Sr_{1.3}Co_{0.5}Ni_{0.5}O_{4\pm\delta}$), with a K_2NiF_4-type structure, on a 10Sc1CeSZ electrolyte and Ni-YSZ fuel electrode [255]. The performance was similar in both SOFC and SOEC modes, with ASR values at 850 °C of 1.92 and 2.05 Ω·cm^2, respectively. For high-order RP nickelate electrodes, Amow et al. [40] reported Pechini-synthetized $La_4Ni_{2.6}Co_{0.4}O_{10-\delta}$ oxygen electrodes on LSGM electrolytes in symmetric SOC, displaying a R_{pol} = 0.06 Ω·cm^2 at 800 °C.

3.5. Calcium-doped nickelate oxygen electrodes

Sadykov et al. [159] reported the performance of symmetrical cells formed by painting with intermediate pre-sintering of the functional electrode layers of $Pr_{1.7}Ca_{0.3}NiO_{4+\delta}$ / $LaNi_{0.6}Fe_{0.4}O_{3-\delta}$, obtaining R_{pol} = 0.40 Ω·cm^2 at 700 °C. Similarly, for LNO-based electrodes, Pikalova et al. [256] verified the changes in R_{pol} of the $La_{2-x}Ca_xNiO_{4+\delta}$ and $La_{2-x}Sr_xNiO_{4+\delta}$ electrodes in contact with CGO electrolytes, determining an increase with Ca content [131,256]. Ca-enriched materials in orthorhombic and tetragonal structures did not decompose after 250 h of heating at 850 °C. Also, the TEC values diminished, the most for $Pr_{1.5}Ca_{0.5}NiO_{4+\delta}$ to 13.4 × 10^{-6} K^{-1}, compared to PNO values of 14.0 × 10^{-6} K^{-1}. PNO had a higher chemical activity to interact with electrolytes of LSGM, SDC, and BCZY, than the Ca-containing PNO. However, the latter reacted more with YSZ due to the formation of the thermodynamically stable calcium zirconate [77].

3.6. Copper-doped nickelate oxygen electrodes

Another common dopant used along lanthanide nickelates is copper. Some of the highlights include the works of Zheng et al. [186], who reported an MPD = 0.13 W·cm^{-2} at 800 °C for a $Pr_2Ni_{0.5}Cu_{0.5}O_4$-based SOC, and a single cell with a $Pr_2Ni_{0.6}Cu_{0.4}O_4$ oxygen electrode and SDC electrolyte showed an MPD = 0.24 W·cm^{-2} at 700 °C [187]. However, stability issues arise from the partial decomposition of the materials at 1000 °C. The presence of secondary phases induced by the Cu presence increase in $Pr_2Ni_{1-x}Cu_xO_4$, causing a decrease in power output. Kharton et al. [257] studied $La_2Ni_{0.8}Cu_{0.2}O_{4+\delta}$ as an oxygen electrode on symmetric cells with LSGM electrolyte, emphasizing in the pO_2 dependence of R_{pol} values. They concluded that the cathodic reaction rate was affected by surface-related processes, and in consequence, electrode performance can be considerably enhanced by surface activation, particularly via impregnation with Pr-containing solutions.

Also, modifications in A-site cation with Ce have been mentioned in different publications by Khandale et al. [258,259], who employed several approaches for $Nd_{2-x}Ce_xCuO_{4\pm\delta}$ for microstructural optimization, such as combustion, mechano-chemical, microwave, ball-milled solid-state and sol-gel syntheses. This was possible through modifications of the calcination temperature during the fabrication process [55, 254,260]. The outlined results for the $Nd_{2-x}Ce_xCuO_{4\pm\delta}$ ($x = 0.1 – 0.25$) electrode in symmetrical cells displayed a proportional increase of the R_{pol} from 0.93 to 3.92 Ω·cm^2 as the sintering temperature increased from 800 to 1200 °C [259]. The authors attributed such phenomenon to the enlarged grain size with the increase in sintering temperature. The use of spin coating [190] for $Nd_{1.8}Ce_{0.2}Cu_{1-x}Ni_xO_{4+\delta}$ resulted in better R_{pol} values (0.44 Ω·cm^2 at 700 °C). Although improved results are perceived from the NNO electrode, this performance is not as effective as in the impregnated NNO-SDC / NNO electrodes [85].

3.7. Other novel composites

In addition to all the above developments, many other efforts to improve the microstructural properties for better electrochemical performance in oxygen electrodes have been documented. The NNO symmetrical cells deposited by ultrasonic spray-pyrolysis [223] showed a R_{pol} = 0.50 Ω·cm^2 at 700 °C. The good sintering capability of NNO nanoparticles improved the adhesion with the electrolyte, and the particles inside the electrode were also well connected [261]. As reference, an impregnated $Nd_{1.6}Sr_{0.4}NiO_4$ electrode previously showed a R_{pol} = 0.93 Ω·cm^2 at 700 °C [88]. An improvement over these prototypes was made by Arias-Serrano et al. [262], who worked on Pechini-synthesized symmetrical cells with PrO_x surface modifications. The $Nd_{0.8}Sr_{1.2}Ni_{0.8}M_{0.2}O_{4-\delta}$ oxygen electrodes (23 wt% of PrO_x in M = Ni + PrO_x) showed R_{pol} = 0.04 Ω·cm^2 at 800 °C. Further incorporations of Co or Fe into the Ni sub-lattice of $Nd_{0.8}Sr_{1.2}NiO_{4-\delta}$ reduced the oxygen deficiency and electrical conductivity.

Garali et al. [161] studied the incorporation of europium (instead of Sr) as a dopant, observing a well-bonded porous lattice with sufficient TPB density. In their electrochemical characterizations, the lowest R_{pol} was obtained for $La_{0.8}Eu_{0.2}NiO_{4+\delta}$ at a temperature of 700 °C in air, obtaining a value of 1.30 Ω·cm^2.

Finally, He et al. [263] introduced the ion-conductive $Er_{0.4}Bi_{1.6}O_{3-\delta}$ (EBO) oxide into the LNO air electrode, improving the MPD of the LNO electrode (from 0.12 to 0.85 W cm^{-2} at 750 ºC) when operating on a YSZ electrolyte. The LNO-EBO electrode provided a stable performance for 200 h at 750 °C.

3.8. Perovskite nickelates

One of the most prominent works on perovskite nickelate oxygen electrodes is that of Chiba et al. [264] who tested the B-site substitutions of Al, Cr, Mn, Fe, Co, and Ga into $LaNiO_3$ to stabilize the perovskite phase, which is unstable at less than 850 ºC [265]. They found that doping the Ni-site of LNF was the most viable option for oxygen electrodes in terms of conductivity and thermal expansion [264]. Later, on a single SOC with Nickel-Scandia and alumina stabilized zirconia (Ni-SASZ) / SASZ / LNF, Orui et al. [266] applied a current loading of 3.00 A·cm^{-2} for several days to activate the LNF electrode. After the activation, the cell MPD reached 1.56 W·cm^{-2} at 800 °C, up to ten times higher than the same cell before activation. Pikalova et al. [267] managed to improve the electrochemical activity of LNF by introducing $Bi_{1.75}Y_{0.25}O_{3-\delta}$ (YDB) and $Bi_{0.6}Er_{0.4}O_{3-\delta}$ (EDB) additives into the current collector. The addition of CuO increased the sintering ability and electrochemical activity of the LNF-YDB cell, obtaining stability for 600 h at 700 ºC. The composite LNF-SDC performed better than LNF-EDB, 0.69

and 0.76 W·cm^{-2}, respectively, at 750 ºC [268].

As in the case of RP nickelates, the influence of Ni particles seems to reduce the thermal expansion, but ionic conductivity is decreased as compared with lanthanum cobaltites [27] and substitutions in the Ni site are favored. Hjalmarsson et al. [269] discovered in $La_{0.99}Co_{0.4}Ni_{0.6}O_{3-\delta}$-CGO composites operating at low temperatures that the ORR activity was even higher, while the activation energy of the R_{pol} is lower than in LSM–YSZ. A $R_{pol} = 0.05$ Ω·cm^2 at 750 °C was measured for this particular oxygen electrode. Other researchers compared the R_{pol} of functionally-graded [270] and composite [271] LNF - CGO electrodes with LNF-impregnated CGO under similar testing conditions, finding the lowest values in the latter (0.29 Ω·cm^2 at 700 ºC).

Perovskite nickelate infiltrated into YSZ backbones has been seen as a viable option for single cell construction, as power density values are reported to be higher than in non-infiltrated electrodes [213]. Another remarkable work is that of Huang et al. [270], who constructed single cells with $PrNi_{0.6}Co_{0.4}O_3$ – $Ce_{0.8}Sm_{0.2}O_{1.9}$ mixtures at a ratio of 1:1, resulting in a very low $R_{pol} = 0.03$ Ω·cm^2 at 700 °C and particularly high MPD = 1.09 W·cm^{-2}.

Khoshkalam et al. [272] incorporated Pr_6O_{11}-infiltrated layers into two different compositions of LSFC - CGO and LNF - CGO, where the best electrochemical performance is obtained in the latter ($R_{pol} = 0.07$ Ω·cm^2 at 600 °C). The samples sintered at 650 °C showed the best electrochemical performance among all the tested symmetrical cells. Finally, Zhang et al. [273] used the effects of mixing MIEC materials to improve the electrochemical response of the oxygen electrodes. The result was the LNO infiltration into an LSFC oxygen electrode, giving a significant decrease in the R_{pol} values from 0.30 to 0.04 Ω·cm^2 at 700 °C.

4. Concluding remarks

In the present work, a comprehensive review of the current state of the development of nickelates as SOC air electrodes, their material selection, and their electrochemical performance have been reviewed in detail. Further optimizations of these advanced materials are still required for complete implementation in industry and commercial markets, and it is of great importance to develop a better understanding of how the factors associated with synthesis, microstructure, phase evolution and transitions, as well as SOC configuration, affect the SOC electrochemistry. This could allow the development of strategies for the enhancement of nickelate air electrodes.

The intermediate-to-high temperature electrochemical performance of featured nickelate air electrodes was compiled from the different configurations studied by several research groups, with some of them achieving remarkable success. A summary highlighting the relevant nickelate SOC air electrode performances of symmetrical and single cells found in the literature are compiled in Tables 1-3, respectively to compare the different strategies covered in this review. It has been demonstrated that they could be used for SOFC, SOEC, and reversible SOC operation due to the chemical flexibility of those devices.

The use of cation mismatch substitutions in nickelate synthesis to suppress dopant segregation is an interesting development, but it requires a careful compromise between stability and performance to obtain the best possible results. Amid the most promising electrochemical performances of nickelate-based air electrodes, the Cu B-site cation modification, the use of ceria barrier layers in composites, and nickelate infiltrations have stood out for providing a high-power output, low interaction with electrolytes, and increase in charge transfer, respectively.

The most promising perspectives fundamentally involve the achievement of the highest possible amount of pure nickelate phases, where diminishing decomposition and formation of secondary phases becomes a critical objective for air electrode optimization and SOC durability studies. Improved synthesis optimization, innovative deposition techniques, long-term heating for electrode activation, and the use of high-order nickelates are among the most optimistic regarding a more stable SOC performance.

Declaration of Competing Interest

The authors declare that they have no known competing financial interests or personal relationships that could have appeared to influence the work reported in this paper.

Acknowledgements

This research has received funding from PID2019–107106RB-C32 (MCIU/AEI/FEDER, UE) and T02-20R (DGA) grants, and the Institute for Training and Development of Human Resources and Panamanian National Secretary of Science and Technology (IFARHU-SENACYT) for Miguel Morales-Zapata's PhD. scholarship. This research was also supported by MCIN with funding from NextGenerationEU (PRTR-C17.I1) within the Planes Complementarios con CCAA (Area of Green Hydrogen and Energy) and it has been carried out in the CSIC Interdisciplinary Thematic Platform (PTI+) Transición Energética Sostenible+ (PTI-TRANSENER+).

References

[1] V. Smil, Energy Transitions: History, Requirements, Prospects, Praeger, 2010.
[2] S.H. Jensen, C. Graves, M. Mogensen, C. Wendel, R. Braun, G. Hughes, Z. Gao, S. A. Barnett, Large-scale electricity storage utilizing reversible solid oxide cells combined with underground storage of CO2 and CH4, Energy Environ. Sci. 8 (2015) 2471–2479, https://doi.org/10.1039/c5ee01485a.
[3] M.A. Morales-Zapata, A. Larrea, M.A. Laguna-Bercero, Reversible operation performance of microtubular solid oxide cells with a nickelate-based oxygen electrode, Int. J. Hydrogen Energy. 45 (2020) 5535–5542, https://doi.org/10.1016/j.ijhydene.2019.05.122.
[4] M.B. Mogensen, M. Chen, H.L. Frandsen, C. Graves, J.B. Hansen, K.V. Hansen, A. Hauch, T. Jacobsen, S.H. Jensen, T.L. Skafte, X. Sun, Reversible solid-oxide cells for clean and sustainable energy, Clean Energy 3 (2019) 175–201, https://doi.org/10.1093/ce/zkz023.
[5] Q. Fang, L. Blum, D. Stolten, Electrochemical performance and degradation analysis of an SOFC short stack following operation of more than 100,000 H, J. Electrochem. Soc. 166 (2019) F1320–F1325, https://doi.org/10.1149/2.0751916jes.
[6] J. Schefold, A. Brisse, A. Surrey, C. Walter, 80,000 current on/off cycles in a one year long steam electrolysis test with a solid oxide cell, Int. J. Hydrogen Energy. 45 (2020) 5143–5154, https://doi.org/10.1016/j.ijhydene.2019.05.124.
[7] M.A. Laguna-Bercero, H. Monzón, A. Larrea, V.M. Orera, Improved stability of reversible solid oxide cells with a nickelate-based oxygen electrode, J. Mater. Chem. A. 4 (2016) 1446–1453, https://doi.org/10.1039/c5ta08531d.
[8] C. Graves, S.D. Ebbesen, S.H. Jensen, S.B. Simonsen, M.B. Mogensen, Eliminating degradation in solid oxide electrochemical cells by reversible operation, Nat. Mater. 14 (2015) 239–244, https://doi.org/10.1038/nmat4165.
[9] M. Lang, M. Braig, N. Alqubati, P. Szabo, Long-term behavior of a SOC stack in reversible fuel cell/electrolysis operation, in: ECS Meet. Abstr. 17th Int. Symp. Solid Oxide Fuel Cells July 18, 2021 - July 23, 2021. MA2021-03, 2021, https://doi.org/10.1149/MA2021-031248mtgabs.
[10] M. Greenblatt, Ruddlesden-Popper properties Ln n+1 NinO3n + 1 nickelates : structure and properties, Curr. Opin. Solid State Mater. Sci. 2 (1997) 174–183.
[11] V.V. Kharton, A.P. Viskup, E.N. Naumovich, F.M.B. Marques, Oxygen ion transport in La 2 NiO 4 -based ceramics, J. Mater. 9 (1999) 2623–2629.
[12] S.J. Skinner, J.A. Kilner, Oxygen diffusion and surface exchange in La2-xSrxNiO4+δ, Solid State Ionics 135 (2000) 709–712, https://doi.org/10.1016/S0167-2738(00)00388-X.
[13] J.M. Bassat, P. Odier, A. Villesuzanne, C. Marin, M. Pouchard, Anisotropic ionic transport properties in La2NiO 4+δ single crystals, Solid State Ionics 167 (2004) 341–347, https://doi.org/10.1016/j.ssi.2003.12.012.
[14] J. Zhou, G. Chen, K. Wu, Y. Cheng, Interaction of La 2 NiO 4 (100) surface with oxygen molecule : a first- principles study, J. Phys. Chem. C 117 (2013) 12991–12999, 2013.
[15] R.J. Woolley, M.P. Ryan, S.J. Skinner, In situ measurements on solid oxide fuel cell cathodes - simultaneous X-ray absorption and ac impedance spectroscopy on symmetrical cells, Fuel Cells 13 (2013) 1080–1087, https://doi.org/10.1002/fuce.201300174.
[16] R.J. Wold, Aaron; Arnott, Preparation and crystallographic of the systems LaMn1-xMnxO3+d and LaMn1-xNixO3+d, J. Phys. Chem. Solids. 9 (1959) 176–180.
[17] F. Chauveau, J. Mougin, J.M. Bassat, F. Mauvy, J.C. Grenier, A new anode material for solid oxide electrolyser: the neodymium nickelate Nd2NiO4+δ, J. Power Sources. 195 (2010) 744–749, https://doi.org/10.1016/j.jpowsour.2009.08.003.
[18] M.A. Laguna-Bercero, A.R. Hanifi, H. Monzón, J. Cunningham, T.H. Etsell, P. Sarkar, High performance of microtubular solid oxide fuel cells using Nd2NiO4

+δ-based composite cathodes, J. Mater. Chem. A. 2 (2014) 9764–9770, https://doi.org/10.1039/c4ta00665h.
[19] P. Ding, W. Li, H. Zhao, C. Wu, L. Zhao, B. Dong, S. Wang, Review on Ruddlesden-Popper perovskites as cathode for solid oxide fuel cells, JPhys Mater 4 (2021), https://doi.org/10.1088/2515-7639/abe392.
[20] A.V. Kasyanova, A.O. Rudenko, Y.G. Lyagaeva, D.A. Medvedev, Lanthanum-containing proton-conducting electrolytes with perovskite structures, Membr. Membr. Technol. 3 (2021) 73–97, https://doi.org/10.1134/S2517751621020050.
[21] A.P. Tarutin, J.G. Lyagaeva, D.A. Medvedev, L. Bi, A.A. Yaremchenko, Recent advances in layered Ln2NiO4+ δ nickelates: fundamentals and prospects of their applications in protonic ceramic fuel and electrolysis cells, J. Mater. Chem. A. 9 (2021) 154–195, https://doi.org/10.1039/d0ta08132a.
[22] X. Xu, Y. Pan, Y. Zhong, R. Ran, Z. Shao, Ruddlesden-Popper perovskites in electrocatalysis, Mater. Horizons. 7 (2020) 2519–2565, https://doi.org/10.1039/d0mh00477d.
[23] J. Song, D. Ning, B. Boukamp, J.-M.M. Bassat, H.J.M.M. Bouwmeester, Structure, electrical conductivity and oxygen transport properties of Ruddlesden-Popper phases Lnn+1NinO3n+1(Ln=La, Pr and Nd; n=1, 2 and 3), J. Mater. Chem. A 8 (2020) 22206–22221, https://doi.org/10.1039/d0ta06731h.
[24] A.P. Tarutin, J.G. Lyagaeva, A.S. Farlenkov, A.I. Vylkov, D.M. Medvedev, Cu-substituted La2NiO4+δ as oxygen electrodes for protonic ceramic electrochemical cells, Ceram. Int. 45 (2019) 16105–16112, https://doi.org/10.1016/j.ceramint.2019.05.127.
[25] A. Tarutin, J. Lyagaeva, A. Farlenkov, S. Plaksin, G. Vdovin, A. Demin, D. Medvedev, A reversible protonic ceramic cell with symmetrically designed Pr2NiO4+δ-based electrodes: fabrication and electrochemical features, Materials (Basel) 12 (2019), https://doi.org/10.3390/ma12010118.
[26] M. Bevilacqua, T. Montini, C. Tavagnacco, E. Fonda, P. Fornasiero, M. Graziani, Preparation, characterization, and electrochemical properties of pure and composite LaNi 0.6 Fe 0.4 O 3 -based cathodes for IT-SOFC, Chem. Mater. 19 (2007) 5926–5936, https://doi.org/10.1021/cm071622n.
[27] K.K. Hansen, The effect of A-site deficiency on the performance of La1-sFe0.4Ni0.6O3-δ cathodes, Mater. Res. Bull. 45 (2010) 197–199, https://doi.org/10.1016/j.materresbull.2009.09.024.
[28] Z. Zhu, J. Qian, Z. Wang, J. Dang, W. Liu, High-performance anode-supported solid oxide fuel cells based on nickel-based cathode and Ba(Zr0.1Ce0.7Y 0.2)O3-δ electrolyte, J. Alloys Compd. 581 (2013) 832–835, https://doi.org/10.1016/j.jallcom.2013.07.210.
[29] X.D. Zhou, J.W. Templeton, Z. Nie, H. Chen, J.W. Stevenson, L.R. Pederson, Electrochemical performance and stability of the cathode for solid oxide fuel cells: V. high performance and stable Pr2NiO4 as the cathode for solid oxide fuel cells, Electrochim. Acta. 71 (2012) 44–49, https://doi.org/10.1016/j.electacta.2012.03.067.
[30] W. Zhou, R. Ran, Z. Shao, Progress in understanding and development of Ba0.5Sr0.5Co0.8Fe0.2O3-δ-based cathodes for intermediate-temperature solid-oxide fuel cells: a review, J. Power Sources. 192 (2009) 231–246, https://doi.org/10.1016/j.jpowsour.2009.02.069.
[31] H. Téllez, J. Druce, Y.W. Ju, J. Kilner, T. Ishihara, Surface chemistry evolution in LnBaCo2O5 + δ double perovskites for oxygen electrodes, Int. J. Hydrogen Energy. 39 (2014) 20856–20863, https://doi.org/10.1016/j.ijhydene.2014.06.102.
[32] F. Mauvy, C. Lalanne, J.-.M. Bassat, J.-.C. Grenier, H. Zhao, L. Huo, P. Stevens, Electrode properties of Ln2NiO4+δ (Ln=La, Nd, Pr), J. Electrochem. Soc 153 (2006) A1547, https://doi.org/10.1149/1.2207059.
[33] B. Philippeau, F. Mauvy, C. Mazataud, S. Fourcade, J.C. Grenier, Comparative study of electrochemical properties of mixed conducting Ln 2NiO4 + δ (Ln = La, Pr and Nd) and La 0.6Sr0.4Fe0.8Co0.2O, Solid State Ionics. 249–250 (2013) 17–25. https://doi.org/10.1016/j.ssi.2013.06.009.
[34] S. Miyoshi, T. Furuno, O. Sangoanruang, H. Matsumoto, T. Ishihara, Mixed conductivity and oxygen permeability of doped Pr2NiO4-based oxides, J. Electrochem. Soc. 154 (2007) B57, https://doi.org/10.1149/1.2387103.
[35] T. Ishihara, N. Sirikanda, K. Nakashima, S. Miyoshi, H. Matsumoto, Mixed oxide ion and hole conductivity in Pr2−αNi0.76−xCu0.24GaxO4+δ membrane, J. Electrochem. Soc. 157 (2010) B141, https://doi.org/10.1149/1.3251004.
[36] E. Boehm, J.M. Bassat, P. Dordor, F. Mauvy, J.C. Grenier, P. Stevens, Oxygen diffusion and transport properties in non-stoichiometric Ln 2 - XNiO4 + δ oxides, Solid State Ionics 176 (2005) 2717–2725, https://doi.org/10.1016/j.ssi.2005.06.033.
[37] E. Boehm, J.M. Bassat, M.C. Steil, P. Dordor, F. Mauvy, J.C. Grenier, Oxygen transport properties of La2Ni1-xCuxO4+δ mixed conducting oxides, Solid State Sci. 5 (2003) 973–981, https://doi.org/10.1016/S1293-2558(03)00091-8.
[38] M. Burriel, G. Garcia, J. Santiso, J.A. Kilner, R.J. Chater, S.J. Skinner, Anisotropic oxygen diffusion properties in epitaxial thin films of La2NiO4+δ, J. Mater. Chem. 18 (2008) 416–422, https://doi.org/10.1039/b711341b.
[39] G. Amow, S.J. Skinner, Recent developments in Ruddlesden-Popper nickelate systems for solid oxide fuel cell cathodes, J. Solid State Electrochem. 10 (2006) 538–546, https://doi.org/10.1007/s10008-006-0127-x.
[40] G. Amow, I.J. Davidson, S.J. Skinner, A comparative study of the Ruddlesden-Popper series, Lan+1NinO3n+1 (n = 1, 2 and 3), for solid-oxide fuel-cell cathode applications, Solid State Ionics 177 (2006) 1205–1210, https://doi.org/10.1016/j.ssi.2006.05.005.
[41] M. Burriel, G. Garcia, M.D. Rossell, A. Figueras, G. Van Tendeloo, J. Santiso, Enhanced high-temperature electronic transport properties in nanostructured epitaxial thin films of the Lan+1NinO3n+1 Ruddlesden-Popper series (n = 1, 2, 3, ∞), Chem. Mater. 19 (2007) 4056–4062, https://doi.org/10.1021/cm070804e.
[42] S. Takahashi, S. Nishimoto, M. Matsuda, M. Miyake, Electrode properties of the ruddlesden-popper series, Lan+1NinO3n+1 (n=1, 2, and 3), as intermediate-temperature solid oxide fuel cells, J. Am. Ceram. Soc. 93 (2010) 2329–2333, https://doi.org/10.1111/j.1551-2916.2010.03743.x.
[43] Z. Lou, J. Peng, N. Dai, J. Qiao, Y. Yan, Z. Wang, J. Wang, K. Sun, High performance La3Ni2O7 cathode prepared by a facile sol-gel method for intermediate temperature solid oxide fuel cells, Electrochem. Commun. 22 (2012) 97–100, https://doi.org/10.1016/j.elecom.2012.06.004.
[44] S. Yoo, S. Choi, J. Shin, M. Liu, G. Kim, Electrical properties, thermodynamic behavior, and defect analysis of La n+1Ni nO 3n+1+δ infiltrated into YSZ scaffolds as cathodes for intermediate-temperature SOFCs, RSC Adv. 2 (2012) 4648–4655, https://doi.org/10.1039/c2ra20402a.
[45] D. Balz, K. Plieth, Die Struktur des Kaliumnickelfluorids, K2NiF4, Zeitschrift Für Elektrochemie, Berichte Der Bunsengesellschaft Für Phys. Chemie 59 (1955) 545–551. http://onlinelibrary.wiley.com/doi/10.1002/bbpc.19550590613/abstract.
[46] S.N. Ruddlesden, P. Popper, The compound Sr3Ti2O7 and its structure, Acta Crystallogr. 11 (1958) 54–55, https://doi.org/10.1107/s0365110×58000128.
[47] R.A. Mohan Ram, L. Ganapathi, P. Ganguly, C.N.R. Rao, Evolution of three-dimensional character across the Lan+1NinO3n+1 homologous series with increase in n, J. Solid State Chem. 63 (1986) 139–147, https://doi.org/10.1016/0022-4596(86)90163-5.
[48] B.W. Arbuckle, K.V. Ramanujachary, Z. Zhang, M. Greenblatt, Investigations on the structural, electrical, and magnetic properties of Nd2-xSrxNiO4+δ, J. Solid State Chem. 88 (1990) 278–290, https://doi.org/10.1016/0022-4596(90)90225-M.
[49] K. Sreedhar, M. McElfresh, D. Perry, D. Kim, P. Metcalf, J.M. Honig, Low-temperature electronic properties of the lan+1nino3n+1 (n = 2, 3, and ∞) system: evidence for a crossover from fluctuating-valence to fermi-liquid-like behavior, J. Solid State Chem. 110 (1994) 208–215, https://doi.org/10.1006/jssc.1994.1161.
[50] Z. Zhang, M. Greenblatt, J.B. Goodenough, Synthesis, structure, and properties of the layered perovskite La3Ni2O7-δ, J. Solid State Chem. 108 (1994) 402–409, https://doi.org/10.1006/jssc.1994.1059.
[51] M.D. Carvalho, M.A. Costa, A. Wattiaux, M. Bassat, J. Claude, M. Pouchard, New preparation method of Lan+1NinO3n+1–δ (n=2, 3), J. Mater. Chem. 7 (1997) 2107–2111.
[52] R. Chiba, H. Ishii, Pr2NiO4+δ cathode properties and reaction at interface with ceria and zirconia, ECS Trans. 68 (2015) 947–955, https://doi.org/10.1149/06801.0947ecst.
[53] R. Sayers, J. Liu, B. Rustumji, S.J. Skinner, Novel K2NiF4-type materials for solid oxide fuel cells: compatibility with electrolytes in the intermediate temperature range, Fuel Cells 8 (2008) 338–343, https://doi.org/10.1002/fuce.200800023.
[54] E. Dogdibegovic, J. Templeton, J. Yan, J.W. Stevenson, X.-.D. Zhou, Compatibility of praseodymium nickelates with various cathode current collectors and electrolytes, ECS Trans. 57 (2013) 1761–1770, https://doi.org/10.1149/05701.1761ecst.
[55] C. Lalanne, G. Prosperi, J.M. Bassat, F. Mauvy, S. Fourcade, P. Stevens, M. Zahid, S. Diethelm, J. Van herle, J.C. Grenier, Neodymium-deficient nickelate oxide Nd1.95NiO4+δ as cathode material for anode-supported intermediate temperature solid oxide fuel cells, J. Power Sources. 185 (2008) 1218–1224, https://doi.org/10.1016/j.jpowsour.2008.06.072.
[56] V.V. Kharton, A.V. Kovalevsky, M. Avdeev, E.V. Tsipis, M.V. Patrakeev, A. A. Yaremchenko, E.N. Naumovich, J.R. Frade, Chemically induced expansion of La2NiO4+δ-based materials, Chem. Mater. 19 (2007) 2027–2033, 2007.
[57] A. Montenegro-Hernández, L. Mogni, A. Caneiro, Microstructure and reactivity effects on the performance of Nd 2NiO 4+δ oxygen electrode on Ce 0.9Gd 0.1O 1.95 electrolyte, Int. J. Hydrogen Energy. 37 (2012) 18290–18301, https://doi.org/10.1016/j.ijhydene.2012.09.071.
[58] A. Flura, S. Dru, C. Nicollet, V. Vibhu, S. Fourcade, E. Lebraud, A. Rougier, J. M. Bassat, J.C. Grenier, Chemical and structural changes in Ln2NiO4+δ (Ln=La, Pr or Nd) lanthanide nickelates as a function of oxygen partial pressure at high temperature, J. Solid State Chem. 228 (2015) 189–198, https://doi.org/10.1016/j.jssc.2015.04.029.
[59] V. Vibhu, A. Rougier, C. Nicollet, A. Flura, S. Fourcade, N. Penin, J.C. Grenier, J. M. Bassat, Pr4Ni3O10+δ: a new promising oxygen electrode material for solid oxide fuel cells, J. Power Sources. 317 (2016) 184–193, https://doi.org/10.1016/j.jpowsour.2016.03.012.
[60] A. Aguadero, J.A. Alonso, M.J. Escudero, L. Daza, Evaluation of the La2Ni1 - xCuxO4 + δ system as SOFC cathode material with 8YSZ and LSGM as electrolytes, Solid State Ionics. 179 (2008) 393–400. https://doi.org/10.1016/j.ssi.2008.01.099.
[61] V. Vibhu, A. Rougier, J.-.C. Grenier, J.-.M. Bassat, Mixed nickelates Pr2-xLaxNiO4+δ used as cathodes in metal supported SOFCs, ECS Trans. Electrochem. Soc. 57 (2013) 2093–2100.
[62] V.A. Tsvinkinberg, A.S. Tolkacheva, E.A. Filonova, O.I. Gyrdasova, S.M. Pikalov, V.A. Vorotnikov, A.I. Vylkov, N.I. Moskalenko, E. Yu, Structure, thermal expansion and electrical conductivity of La2-xGdxNiO4+d (0.0<x<0.6) cathode materials for SOFC applications, J. Alloys Compd. 853 (2021), 156728, https://doi.org/10.1016/j.jallcom.2020.156728.
[63] Y.G. Lyagaeva, N.A. Danilov, M.Y. Gorshkov, G.K. Vdovin, B.D. Antonov, A. K. Demin, D.A. Medvedev, Functionality of lanthanum, neodymium, and praseodymium nickelates as promising electrode systems for proton-conducting

electrolytes, Russ. J. Appl. Chem. 91 (2018) 583–590, https://doi.org/10.1134/S1070427218040080.
[64] Y.P. Wang, Q. Xu, D.P. Huang, K. Zhao, M. Chen, B.H. Kim, Evaluation of La1.8Sr0.2NiO4+δ as cathode for intermediate temperature solid oxide fuel cells, Int. J. Hydrogen Energy. 41 (2016) 6476–6485, https://doi.org/10.1016/j.ijhydene.2016.03.019.
[65] Y.P. Wang, Q. Xu, D.P. Huang, K. Zhao, M. Chen, B.H. Kim, Survey on electrochemical properties of La2−xSrxNiO4±d (x = 0.2 and 0.8, d >0) cathodes related with structural stability under cathodic polarization conditions, Int. J. Hydrogen Energy. 42 (2017) 6290–6302, https://doi.org/10.1016/j.ijhydene.2016.12.041.
[66] Z. Zhu, M. Li, C. Xia, H.J.M. Bouwmeester, Bismuth-doped La1.75Sr0.25NiO4+: δ as a novel cathode material for solid oxide fuel cells, J. Mater. Chem. A. 5 (2017) 14012–14019, https://doi.org/10.1039/c7ta03381h.
[67] E.Y. Pikalova, A.A. Kolchugin, The influence of the substituting element (M = Ca, Sr, Ba) in La1.7M0.3NiO4+δ on the electrochemical performance of the composite electrodes, Eurasian Chem. J 18 (2016) 3–11, https://doi.org/10.1149/ma2014-01/2/252.
[68] T. Inprasit, P. Limthongkul, S. Wongkasemjit, Sol–gel and solid-state synthesis and property study of La2−xSrxNiO4 (x≤0.8), J. Electrochem. Soc. 157 (2010) B1726, https://doi.org/10.1149/1.3489262.
[69] A.R. Gilev, E.A. Kiselev, V.A. Cherepanov, Synthesis, oxygen nonstoichiometry and total conductivity of (La,Sr)2(Mn,Ni)O4± δ, Solid State Ionics. 279 (2015) 53–59. https://doi.org/10.1016/j.ssi.2015.07.017.
[70] A.R. Gilev, E.A. Kiselev, D.M. Zakharov, V.A. Cherepanov, Effect of calcium and copper/iron co-doping on defect-induced properties of La2NiO4-based materials, J. Alloys Compd. 753 (2018) 491–501, https://doi.org/10.1016/j.jallcom.2018.04.178.
[71] E. Pikalova, A. Kolchugin, E. Filonova, N. Bogdanovich, S. Pikalov, M. Ananyev, N. Molchanova, A. Farlenkov, Validation of calcium-doped neodymium nickelates as SOFC air electrode materials, Solid State Ionics 319 (2018) 130–140, https://doi.org/10.1016/j.ssi.2018.02.008.
[72] C. Zhao, Q. Zhou, T. Zhang, L. Qu, X. Yang, T. Wei, Preparation and electrochemical properties of La 1.5 Pr 0.5 NiO 4 and La 1.5 Pr 0.5 Ni 0.9 Cu 0.1 O 4 cathode materials for intermediate-temperature solid oxide fuel cells, Mater. Res. Bull. 113 (2019) 25–30, https://doi.org/10.1016/j.materresbull.2019.01.016.
[73] A. Aguadero, J.A. Alonso, M.T. Fernández-Díaz, M.J. Escudero, L. Daza, In situ high temperature neutron powder diffraction study of La2Ni0.6Cu0.4O4+δ in air: correlation with the electrical behaviour, J. Power Sources. 169 (2007) 17–24, https://doi.org/10.1016/j.jpowsour.2007.01.075.
[74] J. Yeyongchaiwat, K. Nonthawissarut, S. Charojrochkul, N. Sukpirom, Compatibility and conductivity of La2Ni1-xFexO4+δ and LaNi0.6Fe0.4O3–δ with GDC electrolyte, Energy Mater. Mater. Sci. Eng. Energy Syst. 10 (2015) 1–8, https://doi.org/10.1179/1743676114Y.0000000203.
[75] J. Cheng, S. Zhang, B. Meng, J. Ding, X. Tan, Preparation and the superior oxygen permeability of a new CO2-resistant Ruddlesden–Popper composite oxide Pr2Ni0.9Mo0.1O4+δ, J. Alloys Compd. 742 (2018) 966–976, https://doi.org/10.1016/j.jallcom.2018.01.366.
[76] A. Montenegro-Hernández, J.E. Vega-Castillo, A. Caneiro, L. Mogni, Effects of neodymium doping on oxygen reduction activity in Pr2−xNdxNiO4+δ cathodes, Solid State Ionics 347 (2020), 115093, https://doi.org/10.1016/j.ssi.2019.115093.
[77] E.Y. Pikalova, D.A. Medvedev, A.F. Khasanov, Structure, stability, and thermomechanical properties of Ca-substituted Pr2NiO4 + δ, Phys. Solid State. 59 (2017) 694–702, https://doi.org/10.1134/S1063783417040187.
[78] T.W. Chiu, M.X. Lin, H.Y. Shih, B. yinn Hwang, H.Y. Chang, Y.M. Wang, Preparation and performance of PrLaNiO4 and (La0.75Sr0.2 Ba0.05) 0.175Ce0.825O1.891 composite cathode material by solid state reaction for IT-SOFCs, Ceram. Int. 43 (2017) S700–S704, https://doi.org/10.1016/j.ceramint.2017.05.269.
[79] J. Yang, J. Cheng, Q. Jiang, Y. Wang, R. Wang, J. Gao, Preparation and electrochemical properties of strontium doped Pr2NiO4 cathode materials for intermediate-temperature solid oxide fuel cells, Int. J. Hydrogen Energy. 37 (2012) 1746–1751, https://doi.org/10.1016/j.ijhydene.2011.09.146.
[80] H.W. Nie, T.L. Wen, S.R. Wang, Y.S. Wang, U. Guth, V. Vashook, Preparation, thermal expansion, chemical compatibility, electrical conductivity and polarization of A2-αA′αMO4 (A = Pr, Sm; A′ = Sr; M = Mn, Ni; α = 0.3, 0.6) as a new cathode for SOFC, Solid State Ionics 177 (2006) 1929–1932, https://doi.org/10.1016/j.ssi.2006.01.003.
[81] S.Y. Istomin, O.M. Karakulina, M.G. Rozova, S.M. Kazakov, A.A. Gippius, E. V. Antipov, I.A. Bobrikov, A.M. Balagurov, A.A. Tsirlin, A. Michau, J.J. Biendicho, G. Svensson, Tuning the high-temperature properties of Pr2NiO4+δ by simultaneous Pr- and Ni-cation replacement, RSC Adv. 6 (2016) 33951–33958, https://doi.org/10.1039/c6ra03099h.
[82] M. Li, J. Cheng, Y. Gan, S. Li, B. He, W. Sun, Effects of strontium doping on the structure, oxygen nonstoichiometry and electrochemical performance of Pr2-xSrxNi0.6Cu0.4O4+δ (0.1 ≤ x ≤ 0.5) cathode materials, J. Power Sources. 275 (2015) 151–158, https://doi.org/10.1016/j.jpowsour.2014.10.191.
[83] X. Meng, S. Lü, S. Liu, X. Liu, Y. Sui, X. Li, M. Pang, B. Wang, Y. Ji, M.Z. Hu, Electrochemical characterization of B-site cation-excess Pr2Ni0.75Cu0.25Ga0.05O4+δ cathode for IT-SOFCs, Ceram. Int. 41 (2015) 12107–12114, https://doi.org/10.1016/j.ceramint.2015.06.028.
[84] C. Berger, E. Bucher, A. Egger, A.T. Strasser, N. Schrödl, C. Gspan, J. Hofer, W. Sitte, Synthesis and characterization of the novel K2NiF4-type oxide Pr2Ni0.9Co0.1O4 + δ, Solid State Ionics 316 (2018) 93–101, https://doi.org/10.1016/j.ssi.2017.12.024.
[85] T. Chen, Y. Zhou, C. Yuan, M. Liu, X. Meng, Z. Zhan, C. Xia, S. Wang, Impregnated Nd2NiO4+δ- scandia stabilized zirconia composite cathode for intermediate-temperature solid oxide fuel cells, J. Power Sources. 269 (2014) 812–817, https://doi.org/10.1016/j.jpowsour.2014.07.073.
[86] M. Letilly, A.L.G. La Salle, M. Caldes, M. Marrony, O. Joubert, Validation of BaIn0.3Ti0.7O2.85 as SOFC electrolyte with Nd2NiO4, LSM and LSCF as cathodes, Fuel Cells 9 (2009) 622–629, https://doi.org/10.1002/fuce.200900072.
[87] T. Nakamura, K. Yashiro, K. Sato, J. Mizusaki, Thermally-induced and chemically-induced structural changes in layered perovskite-type oxides Nd2 - xSrxNiO4 + δ (x = 0, 0.2, 0.4), Solid State Ionics. 181 (2010) 402–411. https://doi.org/10.1016/j.ssi.2010.02.002.
[88] L.P. Sun, Q. Li, H. Zhao, L.H. Huo, J.C. Grenier, Preparation and electrochemical properties of Sr-doped Nd2NiO4 cathode materials for intermediate-temperature solid oxide fuel cells, J. Power Sources. 183 (2008) 43–48, https://doi.org/10.1016/j.jpowsour.2008.05.001.
[89] E. Kravchenko, D. Khalyavin, K. Zakharchuk, J. Grins, G. Svensson, V. Pankov, A. Yaremchenko, High-temperature characterization of oxygen-deficient K2NiF4-type Nd2-xSrxNiO4-δ (x = 1.0-1.6) for potential SOFC/SOEC applications, J. Mater. Chem. A. 3 (2015) 23852–23863, https://doi.org/10.1039/c5ta06779k.
[90] S.M. Pikalov, L.B. Vedmid, E.A. Filonova, E.Y. Pikalova, J.G. Lyagaeva, N. A. Danilov, A.A. Murashkina, High-temperature behavior of calcium substituted layered neodymium nickelates, J. Alloys Compd. 801 (2019) 558–567, https://doi.org/10.1016/j.jallcom.2019.05.349.
[91] S. Sameshima, M. Kawaminami, Y. Hirata, Thermal expansion of rare-earth-doped ceria ceramics, J. Ceram. Soc. Japan. 110 (2002) 597–600.
[92] J.W. Stevenson, K. Hasinska, N.L. Canfield, T.R. Armstrong, Influence of cobalt and iron additions on the electrical and thermal properties of (La,Sr)(Ga,Mg)O [*sub* 3−δ], J. Electrochem. Soc 147 (2000) 3213, https://doi.org/10.1149/1.1393885.
[93] R.K. Lenka, P.K. Patro, V. Patel, L. Muhmood, T. Mahata, Comparative investigation on the functional properties of alkaline earth metal (Ca, Ba, Sr) doped Nd2NiO4+δ oxygen electrode material for SOFC applications, J. Alloys Compd. 860 (2021), 158490, https://doi.org/10.1016/j.jallcom.2020.158490.
[94] A.P. Tarutin, M.Y. Gorshkov, I.N. Bainov, G.K. Vdovin, A.I. Vylkov, J. G. Lyagaeva, D.A. Medvedev, Barium-doped nickelates Nd2−xBaxNiO4+δ as promising electrode materials for protonic ceramic electrochemical cells, Ceram. Int. 46 (2020) 24355–24364, https://doi.org/10.1016/j.ceramint.2020.06.217.
[95] T. Zhang, Q. Zhou, Y. He, C. Zhao, S. Qi, M. Wang, T. Wei, D. An, Assessment of Nd1.5Pr0.5Ni1−xMxO4+δ (M = Cu, Co, Mo; x = 0, 0.05 and 0.1) as cathode materials for intermediate-temperature solid oxide fuel cell, J. Mater. Sci. Mater. Electron 31 (2020) 949–958, https://doi.org/10.1007/s10854-019-02604-2.
[96] H. Tamura, A. Hayashi, Y. Ueda, Phase diagram of La2NiO4+5 (0 ≤ δ ≤ 0.18) II. Thermodynamics of excess oxygen, phase transitions (0.06 ≤ δ ≤ 0.11) and phase segregation (0.03 ≤ δ ≤ 0.06), Phys. C Supercond. Its Appl. 258 (1996) 61–71, https://doi.org/10.1016/0921-4534(95)00798-9.
[97] J.-.M. Bassat, V. Vibhu, C. Nicollet, A. Flura, S. Fourcade, J.-.C. Grenier, A. Rougier, Comparison of Pr-based cathodes for IT-SOFCs in the Ruddlesden-Popper family, ECS Trans. 78 (2017) 655–665, https://doi.org/10.1149/07801.0655ecst.
[98] J. Bassat, O. Wahyudi, M. Ceretti, P. Veber, I. Weill, A. Villesuzanne, J. Grenier, W. Paulus, J.A. Kilner, Anisotropic oxygen diffusion properties in Pr2NiO4+δ and Nd2NiO4+δ single crystals, J. Phys. Chem. C. (2013).
[99] T. Ogier, J.M. Bassat, F. Mauvy, S. Fourcade, J.C. Grenier, K. Couturier, M. Petitjean, J. Mougin, Enhanced performances of structured oxygen electrodes for high temperature steam electrolysis, Fuel Cells 13 (2013) 536–541, https://doi.org/10.1002/fuce.201200201.
[100] V. Vibhu, J.-M.J. Bassat, A. Flura, C. Nicollet, J.-C.J.-C. Grenier, A. Rougier, Influence of La/Pr ratio on the ageing properties of La2-xPrxNiO4+δ as cathodes in IT-SOFCs, ECS Trans. 68 (2015) 825–835, https://doi.org/10.1149/06801.0825ecst.
[101] R.K. Sharma, M. Burriel, E. Djurado, La4Ni3O10-δ as an efficient solid oxide fuel cell cathode: electrochemical properties versus microstructure, J. Mater. Chem. A. 3 (2015) 23833–23843, https://doi.org/10.1039/c5ta07862h.
[102] M.A. Yatoo, A. Aguadero, S.J. Skinner, LaPr3Ni3O9.76 as a candidate solid oxide fuel cell cathode: role of microstructure and interface structure on electrochemical performance, APL Mater. 7 (2019) 1–8, https://doi.org/10.1063/1.5050249.
[103] M.A. Yatoo, Z. Du, H. Zhao, A. Aguadero, S.J. Skinner, La2Pr2Ni3O10±δ Ruddlesden-Popper phase as potential intermediate temperature-solid oxide fuel cell cathodes, Solid State Ionics 320 (2018) 148–151, https://doi.org/10.1016/j.ssi.2018.02.043.
[104] A.C. Tomkiewicz, M. Tamimi, A. Huq, S. McIntosh, Oxygen transport pathways in Ruddlesden-Popper structured oxides revealed via in situ neutron diffraction, J. Mater. Chem. A. 3 (2015) 21864–21874, https://doi.org/10.1039/c5ta04193g.
[105] M.A. Yatoo, S.J. Skinner, Ruddlesden-Popper phase materials for solid oxide fuel cell cathodes : a short review, Mater. Today Proc. 56 (2022) 3747–3754, https://doi.org/10.1016/j.matpr.2021.12.537.
[106] C.Y. Tsai, A. Aguadero, S.J. Skinner, High electrical conductivity and crystal structure of the solid oxide cell electrode Pr4Ni3O10-δ, J. Solid State Chem. 289 (2020), 121533 https://doi.org/10.1016/j.jssc.2020.121533.
[107] M.U. Nagell, W.A. Sławiński, P. Vajeeston, H. Fjellvåg, A.O. Sjåstad, Temperature induced transitions in La4(Co1−xNix)3O10+δ; oxygen stoichiometry and

mobility, Solid State Ionics 305 (2017) 7–15, https://doi.org/10.1016/j.ssi.2017.04.006.
[108] Z. Tan, S.M. Heald, S.W. Cheong, A.S. Cooper, J.I. Budnick, Rare-earth valence and doping in T-, T, and T*-phase R2CuO4 (R=rare earths), Phys. Rev. B 45 (1992) 2593–2596, https://doi.org/10.1103/PhysRevB.45.2593.
[109] E. Dogdibegovic, N.S. Alabria, C.J. Wright, J.S. Hardy, C.A. Coyle, S.A. Horlick, W. Guan, J.W. Stevenson, X.-.D. Zhou, In situ studies of phase evolution in (Pr1-xNdx)2NiO4 electrodes with various interlayer chemistries, ECS Trans. 78 (2017) 623–635, https://doi.org/10.1149/07801.0623ecst.
[110] P. Odier, Y. Nigara, J. Coutures, M. Sayer, Phase relations in the La–Ni–O system: influence of temperature and stoichiometry on the structure of La2NiO4, J. Solid State Chem. 56 (1985) 32–40, https://doi.org/10.1016/0022-4596(85)90249-X.
[111] C.N.R. Rao, J.M. Thomas, Intergrowth structures: the chemistry of solid-solid interfaces, Acc. Chem. Res. 18 (1985) 113–119, https://doi.org/10.1021/ar00112a003.
[112] J.T. Lewandowski, R.A. Beyerlein, J.M. Longo, R.A. McCauley, Nonstoichiometric KzNiF4-type phases in the lanthanum-cobalt-oxygen system, J. Am. Ceram. Soc. 69 (1986) 699–703.
[113] J... Drennan, C.P... Tavares, B.C.H. Steele, An electron microscope investigation of phases in the system La-Ni-O, Mat. Res. Bull. 17 (1982) 621–626. http://eprints.uanl.mx/5481/1/1020149995.PDF.
[114] J.D... Jorgensen, B... Dabrowski, P... Shiyou, D.R... Richards, D.G. Hinks, Structure of the interstitial oxygen defect in La2NiO4+d, Phys. Rev. B. 40 (1992) 416–419, https://doi.org/10.1016/0163-8343(92)90009-Y.
[115] J.B. Goodenough, S. Ramasesha, Further evidence for the coexistence of localized and itinerant 3d electrons in La2NiO4, Mater. Res. Bull. 17 (1982) 383–390, https://doi.org/10.1016/0025-5408(82)90089-7.
[116] M. Zinkevich, F. Aldinger, Thermodynamic analysis of the ternary La-Ni-O system, J. Alloys Compd. 375 (2004) 147–161, https://doi.org/10.1016/j.jallcom.2003.11.138.
[117] A. Aguadero, J.A. Alonso, M.J. Martínez-Lope, M.T. Fernández-Díaz, M. J. Escudero, L. Daza, In situ high temperature neutron powder diffraction study of oxygen-rich La2NiO4+δ in air: correlation with the electrical behaviour, J. Mater. Chem. 16 (2006) 3402–3408, https://doi.org/10.1039/b605886h.
[118] Z. Zhang, M. Greenblatt, Synthesis, structure and properties of Ln4Ni3O10-d (Ln=La,Pr, and Nd), J. Solid State Chem 117 (1995) 236–246.
[119] A.V. Kovalevsky, V.V. Kharton, A.A. Yaremchenko, Y.V. Pivak, E.V. Tsipis, S. O. Yakovlev, A.A. Markov, E.N. Naumovich, J.R. Frade, Oxygen permeability, stability and electrochemical behavior of Pr 2NiO4+δ-based materials, J. Electroceramics. 18 (2007) 205–218, https://doi.org/10.1007/s10832-007-9024-7.
[120] A. Chroneos, B. Yildiz, A. Tarancón, D. Parfitt, J.A. Kilner, Oxygen diffusion in solid oxide fuel cell cathode and electrolyte materials: mechanistic insights from atomistic simulations, Energy Environ. Sci. 4 (2011) 2774–2789, https://doi.org/10.1039/c0ee00717j.
[121] A. Chroneos, D. Parfitt, J.A. Kilner, R.W. Grimes, Anisotropic oxygen diffusion in tetragonal La2NiO 4+δ: molecular dynamics calculations, J. Mater. Chem. 20 (2010) 266–270, https://doi.org/10.1039/b917118e.
[122] L. Minervini, R.W. Grimes, J.A. Kilner, K.E. Sickafus, Oxygen migration in La2NiO (4+δ), J. Mater. Chem. 10 (2000) 2349–2354, https://doi.org/10.1039/b004212i.
[123] V.A. Sadykov, V.S. Muzykantov, N.F. Yeremeev, V.V. Pelipenko, E. M. Sadovskaya, A.S. Bobin, Y.E. Fedorova, D.G. Amanbaeva, A.L. Smirnova, Solid oxide fuel cell cathodes: importance of chemical composition and morphology, Catal. Sustain. Energy. 2 (2016) 57–70, https://doi.org/10.1515/cse-2015-0004.
[124] A.L. Shaula, E.N. Naumovich, A.P. Viskup, V.V. Pankov, A.V. Kovalevsky, V. V. Kharton, Oxygen transport in La2NiO4 + δ: assessment of surface limitations and multilayer membrane architectures, Solid State Ionics 180 (2009) 812–816, https://doi.org/10.1016/j.ssi.2009.01.005.
[125] H. Zhao, F. Mauvy, C. Lalanne, J.M. Bassat, S. Fourcade, J.C. Grenier, New cathode materials for ITSOFC: phase stability, oxygen exchange and cathode properties of La2 - xNiO4 + δ, Solid State Ionics 179 (2008) 2000–2005, https://doi.org/10.1016/j.ssi.2008.06.019.
[126] V.A. Sadykov, E.Y. Pikalova, A.A. Kolchugin, A.V. Fetisov, E.M. Sadovskaya, E. A. Filonova, N.F. Eremeev, V.B. Goncharov, A.V. Krasnov, P.I. Skriabin, A. N. Shmakov, Z.S. Vinokurov, A.V. Ishchenko, S.M. Pikalov, Transport properties of Ca-doped Ln2NiO4 for intermediate temperature solid oxide fuel cells cathodes and catalytic membranes for hydrogen production, Int. J. Hydrogen Energy. 45 (2020) 13625–13642, https://doi.org/10.1016/j.ijhydene.2018.03.039.
[127] N. Gauquelin, Impact of the Structural Anisotropy of La2NiO4+δ On High Temperature Surface Modifications and Diffusion of Oxygen, University of Rennes, 2010.
[128] M.V. Ananyev, E.S. Tropin, V.A. Eremin, A.S. Farlenkov, A.S. Smirnov, A. A. Kolchugin, N.M. Porotnikova, A.V. Khodimchuk, A.V. Berenov, E. K. Kurumchin, Oxygen isotope exchange in La2NiO4±δ, Phys. Chem. Chem. Phys. 18 (2016) 9102–9111, https://doi.org/10.1039/c5cp05984d.
[129] H.J.M. Bouwmeester, C. Song, J. Zhu, J. Yi, M. Van Sint Annaland, B.A. Boukamp, A novel pulse isotopic exchange technique for rapid determination of the oxygen surface exchange rate of oxide ion conductors, Phys. Chem. Chem. Phys. 11 (2009) 9640–9643, https://doi.org/10.1039/b912712g.
[130] N.M. Porotnikova, A.V. Khodimchuk, M.V. Ananyev, V.A. Eremin, E.S. Tropin, A. S. Farlenkov, E.Y. Pikalova, A.V. Fetisov, Oxygen isotope exchange in praseodymium nickelate, J. Solid State Electrochem. 22 (2018) 2115–2126, https://doi.org/10.1007/s10008-018-3919-x.
[131] A.A. Kolchugin, E.Y. Pikalova, N.M. Bogdanovich, D.I. Bronin, S.M. Pikalov, S. V. Plaksin, M.V. Ananyev, V.A. Eremin, Structural, electrical and electrochemical properties of calcium-doped lanthanum nickelate, Solid State Ionics 288 (2016) 48–53, https://doi.org/10.1016/j.ssi.2016.01.035.
[132] T. Ina, Y. Orikasa, T. Masese, T. Nakao, A. Mineshige, K. Amezawa, H. Tanida, T. Uruga, Y. Uchimoto, Relationship between local structure and oxide ionic diffusion of Nd2NiO4+δ with K2NiF4 structure, Electrochemistry 82 (2014) 875–879, https://doi.org/10.5796/electrochemistry.82.875.
[133] D. Lee, A. Grimaud, E.J. Crumlin, K. Mezghani, M.A. Habib, Z. Feng, W.T. Hong, M.D. Biegalski, H.M. Christen, Y. Shao-horn, Strain influence on the oxygen electrocatalysis of the (100)-oriented epitaxial La2NiO4+d, J. Phys. Chem. C. 117 (2013) 18789–18795.
[134] N. Tsvetkov, Q. Lu, Y. Chen, B. Yildiz, Accelerated oxygen exchange kinetics on Nd2NiO4+δthin films with tensile strain along c-axis, ACS Nano 9 (2015) 1613–1621, https://doi.org/10.1021/nn506279h.
[135] D. Parfitt, A. Chroneos, J.A. Kilner, R.W. Grimes, Molecular dynamics study of oxygen diffusion in Pr2NiO4+δ, Phys. Chem. Chem. Phys. 12 (2010) 6834–6836, https://doi.org/10.1039/c001809k.
[136] A. Kushima, D. Parfitt, A. Chroneos, B. Yildiz, J.A. Kilner, R.W. Grimes, Interstitialcy diffusion of oxygen in tetragonal La2CoO 4+δ, Phys. Chem. Chem. Phys. 13 (2011) 2242–2249, https://doi.org/10.1039/c0cp01603a.
[137] X. Li, N.A. Benedek, Enhancement of ionic transport in complex oxides through soft lattice modes and epitaxial strain, Chem. Mater. 27 (2015) 2647–2652, https://doi.org/10.1021/acs.chemmater.5b00445.
[138] D. Lee, H.N. Lee, Controlling oxygen mobility in ruddlesden-popper oxides, Materials (Basel) 10 (2017) 368–389, https://doi.org/10.3390/ma10040368.
[139] G. Kim, S. Wang, A.J. Jacobson, L. Reimus, P. Brodersen, C.A. Mims, Rapid oxygen ion diffusion and surface exchange kinetics in PrBaCo 2O5+x with a perovskite related structure and ordered a cations, J. Mater. Chem. 17 (2007) 2500–2505, https://doi.org/10.1039/b618345j.
[140] I.D. Seymour, A. Tarancón, A. Chroneos, D. Parfitt, J.A. Kilner, R.W. Grimes, Anisotropic oxygen diffusion in PrBaCo 2O 5.5 double perovskites, Solid State Ionics. 216 (2012) 41–43. https://doi.org/10.1016/j.ssi.2011.09.002.
[141] E. Tropin, M. Ananyev, N. Porotnikova, A. Khodimchuk, S. Saher, A. Farlenkov, E. Kurumchin, D. Shepel, E. Antipov, S. Istomin, H. Bouwmeester, Oxygen surface exchange and diffusion in Pr1.75Sr0.25Ni0.75Co0.25O4±: δ, Phys. Chem. Chem. Phys. 21 (2019) 4779–4790, https://doi.org/10.1039/c9cp00172g.
[142] A. Egger, W. Sitte, Enhanced oxygen surface exchange of La2NiO4+δ by means of a thin surface layer of silver, Solid State Ionics 258 (2014) 30–37, https://doi.org/10.1016/j.ssi.2014.01.038.
[143] W. Li, B. Guan, J. Yan, N. Zhang, X. Zhang, X. Liu, Enhanced surface exchange activity and electrode performance of (La2-2xSr2x)(Ni1-xMnx)O4+δ cathode for intermediate temperature solid oxide fuel cells, J. Power Sources. 318 (2016) 178–183, https://doi.org/10.1016/j.jpowsour.2016.04.022.
[144] E.Y. Pikalova, A.A. Kolchugin, V.A. Sadykov, Structure, transport properties and electrochemical behavior of the layered lanthanide nickelates doped with calcium, Int. J. Hydrogen Energy. 43 (2018) 17373–17386, https://doi.org/10.1016/j.ijhydene.2018.07.115.
[145] J. Railsback, G. Hughes, L. Mogni, A. Montenegro-Hernández, S. Barnett, High-pressure performance of mixed-conducting oxygen electrodes: effect of interstitial versus vacancy conductivity, J. Electrochem. Soc. 163 (2016) F1433–F1439, https://doi.org/10.1149/2.1071613jes.
[146] K. Yakal-Kremski, L.V. Mogni, A. Montenegro-Hernández, A. Caneiro, S. A. Barnett, Determination of electrode oxygen transport kinetics using electrochemical impedance spectroscopy combined with three-dimensional microstructure measurement: application to Nd 2 NiO 4+δ, J. Electrochem. Soc. 161 (2014) F1366–F1374, https://doi.org/10.1149/2.0521414jes.
[147] A. Stangl, A. Riaz, L. Rapenne, J.M. Caicedo, J. De Dios Sirvent, F. Baiutti, C. Jiménez, A. Tarancón, M. Mermoux, M. Burriel, Tailored nano-columnar La2NiO4 cathodes for improved electrode performance, J. Mater. Chem. A. 10 (2022) 2528–2540, https://doi.org/10.1039/d1ta09110g.
[148] P... Ganguly, C.N.R. Rao, Electron transport properties of transition metal oxide systems with the K2NiF4, Mat. Res. Bull. 8 (1973) 405–412.
[149] Z. Lou, N. Dai, Z. Wang, Y. Dai, Y. Yan, J. Qiao, J. Peng, J. Wang, K. Sun, Preparation and electrochemical characterization of Ruddlesden-Popper oxide La4Ni3O10 cathode for IT-SOFCs by sol-gel method, J. Solid State Electrochem. 17 (2013) 2703–2709, https://doi.org/10.1007/s10008-013-2150-z.
[150] T. Nakamura, K. Yashiro, K. Sato, J. Mizusaki, Electrical conductivity, Seebeck coefficient, and defect structure of oxygen nonstoichiometric Nd2-xSrxNiO4+δ, Mater. Chem. Phys. 122 (2010) 250–258, https://doi.org/10.1016/j.matchemphys.2010.02.044.
[151] A. Egger, E. Bucher, W. Sitte, Oxygen exchange kinetics of the IT-SOFC cathode material Nd2NiO4+δ and comparison with La0.6Sr0.4CoO3-δ, J. Electrochem. Soc. 158 (2011) B573, https://doi.org/10.1149/1.3569697.
[152] J. Andreas Schuler, H. Lübbe, A. Hessler-Wyser, J. Van Herle, Nd-nickelate solid oxide fuel cell cathode sensitivity to Cr and Si contamination, J. Power Sources. 213 (2012) 223–228, https://doi.org/10.1016/j.jpowsour.2012.03.112.
[153] A. Egger, W. Sitte, F. Klauser, E. Bertel, Long-term oxygen exchange kinetics of Nd2NiO4+δ in H2O- and CO2-containing atmospheres, J. Electrochem. Soc. 157 (2010) B1537, https://doi.org/10.1149/1.3481420.
[154] M. Yang, E. Bucher, W. Sitte, Effects of chromium poisoning on the long-term oxygen exchange kinetics of the solid oxide fuel cell cathode materials La0.6Sr 0.4CoO3 and Nd2NiO4, J. Power Sources. 196 (2011) 7313–7317, https://doi.org/10.1016/j.jpowsour.2010.10.064.
[155] N. Schrödl, A. Egger, J. Lammer, F. Hofer, W. Sitte, Long-term stability of Pr2NiO4+δ air electrodes for solid oxide cells against chromium poisoning, J. Electrochem. Soc. 168 (2021), 014509, https://doi.org/10.1149/1945-7111/abdc5e.

[156] S. Peng, Y. Wei, J. Xue, Y. Chen, H. Wang, Pr1.8La0.2Ni0.74Cu0.21Ga 0.05O4+δ as a potential cathode material with CO2 resistance for intermediate temperature solid oxide fuel cell, Int. J. Hydrogen Energy. 38 (2013) 10552–10558, https://doi.org/10.1016/j.ijhydene.2013.06.073.

[157] G. Li, H. Jin, Y. Cui, L. Gui, B. He, L. Zhao, Application of a novel (Pr0.9La0.1)2(Ni0.74Cu0.21Nb0.05)O4+δ-infiltrated BaZr0.1Ce0.7Y0.2O3-δ cathode for high performance protonic ceramic fuel cells, J. Power Sources. 341 (2017) 192–198, https://doi.org/10.1016/j.jpowsour.2016.11.008.

[158] E. Dogdibegovic, N.S. Alabri, C.J. Wright, J.S. Hardy, C.A. Coyle, S.A. Horlick, W. Guan, J.W. Stevenson, X.-.D. Zhou, Activity and stability of (Pr1-xNdx)2NiO4 as cathodes for solid oxide fuel cells: part v. in situ studies of phase evolution, J. Electrochem. Soc 164 (2017) F1115–F1121, https://doi.org/10.1149/2.1041707jes.

[159] V.A. Sadykov, E.Y. Pikalova, A.A. Kolchugin, E.A. Filonova, E.M. Sadovskaya, N. F. Eremeev, A.V. Ishchenko, A.V. Fetisov, S.M. Pikalov, Oxygen transport properties of Ca-doped Pr2NiO4, Solid State Ionics 317 (2018) 234–243, https://doi.org/10.1016/j.ssi.2018.01.035.

[160] S.S. Bhoga, A.P. Khandale, B.S. Pahune, Investigation on Pr2 - XSrxNiO4 + δ (x = 0.3-1.0) cathode materials for intermediate temperature solid oxide fuel cell, Solid State Ionics 262 (2014) 340–344, https://doi.org/10.1016/j.ssi.2013.09.041.

[161] M. Garali, M. Kahlaoui, B. Mohammed, A. Mater, C. ben Azouz, C. Chefi, Synthesis, characterization and electrochemical properties of La2-xEuxNiO4+Δ Ruddlesden-Popper-type layered nickelates as cathode materials for SOFC applications, Int. J. Hydrogen Energy. 44 (2019) 11020–11032, https://doi.org/10.1016/j.ijhydene.2019.02.158.

[162] S. Chaianansutcharit, Y.W. Ju, S. Ida, T. Ishihara, Ni doped PrSr3Fe3O10-δ Ruddlesden-Popper oxide for active oxygen reduction cathode for solid oxide fuel cell, Electrochim. Acta. 222 (2016) 1853–1860, https://doi.org/10.1016/j.electacta.2016.11.178.

[163] S.E. Hou, J.A. Alonso, S. Rajasekhara, M.J. Martínez-Lope, M.T. Fernández-Díaz, J.B. Goodenough, Defective Ni perovskites as cathode materials in intermediate-temperature solid-oxide fuel cells: a structure=properties correlation, Chem. Mater. 22 (2010) 1071–1079, https://doi.org/10.1021/cm9020518.

[164] Q. Wang, J. Hou, Y. Fan, X.A. Xi, J. Li, Y. Lu, G. Huo, L. Shao, X.Z. Fu, J.L. Luo, Pr2BaNiMnO7-δ double-layered Ruddlesden-Popper perovskite oxides as efficient cathode electrocatalysts for low temperature proton conducting solid oxide fuel cells, J. Mater. Chem. A. 8 (2020) 7704–7712, https://doi.org/10.1039/c9ta11212j.

[165] V.V. Kharton, A.P. Viskup, A.V. Kovalevsky, E.N. Naumovich, F.M.B. Marques, Ionic transport in oxygen-hyperstoichiometric phases with K2NiF4-type structure, Solid State Ionics 143 (2001) 337–353, https://doi.org/10.1016/S0167-2738(01)00876-1.

[166] E.Y. Pikalova, V.A. Sadykov, E.A. Filonova, N.F. Eremeev, E.M. Sadovskaya, S. M. Pikalov, N.M. Bogdanovich, J.G. Lyagaeva, A.A. Kolchugin, L.B. Vedmid, A. V. Ishchenko, V.B. Goncharov, Structure, oxygen transport properties and electrode performance of Ca-substituted Nd 2 NiO 4, Solid State Ionics 335 (2019) 53–60, https://doi.org/10.1016/j.ssi.2019.02.012.

[167] V. Vashook, E. Girdauskaite, J. Zosel, T.L. Wen, H. Ullmann, U. Guth, Oxygen non-stoichiometry and electrical conductivity of Pr2-xSrxNiO4±δ with x = 0-0.5, Solid State Ionics 177 (2006) 1163–1171, https://doi.org/10.1016/j.ssi.2006.05.018.

[168] J.M. Bassat, P. Odier, J.P. Loup, The semiconductor-to-metal transition in question in la2-xnio4+δ (δ >0 or δ < 0), J. Solid State Chem. 110 (1994) 124–135, https://doi.org/10.1006/jssc.1994.1146.

[169] V. Vibhu, A. Rougier, C. Nicollet, A. Flura, J.C. Grenier, J.M. Bassat, La2 - XPrxNiO4 + δ as suitable cathodes for metal supported SOFCs, Solid State Ionics 278 (2015) 32–37, https://doi.org/10.1016/j.ssi.2015.05.005.

[170] E. Dogdibegovic, Q. Cai, N.S. Alabri, W. Guan, X.-.D. Zhou, Activity and stability of (Pr 1-x Ndx) 2 NiO 4 as cathodes for solid oxide fuel cells, J. Electrochem. Soc. 164 (2017) F99–F106. https://doi.org/10.1149/2.0581702jes.

[171] Y. Shen, H. Zhao, J. Xu, X. Zhang, K. Zheng, K. Świerczek, Effect of ionic size of dopants on the lattice structure, electrical and electrochemical properties of La2-xMxNiO 4+δ (M = Ba, Sr) cathode materials, Int. J. Hydrogen Energy. 39 (2014) 1023–1029, https://doi.org/10.1016/j.ijhydene.2013.10.153.

[172] E. Kravchenko, A. Neagu, K. Zakharchuk, J. Grins, G. Svensson, V. Pankov, A. A. Yaremchenko, High-temperature structural and electrical characterization of reduced oxygen-deficient Ruddlesden–Popper nickelates, Eur. J. Inorg. Chem. 2018 (2018) 3320–3329, https://doi.org/10.1002/ejic.201800091.

[173] Y. Takeda, N. Nishijima, N. Imanishi, R. Kanno, O. Yamamoto, Crystal chemistry and transport properties of Nd2 _ xAxNiO4 Department of Chemistry, Faculty of Engineering, Mie University, J. Solid State Chem. 96 (1992) 72–83.

[174] S.Y. Jeon, B. Singh, H.N. Im, K.P. Seong, S.J. Song, Charge and mass transport properties of La2Ni 0.95Al0.05O4.025+δ, J. Alloys Compd. 589 (2014) 572–578, https://doi.org/10.1016/j.jallcom.2013.12.039.

[175] X. Zhang, L. Zhang, J. Meng, W. Zhang, F. Meng, X. Liu, J. Meng, Highly enhanced electrochemical property by Mg-doping La2Ni1-xMgxO4+Δ (x = 0.0, 0.02, 0.05 and 0.10) cathodes for intermediate-temperature solid oxide fuel cells, Int. J. Hydrogen Energy. 42 (2017) 29498–29510, https://doi.org/10.1016/j.ijhydene.2017.10.091.

[176] E.N. Naumovich, M.V. Patrakeev, V.V. Kharton, A.A. Yaremchenko, E.V. Tsipis, D. I. Logvinovich, J.R. Frade, F.M.B. Marques, Defect formation in $La_2Ni(M)O_{4+\delta}$ (M= Co, Cu): modelling and coulometric titration study, Mater. Sci. Forum 514–516 (2006) 397–401, https://doi.org/10.4028/www.scientific.net/msf.514-516.397.

[177] S. Li, H. Tu, F. Li, M.T. Anwar, L. Yu, Investigation of Nd2Ni0.9M0.1O4+δ(M = Ni, Co, Cu, Fe, and Mn) cathodes for intermediate-temperature solid oxide fuel cell, J. Alloys Compd 694 (2017) 17–23, https://doi.org/10.1016/j.jallcom.2016.09.250.

[178] V.V. Kharton, E.V. Tsipis, E.N. Naumovich, A. Thursfield, M.V. Patrakeev, V. A. Kolotygin, J.C. Waerenborgh, I.S. Metcalfe, Mixed conductivity, oxygen permeability and redox behavior of K2NiF4-type La2Ni0.9Fe0.1O4+δ, J. Solid State Chem. 181 (2008) 1425–1433, https://doi.org/10.1016/j.jssc.2008.03.019.

[179] Z. Li, R. Haugsrud, J.B. Smith, T. Norby, Transport properties and defect analysis of La1.9Sr 0.1NiO4+δ, Solid State Ionics 180 (2009) 1433–1441, https://doi.org/10.1016/j.ssi.2009.08.011.

[180] A.R. Gilev, E.A. Kiselev, D.S. Chezganov, V.A. Cherepanov, Correlation between oxygen surface exchange rate and surface structure in the La1.5Sr0.5Ni1-yCoyO4+δ ceramic membranes, Ceram. Int. 46 (2020) 17553–17560, https://doi.org/10.1016/j.ceramint.2020.04.054.

[181] Y. Shen, H. Zhao, X. Liu, N. Xu, Preparation and electrical properties of Ca-doped La2NiO 4+δ cathode materials for IT-SOFC, Phys. Chem. Chem. Phys. 12 (2010) 15124–15131, https://doi.org/10.1039/c0cp00261e.

[182] F. Mauvy, E. Boehm, J.M. Bassat, J.C. Grenier, J. Fouletier, Oxygen permeation fluxes through La2Cu0.5Ni0.5O4+δ dense ceramics: comparison with oxygen diffusion coefficients, Solid State Ionics 178 (2007) 1200–1204, https://doi.org/10.1016/j.ssi.2007.06.008.

[183] J. Hyodo, K. Tominaga, Y.W. Ju, S. Ida, T. Ishihara, Electrical conductivity and oxygen diffusivity in Cu- and Ga-doped Pr 2NiO4, Solid State Ionics 256 (2014) 5–10, https://doi.org/10.1016/j.ssi.2013.12.036.

[184] X. Wu, C. Gu, J. Cao, L. Miao, C. Fu, W. Liu, Investigations on electrochemical performance of La2NiO4+δcathode material doped at A site for solid oxide fuel cells, Mater. Res. Express. 7 (2020), https://doi.org/10.1088/2053-1591/ab9c60.

[185] A.P. Tarutin, G.K. Vdovin, D.A. Medvedev, A.A. Yaremchenko, Fluorine-containing oxygen electrodes of the nickelate family for proton-conducting electrochemical cells, Electrochim. Acta. 337 (2020), 135808, https://doi.org/10.1016/j.electacta.2020.135808.

[186] K. Zheng, K. Świerczek, Evaluation of La2Ni0.5Cu0.5O4+δ and Pr2Ni0.5Cu0.5O4+δ Ruddlesden-Popper-type layered oxides as cathode materials for solid oxide fuel cells, Mater. Res. Bull. 84 (2016) 259–266, https://doi.org/10.1016/j.materresbull.2016.08.017.

[187] Y. Wang, J. Cheng, Q. Jiang, J. Yang, J. Gao, Preparation and electrochemical performance of Pr2Ni0.6Cu0.4O4 cathode materials for intermediate temperature solid oxide fuel cells, J. Power Sources. 196 (2011) 3104–3108, https://doi.org/10.1016/j.jpowsour.2010.11.106.

[188] V. Vibhu, I.C. Vinke, R.A. Eichel, J.-.M. Bassat, L.G.J. de Haart, Cobalt substituted lanthanide nickelates (Ln2Ni1-xCoxO4+δ, Ln = La, Pr; x=0, 0.1, 0.2) as high performance oxygen electrodes for solid oxide cells, ECS Trans. 91 (2019) 1327–1339.

[189] Y. Wang, X. Zhao, S. Lü, B. Yu, X. Meng, Y. Zhang, J. Yang, C. Fu, Y. Ji, (Pr0.9La0.1)2(Ni0.74Cu 0.21Ga0.05)O4+δ as cathode material for CeO2-based intermediate-temperature solid-oxide fuel cell, Ceram. Int. 40 (2014) 7321–7327, https://doi.org/10.1016/j.ceramint.2013.12.074.

[190] A.P. Khandale, S.S. Bhoga, R.V. Kumar, Effect of Ni doping on structural, electrical and electrochemical properties of Nd1.8Ce0.2Cu1 - XNi xO4 + δ mixed ionic-electronic conductor, Solid State Ionics 238 (2013) 1–6, https://doi.org/10.1016/j.ssi.2013.02.010.

[191] W. Lee, J.W. Han, Y. Chen, Z. Cai, B. Yildiz, Cation size mismatch and charge interactions drive dopant segregation at the surfaces of manganite perovskites, J. Am. Chem. Soc. 135 (2013) 7909–7925, https://doi.org/10.1021/ja3125349.

[192] J. Druce, T. Ishihara, J. Kilner, Surface composition of perovskite-type materials studied by Low Energy Ion Scattering (LEIS), Solid State Ionics 262 (2014) 893–896, https://doi.org/10.1016/j.ssi.2013.09.010.

[193] H. Svengren, M. Chamoun, J. Grins, M. Johnsson, Water splitting catalysis studied by using real-time faradaic efficiency obtained through coupled electrolysis and mass spectrometry, ChemElectroChem 5 (2018) 44–50, https://doi.org/10.1002/celc.201701086.

[194] Z. Feng, Y. Yacoby, M.J. Gadre, Y. Lee, W.T. Hong, H. Zhou, M.D. Biegalski, H. M. Christen, S.B. Adler, D. Morgan, Y. Shao-horn, Anomalous interface and surface strontium segregation in (La1−ySry)2CoO4±δ/La1−xSrxCoO3−δ heterostructured thin films, J. Phys. Chem. Lett. 5 (2014) 1027–1034.

[195] M. Yashima, H. Yamada, S. Nuansaeng, T. Ishihara, Role of Ga3+ and Cu2+ in the high interstitial oxide-ion diffusivity of Pr2NiO4-based oxides: design concept of interstitial ion conductors through the higher-valence d10 dopant and Jahn−Teller effect, Chem. Mater. 24 (2012) 4100–4113, https://doi.org/10.1021/cm3021287.

[196] Y. Chen, Q. Liao, Y. Wei, Z. Li, H. Wang, A CO2-stable K2NiF4-type oxide (Nd0.9La0.1)2(Ni0.74Cu0.21Al0.05)O4+δ for oxygen separation, Ind. Eng. Chem. Res. 52 (2013) 8571–8578.

[197] J. Tang, Y. Wei, L. Zhou, Z. Li, H. Wang, Oxygen permeation through a CO2-tolerant mixed conducting oxide (Pr0.9La0.1)2(Ni0.74Cu0.21Ga0.05)O4+d, Am. Inst. Chem. Eng. AIChE J. 58 (2012) 2473–2478, https://doi.org/10.1002/aic.

[198] C. Nicollet, A. Flura, V. Vibhu, A. Rougier, J.M. Bassat, J.C. Grenier, La2NiO4+δ infiltrated into gadolinium doped ceria as novel solid oxide fuel cell cathodes: electrochemical performance and impedance modelling, J. Power Sources. 294 (2015) 473–482, https://doi.org/10.1016/j.jpowsour.2015.06.077.

[199] V. Vibhu, A. Flura, C. Nicollet, S. Fourcade, N. Penin, J.M. Bassat, J.C. Grenier, A. Rougier, M. Pouchard, Characterization of PrNiO3-δ as oxygen electrode for SOFCs, Solid State Sci. 81 (2018) 26–31, https://doi.org/10.1016/j.solidstatesciences.2018.04.016.

[200] M.S.D. Read, M.S. Islam, F. King, F.E. Hancock, Defect chemistry of La2Ni1-xMxO4 (M) Mn, Fe, Co, Cu): relevance to catalytic behavior, J. Phys. Chem. B (1999) 1558–1562.
[201] J.A. Kilner, C.K.M. Shaw, Mass transport in La2Ni1-xCoxO4+δ oxides with the K2NiF4 structure, Solid State Ionics 154–155 (2002) 523–527, https://doi.org/10.1016/S0167-2738(02)00506-4.
[202] A.A. Yaremchenko, V.V. Kharton, M.V. Patrakeev, J.R. Frade, P-type electronic conductivity, oxygen permeability and stability of La2Ni0.9Co0.1O4+δ, J. Mater. Chem. 13 (2003) 1136–1144, https://doi.org/10.1039/b300357d.
[203] C.N. Munnings, S.J. Skinner, G. Amow, P.S. Whitfield, I.J. Davidson, Oxygen transport in the La2Ni1-xCoxO 4+δ system, Solid State Ionics 176 (2005) 1895–1901, https://doi.org/10.1016/j.ssi.2005.06.002.
[204] G. Amow, P.S. Whitfield, I.J. Davidson, R.P. Hammond, C.N. Munnings, S. J. Skinner, Structural and sintering characteristics of the La2Ni 1-xCoxO4+δ series, Ceram. Int. 30 (2004) 1635–1639, https://doi.org/10.1016/j.ceramint.2003.12.164.
[205] J. Dailly, A. Delrue, M. Ancelin, M. Marrony, Nanoparticles infiltration into SOFC cathode backbones, ECS Trans. 78 (2017) 1979–1991, https://doi.org/10.1149/07801.1979ecst.
[206] A.J. Samson, P. Hjalmarsson, M. Sogaard, J. Hjelm, N. Bonanos, Highly durable anode supported solid oxide fuel cell with an infiltrated cathode, J. Power Sources. 216 (2012) 124–130, https://doi.org/10.1016/j.jpowsour.2012.05.040.
[207] A.J. Samson, M. Søgaard, P.V. Hendriksen, Model for solid oxide fuel cell cathodes prepared by infiltration, Electrochim. Acta. 229 (2017) 73–95, https://doi.org/10.1016/j.electacta.2017.01.088.
[208] O. Ozmen, S. Lee, G. Hackett, H. Abernathy, J.W. Zondlo, E.M. Sabolsky, Efficient and controlled nano-catalyst solid-oxide fuel cell electrode infiltration with poly-norepinephrine surface modification, J. Power Sources. 485 (2021), 229232, https://doi.org/10.1016/j.jpowsour.2020.229232.
[209] M. Shah, S.A. Barnett, Solid oxide fuel cell cathodes by infiltration of La0.6Sr0.4Co0.2Fe0.8O3 - δ into Gd-doped ceria, Solid State Ionics 179 (2008) 2059–2064, https://doi.org/10.1016/j.ssi.2008.07.002.
[210] J.G. Railsback, Z. Gao, S.A. Barnett, Oxygen electrode characteristics of Pr2NiO4 +δ -infiltrated porous (La0.9Sr0.1)(Ga0.8Mg0.2)O3–δ, Solid State Ionics 274 (2015) 134–139, https://doi.org/10.1016/j.ssi.2015.03.030.
[211] C. Nicollet, A. Flura, V. Vibhu, S. Fourcade, A. Rougier, J.-M.M. Bassat, J.-C. C. Grenier, Preparation and characterization of Pr2NiO4+δ infiltrated into Gd-doped ceria as SOFC cathode, J. Solid State Electrochem. 20 (2016) 2071–2078, https://doi.org/10.1007/s10008.
[212] M.A. Laguna-Bercero, H. Luebbe, J. Silva, J. Van Herle, Electrochemical performance of Nd1.95NiO4+δ cathode supported microtubular solid oxide fuel cells, Fuel Cells 15 (2015) 98–104, https://doi.org/10.1002/fuce.201400071.
[213] S. Choi, S. Yoo, J.-Y. Shin, G. Kim, High performance SOFC cathode prepared by infiltration of Lan+1NinO3n+1 (n = 1, 2, and 3) in porous YSZ, J. Electrochem. Soc. 158 (2011) B995, https://doi.org/10.1149/1.3598170.
[214] W. Zhou, F. Liang, Z. Shao, Z. Zhu, Hierarchical CO 2-protective shell for highly efficient oxygen reduction reaction, Sci. Rep. 2 (2012) 327–332, https://doi.org/10.1038/srep00327.
[215] G. Yang, C. Su, R. Ran, M.O. Tade, Z. Shao, Advanced symmetric solid oxide fuel cell with an infiltrated K2NiF4-type La2NiO4 electrode, Energy and Fuels 28 (2014) 356–362, https://doi.org/10.1021/ef401473w.
[216] L. Petit, A. Svane, Z. Szotek, W.M. Temmerman, First-principles study of rare-earth oxides, Phys. Rev. B - Condens. Matter Mater. Phys. 72 (2005) 1–9, https://doi.org/10.1103/PhysRevB.72.205118.
[217] A. Montenegro-Hernández, A. Soldati, L. Mogni, H. Troiani, A. Schreiber, F. Soldera, A. Caneiro, Reactivity at the Ln2NiO4+δ/electrolyte interface (Ln = La, Nd) studied by electrochemical impedance spectroscopy and transmission electron microscopy, J. Power Sources. 265 (2014) 6–13, https://doi.org/10.1016/j.jpowsour.2014.04.082.
[218] K. Zhao, Y.P. Wang, M. Chen, Q. Xu, B.H. Kim, D.P. Huang, Electrochemical evaluation of La2NiO4+δ as a cathode material for intermediate temperature solid oxide fuel cells, Int. J. Hydrogen Energy. 39 (2014) 7120–7130, https://doi.org/10.1016/j.ijhydene.2014.02.106.
[219] Y. Lee, H. Kim, Electrochemical performance of La2NiO4+δ cathode for intermediate-temperature solid oxide fuel cells, Ceram. Int. 41 (2015) 5984–5991, https://doi.org/10.1016/j.ceramint.2015.01.037.
[220] M.J. Escudero, A. Fuerte, L. Daza, La2NiO4+δ potential cathode material on La 0.9Sr0.1Ga0.8Mg0.2O2.85 electrolyte for intermediate temperature solid oxide fuel cell, J. Power Sources. 196 (2011) 7245–7250, https://doi.org/10.1016/j.jpowsour.2010.11.068.
[221] R.K. Sharma, S.K. Cheah, M. Burriel, L. Dessemond, J.M. Bassat, E. Djurado, Design of La2-xPrxNiO4+δ SOFC cathodes: a compromise between electrochemical performance and thermodynamic stability, J. Mater. Chem. A. 5 (2017) 1120–1132, https://doi.org/10.1039/c6ta08011a.
[222] A.R. Hanifi, M.A. Laguna-Bercero, N.K. Sandhu, T.H. Etsell, P. Sarkar, Tailoring the microstructure of a solid oxide fuel cell anode support by calcination and milling of YSZ, Sci. Rep. 6 (2016) 1–9, https://doi.org/10.1038/srep27359.
[223] D. Mesguich, J.M. Bassat, C. Aymonier, A. Brüll, L. Dessemond, E. Djurado, Influence of crystallinity and particle size on the electrochemical properties of spray pyrolyzed Nd2NiO4+δ powders, Electrochim. Acta. 87 (2013) 330–335, https://doi.org/10.1016/j.electacta.2012.07.134.
[224] V. Vibhu, A. Flura, A. Rougier, C. Nicollet, S. Fourcade, T. Hungría, J. Grenier, J. Bassat, Electrochemical ageing study of mixed lanthanum /praseodymium nickelates La2-PrNiO4 + δ as oxygen electrodes for solid oxide fuel or electrolysis cells, J. Energy Chem. (2020) 62–70, https://doi.org/10.1016/j.jechem.2019.10.012.
[225] S. Saher, J. Song, V. Vibhu, C. Nicollet, A. Flura, J.M. Bassat, H.J. M. Bouwmeester, Influence of annealing at intermediate temperature on oxygen transport kinetics of Pr2NiO4+δ, J. Mater. Chem. A. 6 (2018) 8331–8339, https://doi.org/10.1039/c7ta08885j.
[226] E. Dogdibegovic, C.J. Wright, X.D. Zhou, W.C. Wei, Stability and activity of (Pr1-xNdx)2NiO4 as cathodes for solid oxide fuel cells: i. quantification of phase evolution in Pr2NiO4, J. Am. Ceram. Soc. 99 (2016) 2737–2741, https://doi.org/10.1111/jace.14291.
[227] M. Lin, S. Sakthinathan, T. Chiu, H. Chang, Y. Wang, Preparation of IT-SOFC with Pr2NiO4 cathode and hybrid Ce0.8Sm0.2O1.9 electrolyte, J. Ceram. Soc. Japan. 127 (2019) 249–253.
[228] S. Kim, S. Choi, A. Jun, J. Shin, G. Kim, Scale-down and Sr-doping effects on La4Ni3O10-δ –YSZ nanocomposite cathodes for IT-SOFCs, J. Electrochem. Soc. 161 (2014) F1468–F1473, https://doi.org/10.1149/2.0791414jes.
[229] S. Chaianansutcharit, K. Hosoi, J. Hyodo, Y.W. Ju, T. Ishihara, Ruddlesden Popper oxides of LnSr3Fe3O10-δ (Ln = La, Pr, Nd, Sm, Eu, and Gd) as active cathodes for low temperature solid oxide fuel cells, J. Mater. Chem. A. 3 (2015) 12357–12366, https://doi.org/10.1039/c5ta01273b.
[230] A. Flura, C. Nicollet, V. Vibhu, B. Zeimetz, A. Rougier, J.-.M. Bassat, J.-. C. Grenier, Application of the adler-lane-steele model to porous La2NiO4+δ SOFC cathode: influence of interfaces with gadolinia doped ceria, J. Electrochem. Soc. 163 (2016) F523–F532, https://doi.org/10.1149/2.0891606jes.
[231] A. Flura, C. Nicollet, V. Vibhu, A. Rougier, J.M. Bassat, J.C. Grenier, Ceria doped with praseodymium instead of gadolinium as efficient interlayer for lanthanum nickelate SOFC oxygen electrode, Electrochim. Acta. 231 (2017) 103–114, https://doi.org/10.1016/j.electacta.2017.02.019.
[232] B. Huang, X.J. Zhu, H.W. Nie, Y.R. Niu, Y. Li, N. Cheng, Comparison of the electrochemical properties of impregnated and functionally gradient LaNi0.6Fe0.4O3-Gd 0.2Ce0.8O2 composite cathodes for Solid Oxide Fuel Cell, J. Power Sources. 235 (2013) 20–28, https://doi.org/10.1016/j.jpowsour.2013.02.010.
[233] S.R. Gandavarapu, K. Sabolsky, K. Gerdes, E.M. Sabolsky, Direct foamed and nano-catalyst impregnated solid-oxide fuel cell (SOFC) cathodes, Mater. Lett. 95 (2013) 131–134, https://doi.org/10.1016/j.matlet.2012.12.099.
[234] Y. Huang, J.M. Vohs, R.J. Gorte, Fabrication of Sr-doped LaFeO3 YSZ composite cathodes, J. Electrochem. Soc. 151 (2004) A646, https://doi.org/10.1149/1.1652053.
[235] X. Chen, J. Wang, Q. Liang, X. Sun, X. Zhu, D. Zhou, J. Meng, Pr2NiO4-Pr0.2Ce0·8O1.9 composite cathode as a potential cathode material for intermediate temperature solid oxide fuel cells, Solid State Sci. 100 (2020), 106108, https://doi.org/10.1016/j.solidstatesciences.2019.106108.
[236] T... Takasu, T... Sugino, Y. Matsuda, Electrical conductivity of praseodymia doped ceria, J. Appl. Electrochem. 14 (1984) 79–81, https://doi.org/10.1007/BF00611261.
[237] K. Eguchi, T. Setoguchi, T. Inoue, H. Arai, Electrical properties of ceria-based oxides and their application to solid oxide fuel cells, Solid State Ionics 52 (1992) 165–172, https://doi.org/10.1016/0167-2738(92)90102-U.
[238] R. Chiba, H. Taguchi, T. Komatsu, H. Orui, K. Nozawa, H. Arai, High temperature properties of Ce1-xPrxO 2-δ as an active layer material for SOFC cathodes, Solid State Ionics 197 (2011) 42–48, https://doi.org/10.1016/j.ssi.2011.03.022.
[239] R. Chiba, T. Komatsu, H. Orui, H. Taguchi, K. Nozawa, H. Arai, An SOFC cathode composed of LaNi0.6Fe0.4O3 and Ce(Ln)O2 (Ln=Sm, Gd, Pr), J. Korean Ceram. Soc 45 (2008) 766–771.
[240] E.V. Tsipis, V.V. Kharton, Electrode materials and reaction mechanisms in solid oxide fuel cells : a brief review, J. Solid State Electrochem. 12 (2008) 1039–1060, https://doi.org/10.1007/s10008-007-0468-0.
[241] S.R. Bishop, D. Chen, Y. Kuru, J.J. Kim, T.S. Stefanik, H.L. Tuller, Measurement and modeling of electrical, mechanical, and chemical properties of a model mixed ionic electronic conductor: PR doped Ceria, ECS Trans. 33 (2011) 51–57.
[242] M. Nauer, C. Ftikos, B.C.H. Steele, An evaluation of Ce-Pr oxides and Ce-Pr-Nb oxides mixed conductors for cathodes of solid oxide fuel cells: structure, thermal expansion and electrical conductivity, J. Eur. Ceram. Soc. 14 (1994) 493–499, https://doi.org/10.1016/0955-2219(94)90118-X.
[243] S.R. Bishop, H.L. Tuller, Y. Kuru, B. Yildiz, Chemical expansion of nonstoichiometric Pr0.1Ce0.9O2-δ: correlation with defect equilibrium model, J. Eur. Ceram. Soc. 31 (2011) 2351–2356, https://doi.org/10.1016/j.jeurceramsoc.2011.05.034.
[244] D.P. Fagg, V.V. Kharton, A. Shaula, I.P. Marozau, J.R. Frade, Mixed conductivity, thermal expansion, and oxygen permeability of Ce(Pr,Zr)O2 - δ, Solid State Ionics 176 (2005) 1723–1730, https://doi.org/10.1016/j.ssi.2005.04.023.
[245] D.P. Fagg, I.P. Marozau, A.L. Shaula, V.V. Kharton, J.R. Frade, Oxygen permeability, thermal expansion and mixed conductivity of GdxCe0.8-xPr0.2O2-δ, x=0, 0.15, 0.2, J. Solid State Chem. 179 (2006) 3347–3356, https://doi.org/10.1016/j.jssc.2006.06.028.
[246] Z. Gao, X. Ding, D. Ding, L. Ding, S. Zhang, G. Yuan, Infiltrated Pr2NiO4 as promising bi-electrode for symmetrical solid oxide fuel cells, Int. J. Hydrogen Energy. 43 (2018) 8953–8961, https://doi.org/10.1016/j.ijhydene.2018.03.164.
[247] D. Pérez-Coll, A. Aguadero, M.J. Escudero, P. Núñez, L. Daza, Optimization of the interface polarization of the La2NiO4-based cathode working with the Ce1-xSmxO2-δ electrolyte system, J. Power Sources. 178 (2008) 151–162, https://doi.org/10.1016/j.jpowsour.2007.12.030.
[248] K. Zhao, Q. Xu, D.P. Huang, M. Chen, B.H. Kim, Electrochemical evaluation of La 2NiO 4+δ-based composite electrodes screen-printed on Ce 0.8Sm 0.2O 1.9 electrolyte, J. Solid State Electrochem. 16 (2012) 2797–2804, https://doi.org/10.1007/s10008-012-1702-y.

[249] J. Druce, H. Téllez, M. Burriel, M.D. Sharp, L.J. Fawcett, S.N. Cook, D.S. McPhail, T. Ishihara, H.H. Brongersma, J.A. Kilner, Surface termination and subsurface restructuring of perovskite-based solid oxide electrode materials, Energy Environ. Sci. 7 (2014) 3593–3599, https://doi.org/10.1039/c4ee01497a.
[250] Y. Tan, A. Wang, L. Jia, D. Yan, B. Chi, J. Pu, J. Li, High-performance oxygen electrode for reversible solid oxide cells with power generation and hydrogen production at intermediate temperature, Int. J. Hydrogen Energy. 42 (2017) 4456–4464, https://doi.org/10.1016/j.ijhydene.2016.10.121.
[251] T. Chen, Y. Zhou, M. Liu, C. Yuan, X. Ye, Z. Zhan, S. Wang, High performance solid oxide electrolysis cell with impregnated electrodes, Electrochem. Commun. 54 (2015) 23–27, https://doi.org/10.1016/j.elecom.2015.02.015.
[252] C. Sun, S. Yang, Y. Lu, J. Wen, X. Ye, Z. Wen, Tailoring a micro-nanostructured electrolyte-oxygen electrode interface for proton-conducting reversible solid oxide cells, J. Power Sources. 449 (2020), 227498, https://doi.org/10.1016/j.jpowsour.2019.227498.
[253] Z. Chen, J. Wang, D. Huan, S. Sun, G. Wang, Z. Fu, W. Zhang, X. Zheng, H. Pan, R. Peng, Y. Lu, Tailoring the activity via cobalt doping of a two-layer Ruddlesden-Popper phase cathode for intermediate temperature solid oxide fuel cells, J. Power Sources. 371 (2017) 41–47, https://doi.org/10.1016/j.jpowsour.2017.10.011.
[254] C. Ferchaud, J.C. Grenier, Y. Zhang-Steenwinkel, M.M.A. Van Tuel, F.P.F. Van Berkel, J.M. Bassat, High performance praseodymium nickelate oxide cathode for low temperature solid oxide fuel cell, J. Power Sources. 196 (2011) 1872–1879, https://doi.org/10.1016/j.jpowsour.2010.09.036.
[255] M.A. Laguna-Bercero, N. Kinadjan, R. Sayers, H. El Shinawi, C. Greaves, S. J. Skinner, Performance of La2-xSrxCo 0.5Ni0.5O4 ± δ as an oxygen electrode for solid oxide reversible cells, Fuel Cells 11 (2011) 102–107, https://doi.org/10.1002/fuce.201000067.
[256] E.Y. Pikalova, N.M. Bogdanovich, A.A. Kolchugin, D.A. Osinkin, D.I. Bronin, Electrical and electrochemical properties of La2NiO4+δ-based cathodes in contact with Ce0.8Sm0.2O2-δ electrolyte, Procedia Eng 98 (2014) 105–110, https://doi.org/10.1016/j.proeng.2014.12.495.
[257] V.V. Kharton, E.V. Tsipis, A.A. Yaremchenko, J.R. Frade, Surface-limited oxygen transport and electrode properties of La 2Ni0.8Cu0.2O4+δ, Solid State Ionics 166 (2004) 327–337, https://doi.org/10.1016/j.ssi.2003.11.020.
[258] A.P. Khandale, S.S. Bhoga, Combustion synthesized Nd2-xCexCuO4 (x = 0-0.25) cathode materials for intermediate temperature solid oxide fuel cell applications, J. Power Sources. 195 (2010) 7974–7982, https://doi.org/10.1016/j.jpowsour.2010.06.044.
[259] A.P. Khandale, S.S. Bhoga, Study of Nd 2-xCe xCuO 4±δ (x=0.1-0.25) as cathode material for intermediate-temperature solid oxide fuel cells, J. Solid State Electrochem. 16 (2012) 341–352, https://doi.org/10.1007/s10008-011-1332-9.
[260] K. Zhao, Q. Xu, D.P. Huang, W. Chen, M. Chen, B.H. Kim, Microstructure and electrochemical properties of porous La 2NiO 4+δ electrode screen-printed on Ce 0.8Sm 0.2O 1.9 electrolyte, J. Solid State Electrochem. 16 (2012) 9–16, https://doi.org/10.1007/s10008-010-1270-y.
[261] D. Mesguich, J.M. Bassat, C. Aymonier, E. Djurado, Nanopowder synthesis of the SOFC cathode material Nd2NiO 4+δ by ultrasonic spray pyrolysis, Solid State Ionics 181 (2010) 1015–1023, https://doi.org/10.1016/j.ssi.2010.05.041.
[262] B.I. Arias-Serrano, E.S. Kravchenko, K. Zakharchuk, J. Grins, G. Svensson, V. Pankov, A.A. Yaremchenko, Oxygen-deficient Nd0.8Sr1.2Ni0.8M0.2O4-δ (M = Ni, Co, Fe) nickelates as oxygen electrode materials for SOFC/SOEC, ECS Trans. 91 (2019) 2387–2397.
[263] Z. He, N. Ai, S. He, S.P. Jiang, L. Zhang, W.D.A. Rickard, D. Tang, K. Chen, Positive effect of incorporating Er0.4Bi1.6O3 on the performance and stability of La2NiO4+δ cathode, J. Electrochem. Soc. 166 (2019) F796–F804, https://doi.org/10.1149/2.0841912jes.
[264] R. Chiba, F. Yoshimura, Y. Sakurai, Investigation of LaNi1-xFexO3 as a cathode material for solid oxide fuel cells, Solid State Ionics 124 (1999) 281–288, https://doi.org/10.1016/S0167-2738(99)00222-2.
[265] A. Aguadero, L. Fawcett, S. Taub, R. Woolley, K.T. Wu, N. Xu, J.A. Kilner, S. J. Skinner, Materials development for intermediate-temperature solid oxide electrochemical devices, J. Mater. Sci. 47 (2012) 3925–3948, https://doi.org/10.1007/s10853-011-6213-1.
[266] H. Orui, K. Watanabe, R. Chiba, M. Arakawa, Application of LaNi(Fe)O3 as SOFC cathode, J. Electrochem. Soc. 151 (2004) A1412, https://doi.org/10.1149/1.1779628.
[267] E. Pikalova, N. Bogdanovich, A. Kolchugin, L. Ermakova, A. Khrustov, A. Farlenkov, D. Bronin, Methods to increase electrochemical activity of lanthanum nickelate-ferrite electrodes for intermediate and low temperature SOFCs, Int. J. Hydrogen Energy. 46 (2021) 35923–35937, https://doi.org/10.1016/j.ijhydene.2021.01.226.
[268] E. Pikalova, N. Bogdanovich, A. Kolchugin, K. Shubin, L. Ermakova, N. Eremeev, A. Farlenkov, A. Khrustov, E. Filonova, V. Sadykov, Development of composite LaNi0.6Fe0.4O3-δ-based air electrodes for solid oxide fuel cells with a thin-film bilayer electrolyte, Int. J. Hydrogen Energy. 46 (2021) 16947–16964, https://doi.org/10.1016/j.ijhydene.2021.02.217.
[269] P. Hjalmarsson, M. Mogensen, La0.99Co0.4Ni0.6O3-δ- Ce0.8Gd0.2O1.95 as composite cathode for solid oxide fuel cells, J. Power Sources 196 (2011) 7237–7244, https://doi.org/10.1016/j.jpowsour.2010.11.065.
[270] S. Huang, Q. Lu, S. Feng, G. Li, C. Wang, PrNi0.6Co0.4O3-Ce0.8Sm 0.2O1.9 composite cathodes for intermediate temperature solid oxide fuel cells, J. Power Sources. 199 (2012) 150–154, https://doi.org/10.1016/j.jpowsour.2011.10.025.
[271] B. Huang, X.J. Zhu, Y. Lv, H. Liu, High-performance Gd 0.2Ce 0.8O 2-impregnated LaNi 0.6Fe 0.4O 3-δ cathodes for intermediate temperature solid oxide fuel cell, J. Power Sources. 209 (2012) 209–219, https://doi.org/10.1016/j.jpowsour.2012.02.103.
[272] M. Khoshkalam, M.A. Faghihi-Sani, X. Tong, M. Chen, P.V. Hendriksen, Enhanced activity of Pr 6 O 11 and CuO infiltrated Ce 0.9 Gd 0.1 O 2 based composite oxygen electrodes, J. Electrochem. Soc. 167 (2020), 024505, https://doi.org/10.1149/1945-7111/ab6821.
[273] X. Zhang, H. Zhang, X. Liu, High performance La2NiO4+δ-infiltrated (La 0.6Sr0.4)0.995Co0.2Fe 0.8O3-δ cathode for solid oxide fuel cells, J. Power Sources. 269 (2014) 412–417, https://doi.org/10.1016/j.jpowsour.2014.06.132.
[274] T. Ogier, F. Mauvy, J.M. Bassat, J. Laurencin, J. Mougin, J.C. Grenier, Overstoichiometric oxides Ln2NiO4+δ (Ln = La, Pr or Nd) as oxygen anodic electrodes for solid oxide electrolysis application, Int. J. Hydrogen Energy. 40 (2015) 15885–15892, https://doi.org/10.1016/j.ijhydene.2015.09.107.
[275] T. Chen, M. Liu, C. Yuan, Y. Zhou, X. Ye, Z. Zhan, C. Xia, S. Wang, High performance of intermediate temperature solid oxide electrolysis cells using Nd2NiO4+δ impregnated scandia stabilized zirconia oxygen electrode, J. Power Sources. 276 (2015) 1–6, https://doi.org/10.1016/j.jpowsour.2014.11.042.
[276] S. Huang, S. Feng, H. Wang, Y. Li, C. Wang, LaNi0.6Fe0.4O3-Ce0.8Sm 0.2O1.9-Ag composite cathode for intermediate temperature solid oxide fuel cells, Int. J. Hydrogen Energy 36 (2011) 10968–10974, https://doi.org/10.1016/j.ijhydene.2011.05.135.
[277] S. Hashimoto, K. Kammer, F.W. Poulsen, M. Mogensen, Conductivity and electrochemical characterization of PrFe1-xNixO3-δ at high temperature, J. Alloys Compd. 428 (2007) 256–261, https://doi.org/10.1016/j.jallcom.2006.02.068.
[278] E.P. Antonova, A.V. Khodimchuk, E.S. Tropin, N.M. Porotnikova, A.S. Farlenkov, M.I. Vlasov, M.V. Ananyev, Influence of modifying additives on electrochemical performance of La2NiO4+δ - based oxygen electrodes, Solid State Ionics 346 (2020), 115215, https://doi.org/10.1016/j.ssi.2019.115215.
[279] R.J. Woolley, S.J. Skinner, Novel La2NiO4+δ and La4Ni 3O10-δ composites for solid oxide fuel cell cathodes, J. Power Sources. 243 (2013) 790–795, https://doi.org/10.1016/j.jpowsour.2013.06.106.
[280] J. Dailly, F. Mauvy, M. Marrony, M. Pouchard, J.C. Grenier, Electrochemical properties of perovskite and A2MO 4-type oxides used as cathodes in protonic ceramic half cells, J. Solid State Electrochem. 15 (2011) 245–251, https://doi.org/10.1007/s10008-010-1188-4.
[281] K. Kammer, L. Mikkelsen, J.B. Bilde-Sørensen, Electrical and electro-chemical characterisation of La 0.99Fe1-x Ni x O3-δ perovskites, J. Solid State Electrochem. 10 (2006) 934–940, https://doi.org/10.1007/s10008-006-0153-8.
[282] R. Chiba, H. Orui, T. Komatsu, Y. Tabata, K. Nozawa, M. Arakawa, K. Sato, H. Arai, LaNi0.6Fe0.4O3–Ceria composite cathode for sofcs operating at intermediate temperatures, J. Electrochem. Soc. 155 (2008) B575, https://doi.org/10.1149/1.2901872.
[283] H. Tang, Z. Gong, Y. Wu, Z. Jin, W. Liu, Electrochemical performance of nanostructured LNF infiltrated onto LNO cathode for BaZr0.1Ce0.7Y0.2O3-Δ–based solid oxide fuel cell, Int. J. Hydrogen Energy. 43 (2018) 19749–19756, https://doi.org/10.1016/j.ijhydene.2018.09.008.
[284] L. Miao, J. Hou, Z. Gong, Z. Jin, W. Liu, A high-performance cobalt-free Ruddlesden-Popper phase cathode La1·2Sr0·8Ni0·6Fe0·4O4+Δ for low temperature proton-conducting solid oxide fuel cells, Int. J. Hydrogen Energy. 44 (2019) 7531–7537, https://doi.org/10.1016/j.ijhydene.2019.01.255.
[285] S. Li, H. Tu, L. Yu, M.T. Anwar, Fabrication and electrochemical characterizations of Nd2NiO4+δ-Ce0.8Gd0.2O2−δ composite cathodes for anode-supported intermediate temperature solid oxide fuel cells, Electrochim. Acta. 212 (2016) 303–312, https://doi.org/10.1016/j.electacta.2016.07.034.
[286] J. Hou, Z. Zhu, J. Qian, W. Liu, A new cobalt-free proton-blocking composite cathode La2NiO 4+δ-LaNi0.6Fe0.4O3-δ for BaZr0.1Ce0.7Y0.2O3-δ-based solid oxide fuel cells, J. Power Sources. 264 (2014) 67–75, https://doi.org/10.1016/j.jpowsour.2014.04.089.
[287] H. An, D. Shin, H. Ji, Pr2NiO4+δ for Cathode in Protonic Ceramic Fuel Cells, J. Korean Ceram. Soc. 55 (2018) 358–363.
[288] S.J. Kim, T. Akbay, J. Matsuda, A. Takagaki, T. Ishihara, Strain effects on oxygen reduction activity of Pr2NiO4 caused by gold bulk dispersion for low temperature solid oxide fuel cells, ACS Appl. Energy Mater. 2 (2019) 1210–1220, https://doi.org/10.1021/acsaem.8b01776.
[289] S. Yang, S. Zhang, C. Sun, X. Ye, Z. Wen, Lattice Incorporation of Cu 2+ into the BaCe 0.7 Zr 0.1 Y 0.1 Yb 0.1 O 3âî electrolyte on boosting its sintering and proton-conducting abilities for reversible solid oxide cells, ACS Appl. Mater. Interfaces. 10 (2018) 42387–42396, https://doi.org/10.1021/acsami.8b15402.
[290] V. Vibhu, I.C. Vinke, R.A. Eichel, L.G.J.J. De Haart, Cobalt substituted Pr2Ni1-xCoxO4+δ (x = 0, 0.1, 0.2) oxygen electrodes: impact on electrochemical performance and durability of solid oxide electrolysis cells, J. Power Sources. 482 (2021), 228909, https://doi.org/10.1016/j.jpowsour.2020.228909.
[291] W. Li, B. Guan, L. Ma, H. Tian, X. Liu, Synergistic Coupling of proton conductors BaZr0.1Ce0.7Y0.1Yb0.1O3-δ and La2Ce2O7 to create chemical stable, interface active electrolyte for steam electrolysis cells, ACS Appl. Mater. Interfaces 11 (2019) 18323–18330, https://doi.org/10.1021/acsami.9b00303.
[292] S. Yang, Y. Lu, Q. Wang, C. Sun, X. Ye, Z. Wen, Effects of porous support microstructure enabled by the carbon microsphere pore former on the performance of proton-conducting reversible solid oxide cells, Int. J. Hydrogen Energy. 43 (2018) 20050–20058, https://doi.org/10.1016/j.ijhydene.2018.09.011.
[293] S. Yang, Y. Wen, J. Zhang, Y. Lu, X. Ye, Z. Wen, Electrochemical performance and stability of cobalt-free Ln1.2Sr0.8NiO4 (Ln=La and Pr) air electrodes for proton-conducting reversible solid oxide cells, Electrochim. Acta. 267 (2018) 269–277, https://doi.org/10.1016/j.electacta.2018.02.053.

[294] W. Li, B. Guan, L. Ma, S. Hu, N. Zhang, X. Liu, High performing triple-conductive Pr2NiO4+: δ anode for proton-conducting steam solid oxide electrolysis cell, J. Mater. Chem. A. 6 (2018) 18057–18066, https://doi.org/10.1039/c8ta04018d.
[295] A. Tarutin, A. Kasyanova, J. Lyagaeva, G. Vdovin, D. Medvedev, Towards high-performance tubular-type protonic ceramic electrolysis cells with all-Ni-based functional electrodes, J. Energy Chem. 40 (2020) 65–74, https://doi.org/10.1016/j.jechem.2019.02.014.
[296] N. Danilov, J. Lyagaeva, G. Vdovin, E. Pikalova, D. Medvedev, Electricity/hydrogen conversion by the means of a protonic ceramic electrolysis cell with Nd2NiO4+Δ-based oxygen electrode, Energy Convers. Manag. 172 (2018) 129–137, https://doi.org/10.1016/j.enconman.2018.07.014.
[297] J. Lyagaeva, N. Danilov, G. Vdovin, J. Bu, D. Medvedev, A. Demin, P. Tsiakaras, A new Dy-doped BaCeO3-BaZrO3 proton-conducting material as a promising electrolyte for reversible solid oxide fuel cells, J. Mater. Chem. A. 4 (2016) 15390–15399, https://doi.org/10.1039/c6ta06414k.